2017

# Functions of the Apical Na+/ K+/ 2cl- Cotransporter 1 in Choroid Plexus Epithelial Cells

Jeannine Marie Crum Gregoriades
*Wright State University*

# Functions of the apical $Na^+/K^+/2Cl^-$ Cotransporter 1 in choroid plexus epithelial cells.

A dissertation submitted in partial fulfillment of the requirements for the degree of Doctor of Philosophy

By

Jeannine Marie Crum Gregoriades

B.S., The Ohio State University, 2004

2017

Wright State University

WRIGHT STATE UNIVERSITY

GRADUATE SCHOOL

August 28, 2017

I HEREBY RECOMMEND THAT THE DISSERTATION PREPARED UNDER MY SUPERVISION BY Jeannine Marie Crum Gregoriades ENTITLED Functions of the apical $Na^+/K^+/2Cl^-$ Cotransporter 1 in choroid plexus epithelial cells. BE ACCEPTED IN PARTIAL FULFILLMENT OF THE REQUIREMENTS FOR THE DEGREE OF Doctor of Philosophy.

_____

Francisco Javier Alvarez-Leefmans, M.D., Ph.D.
Dissertation Director

_____

Mill W. Miller, Ph.D.
Director, Biomedical Sciences
Ph.D. Program

_____

Robert E. W. Fyffe, Ph.D.
Vice President for Research and
Dean of the Graduate School

Committee on Final Examination

_____

James E. Olson, Ph.D.

_____

Kathrin Engisch, Ph.D.

_____

Dan R. Halm, Ph.D.

_____

Michael L. Raymer, Ph.D.

ABSTRACT

Gregoriades, Jeannine Marie Crum. Ph.D., Biomedical Sciences PhD Program, Wright State University, 2017. Functions of the apical $Na^+/K^+/2Cl^-$ Cotransporter 1 in choroid plexus epithelial cells.

Choroid plexus epithelial cells (CPECs) secrete cerebrospinal fluid (CSF) and regulate its electrolyte composition. CPECs express both the $Na^+/K^+$ ATPase and the $Na^+/K^+/2Cl^-$ cotransporter 1 (NKCC1) on their apical membrane (CSF facing), deviating from the typical basolateral membrane location in chloride secretory epithelia. Given this unusual location of NKCC1 and the unknown intracellular $Na^+$ and $Cl^-$ concentrations of CPECs, the cotransporter function in these cells is not understood. Further, the direction of net ion and associated water fluxes mediated by NKCC1 under basal physiological conditions in CPECs is controversial. Determining the direction of NKCC1- mediated fluxes is critical to understanding the function of this cotransporter in CPECs. If NKCC1 works in the net efflux mode, it may be involved in CSF secretion as suggested by some investigators. Conversely, if NKCC1 works in the net influx mode, as it does in the basolateral membrane of other chloride secreting epithelia, then it would have an absorptive function in CPECs and could be involved in CSF $K^+$ regulation, as we and others propose. NKCC1-mediated ion and water fluxes are tightly linked; thus, their direction is inferred by measuring cell water volume (CWV) changes in calcein-loaded CPECs following NKCC1 inactivation. Both genetic and pharmacological inactivation of NKCC1 produces CPEC shrinkage of ~16 %, due to unbalanced solute and water effluxes. $[Na^+]_i$ and $[Cl^-]_i$ measurements using the fluorescent

indicator dyes ANG-2 and MQAE show that $[Na^+]_i$ = 8.4 ± 1.0 mM and $[Cl^-]_i$ = 62.1 ± 3.5 mM. NKCC1 -/- CPECs have ~ 50% less $[Cl^-]_i$ than WT. WT CPECs are exquisitely sensitive to isosmotic changes in $[K^+]_o$ (± 2 mM), as shown by CWV responses. CPECs of NKCC1-/- mouse lose the response to $[K^+]_o$. These results suggest that under basal conditions, NKCC1 is constitutively active and works in the inward mode near its thermodynamic equilibrium in CPECS. We propose NKCC1 has absorptive functions and contributes to the-maintenance of normal and constant CWV. The $K_m$ for $[K^+]_o$ and the thermodynamic forces driving NKCC1 transport in CPECs suggest that it functions as a sensor and regulator of CSF $[K^+]$.

## *Table of contents*

## *List of figures*

## *List of tables*

## *List of equations*

*I dedicate my dissertation to my parents,*

*Bill and Jean Crum.*

## *Acknowledgment*

This dissertation would not have been possible without my advisor, Dr. F.J. Alvarez-Leefmans. His door was always open when I had a question or needed help. His guidance and support have made me a better scientist and writer. I will always be grateful for all that I have learned from you. Thank you, Dr. Alvarez-Leefmans! I thank my Committee members, Dr. Olson, Dr. Halm, Dr. Engisch, and Dr. Raymer for the time and mentorship that you have graciously offered during my education. I am also grateful for the support I received from the Biomedical Sciences Ph.D. Program, the Technology-based Learning with Disabilities PhD Program, the Department of Pharmacology and Toxicology, and the National Science Foundation. I would like to thank the former members of the Alvarez-Leefmans Lab: Dr. Mauricio Di Fulvio, Dr. Shihong Mao, Dr. Karen Flues, David Cha, Baiju Raval, Pankaj Patyal, and Aaron Madaris. Special thanks go to the late Dr. Robert Putnam. It was in his Quantitative Aspects of Membrane Transport class that I first started thinking about the function of apical NKCC1 as a potassium regulator in choroid plexus epithelial cells. Dr. Putnam was a great scientist, mentor, and friend. Thank you, Dr. Putnam. Of course, I would not have reached this point without the love and support of my family and friends. Most importantly, I must thank my husband, Greg. Your unending love, encouragement, generosity, and support have helped me to complete this journey. Words cannot express my gratitude—thank you, Greg!

# *Chapter 1: Background*

## *Choroid plexus*

The choroid plexus epithelium makes up the blood-cerebrospinal fluid-barrier, and consists of a monolayer of cuboidal epithelial cells bound together by tight-junctions, surrounding highly-fenestrated capillaries that maintain an impressive blood-flow of 3 –5 ml/ min/ gram (Damkier, Brown, & Praetorius, 2010; Johanson, Stopa, & McMillan, 2011). On the apical membrane, choroid plexus epithelial cells (CPECs) have beating cilia that protrude from the densely packed microvilli surface, and function to agitate unstirred layers and facilitate cerebrospinal fluid (CSF) circulation (Redzic & Segal, 2004). A convection current/ flow of CSF is generated by the beating cilia on CPECs and directs the CSF from the lateral ventricles through the third and fourth ventricles, and around the spinal cord and brain (Bulat & Klarica, 2011; Damkier et al., 2010). Floating in the brain ventricles, the choroid plexus epithelium is continuous with the ependymal cells lining the ventricles. It has several functions, many which are still under investigation, though the most common function ascribed to the choroid plexus is the ability to secrete CSF (Praetorius & Damkier, 2017; Spector, Keep, Robert Snodgrass, Smith, & Johanson, 2015). CSF flows through the ventricles and around

the brain and spinal cord, freely diffusing with the interstitial fluid (ISF) that fills the extracellular spaces between neurons and glia. Ependymal cells that line the cerebral ventricles are very permeable and allow free diffusion of small solutes between ventricular CSF and brain ISF (Johanson et al., 2008; Johanson et al., 2011). CPECs maintain a net efflux of $Na^+$, $Cl^-$, $HCO_3^-$, and $H_2O$ into the ventricles, while simultaneously mediating a net influx of $K^+$ from the CSF to blood (Brown, Davies, Speake, & Millar, 2004; Damkier et al., 2010; Husted & Reed, 1976; Wright, 1978).

Constantly flowing CSF through the ventricles provides a sink for excess extracellular ions (e.g., $K^+$), neurotransmitters, metabolites, and other waste products to diffuse into for removal by the choroid plexus (Brown et al., 2004). The choroid plexus absorbs these waste products from the CSF and transfers them to the plasma for later processing by the kidney (Johanson et al., 2011). This leads to the choroid plexus being coined "the kidney of the brain" (Spector & Johanson, 1989). Another similarity between the kidney and the choroid plexus is the apical expression of a $Na^+$/ $K^+$/ $2Cl^-$ Cotransporter (NKCC), in the pattern of a $Cl^-$ absorptive epithelium (Alvarez-Leefmans, 2012; Russell, 2000; Spector & Johanson, 1989). In $Cl^-$ absorbing epithelia (Figure 1.1B), such as in the thick ascending limb of Henle's loop and the macula densa of the kidney, NKCC2 is expressed on the apical membrane and $Na^+/K^+$ ATPase (NKATP) remains on the basolateral membrane (Alvarez-Leefmans, 2012). However, the choroid plexus is considered a chloride secreting epithelium, producing CSF with a higher chloride concentration ($[Cl^-]$) than that of the plasma (Alvarez-Leefmans, 2012; Brown et al., 2004; Wright, 1978).

In $Cl^-$ secreting epithelia (Figure 1.1A), such as those found in exocrine glands (e.g., salivary glands or tracheal epithelium) or the ciliary body of the eye, NKATP and NKCC1 are expressed in the basolateral membrane where NKCC1 functions as a $Cl^-$ loader (Alvarez-Leefmans, 2012; Hamann, Herrera-Perez, Zeuthen, & Alvarez-Leefmans, 2010). It should be noted that in both $Cl^-$ secreting and $Cl^-$ absorbing epithelia, NKCC-mediated cotransport occurs in the net influx mode (Figure 1.1A, B). However, in CPECs the direction of net ion fluxes mediated by NKCC1 is uncertain (Figure 1.1C). It has been hypothesized that the cotransporter works near its thermodynamic equilibrium given the low CSF $[K^+]$, approximately 2.9 –3.0 mM, which may favor the cotransporter to fluctuate between inward-directed and outward-directed modes (Keep, Xiang, & Betz, 1994). The uncertainty regarding NKCC1 cotransport direction is the result of its unusual apical location for a $Cl^-$ secreting epithelium, combined with conflicting reports of the $[Na^+]_i$ (Amin, Reza, Wang, & Leenen, 2009; Johanson & Murphy, 1990; Keep et al., 1994; Saito & Wright, 1987; Smith & Johanson, 1985; Zeuthen, 1987). Determining the direction of NKCC1- mediated fluxes is critical to understanding the function of this cotransporter in CPECs. If NKCC1 works in the net efflux mode, it may be involved in CSF secretion. Conversely, if NKCC1 works in the net influx mode, as it does in the basolateral membrane of other chloride secreting epithelia, then it would have an absorptive function in CPECs and could be involved in cell water volume (CWV) maintenance and CSF $K^+$ regulation.

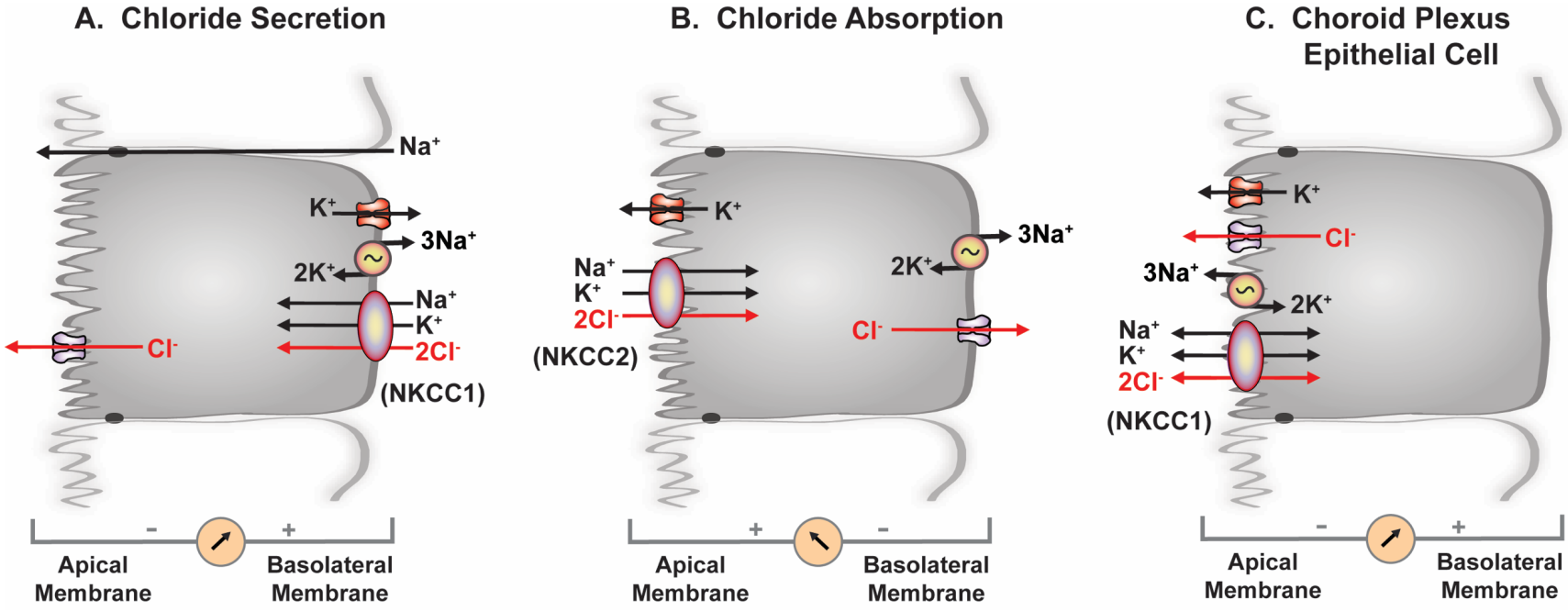


***Figure 1.1: Basic mechanisms for active Cl⁻ secretion and absorption in Cl⁻ transporting epithelia.*** *Cl⁻ secreting epithelia* ***(A)*** *have NKCC1 and NKATP on the basolateral membrane. $K^+$ is recycled on the basolateral membrane through $K^+$ channels, and $Na^+$ is transported out through NKATP activity on the basolateral membrane. NKCC1 maintains $[Cl^-]_i$ above electrochemical equilibrium, and Cl⁻ secretion occurs through apical Cl⁻ channels. Cl⁻ absorbing epithelia* ***(B)*** *have NKCC2 on the apical membrane and NKATP on the basolateral membrane. $K^+$ is recycled on the apical membrane*

*through $K^+$ channels, and $Na^+$ is transported out through NKATP activity on the basolateral membrane. $Cl^-$ efflux occurs through basolateral $Cl^-$ channels. CPECs **(C)** have NKCC1, NKATP, and $Cl^-$ and $K^+$ channels on the apical membrane, which leads to the debate over the function of NKCC1 in these cells.*

### *Importance of CSF potassium regulation*

Maintaining a low CSF [$K^+$] is critical for normal brain function. Under normal conditions the CNS [$K^+$] is approximately 2.9 mM, lower than the plasma [$K^+$] of ~4.7 mM (Damkier et al., 2010; Somjen, 2002). The CSF [$K^+$] remains constant through the combination of glia and CP $K^+$ absorption (Bradbury & Kleeman, 1967; Jones & Keep, 1987; Keep & Xiang, 1995; Keep et al., 1994; Stummer, Keep, & Betz, 1994). Glial cells utilize NKCC1 to absorb $K^+$ from the small extracellular spaces around neurons and transport it away to either the blood vessels or the CSF in the ventricles (Kahle et al., 2009; Lu et al., 2006). Once $K^+$ enters into the CSF filled ventricles (in these experiments, a portion of the CP of the lateral ventricles was isolated using an oil filled chamber. A small amount of artificial CSF, with varying [$K^+$], was added to the isolation chamber and freshly secreted fluid from the CP was collected from under the oil of the chamber.), any excess is removed by CPECs (Ames, Higashi, & Nesbett, 1965; Cserr, 1965; Husted & Reed, 1976). The apical membrane of CPECs is considerably more permeable to $K^+$ than the basolateral membrane (Keep & Xiang, 1995; Zeuthen & Wright, 1981), and CPECs respond to a rise in CSF [$K^+$] by increasing their apical $K^+$ uptake (Parmelee, Bairamian, & Johanson, 1991). Early studies proposed that CPECs regulate the [$K^+$] of freshly secreted CSF in response to the [$K^+$] directly around them (Ames et al., 1965; Husted & Reed, 1976). CPECs are very responsive to high CSF [$K^+$] by reducing the amount [$K^+$] secreted, however lowering CSF [$K^+$] elicits only a slight increase in the [$K^+$] secreted (Ames et al., 1965; Husted & Reed, 1976). Moreover, CPECs maintain the CSF $K^+$ homeostasis

even with severe changes in plasma [$K^+$]: CSF [$K^+$] increases only ~0.2 mM when plasma concentrations of $K^+$ increased up to 9 mM, and CSF [$K^+$] decreases only ~0.5 mM when plasma [$K^+$] is reduced to almost 2 mM (Ames et al., 1965; Bekaert & Demeester, 1954; Cserr, 1965; Husted & Reed, 1976). Both NKATP and NKCC1 can uptake CSF $K^+$ on the apical membrane of CPECs, but NKCC1 is more capable of CSF $K^+$ sensing and regulation because, unlike NKATP, NKCC1 can reverse its direction of transport under physiological conditions (Russell, 2000). The low CSF [$K^+$] is often attributed to the presence of NKATP on the apical membrane of CPECs (Redzic & Segal, 2004). The NKATP subunits expressed in CPECs are $\alpha1\beta1$ and $\alpha1\beta2$ that have a $K_m$ for $K^+$ of 0.92 and 1.16 mM, respectively (Brown et al., 2004; Crambert et al., 2000; Watts, Sanchez-Watts, Emanuel, & Levenson, 1991). This means that while NKATP$\alpha1\beta1/\beta2$ has a high affinity for $[K^+]_o$, the pump is working close to maximal capacity, or $V_{max}$ , for normal external [$K^+$] in CPECs. Additionally, NKATP alone cannot account for the $K^+$-induced cell swelling observed in glia and CPECs since the pump does not transport anions (Macaulay & Zeuthen, 2012; Wu, Delpire, Hebert, & Strange, 1998). In comparison, human NKCC1 has a $K_m$ for external $K^+$ of ~2.7 mM (Payne & Forbush, 1995). NKCC1's lower affinity and higher capacity for $[K^+]_o$ bestows the cotransporter with the ability to sense and respond to changes in CSF $K^+$.

### *NKCC1*

The NKCC1 cotransporter is a member of the larger Slc12a cation-chloride

cotransporter family (Alvarez-Leefmans, 2012). NKCC1 has a predicted 12-transmembrane domain structure, cotransports $Na^+$, $K^+$, and $Cl^-$ ions across the plasma membrane with a stoichiometry of $1Na^+$: $1K^+$: $2Cl^-$ , and is inhibited by the loop-diuretic bumetanide (Alvarez-Leefmans, 2012; Russell, 2000). NKCC1 is a secondary active transporter, meaning that it depends indirectly on the energy generated from ATP by using the sum of chemical potential gradients of $2Cl^-$, $K^+$, and $Na^+$ that is established by NKATP (Alvarez-Leefmans, 2012). The cotransport of two cations ($Na^+$ and $K^+$) and two anions ($2x\ Cl^-$) per cycle is electroneutral and coupled, thus all four ions must first bind to the cotransporter on the uptake side in order for NKCC1 to transport across the membrane (Alvarez-Leefmans, 2012; Lytle, McManus, & Haas, 1998). NKCC1 is ubiquitously expressed in most cell types and cotransports both ions and water (Hamann, Herrera-Perez, Bundgaard, Alvarez-Leefmans, & Zeuthen, 2005; Hamann et al., 2010; Macaulay & Zeuthen, 2012; Zeuthen & Macaulay, 2012).

Activation of the NKCC1 cotransporter occurs through the phosphorylation of serine/threonine residues located on the amino-terminal (Gagnon, England, & Delpire, 2007). The cotransporter is phosphorylated by the WNKs/SPAK/OSR1 pathway: WNKs (with no lysine (K) kinases) are a family of kinases (WNK1-WNK4) activated by phosphorylation in response to osmotic stress, and then WNKs phosphorylate and activate SPAK (SPS1-related proline/alanine-rich kinase) and OSR1 (oxidative stress-response kinase 1), which will phosphorylate and activate NKCC1 (Delpire & Gagnon, 2006; Gagnon, England, & Delpire, 2006; Grimm et al.,

2012; Thastrup et al., 2012). Increased phosphorylation of NKCC1 occurs in response to a drop in $[Cl^-]_i$ and to cell shrinkage, when NKCC1-mediate ion and associated water fluxes are needed to maintain cell volume and $[Cl^-]_i$ (Alvarez-Leefmans, 2012; Delpire & Gagnon, 2006).

### *Significance*

The unusual location of NKCC1, together with NKATP, on the apical membrane of CPECs has led to much debate about the function of the cotransporter in the choroid plexus, including its role in cerebrospinal fluid secretion. Uncertainty of the direction of NKCC1-mediated activity under physiological conditions impedes our understanding of CSF secretion and our ability to develop effective treatment strategies to control conditions such as brain edema and hydrocephalus. Both edema and hydrocephalus can occur subsequent to brain injury (Unterberg, Stover, Kress, & Kiening, 2004), with hydrocephalus being more commonly linked with intracerebral hemorrhages, usually resulting from a blood clot in a weakened artery, that extend into the ventricles (Strahle et al., 2012). In the latter example, CSF drainage is usually obstructed by swelling in the cerebral aqueduct, or at the arachnoid villi or granulations (Strahle et al., 2012). As the pressure of CSF increases, so does the chance of cell death and brain damage (Strahle et al., 2012). Treatments for brain edema and hydrocephalus are often invasive, such as inserting a drainage stent or performing a decompressive craniectomy, and come with a risk of infection. By better understanding the mechanisms of CSF secretion at the choroid plexus, non-invasive medications can be developed for the long-term

control of CSF secretion.

Whether CPECs utilize NKCC1 for CSF secretion is unclear. Blocking NKCC1 activity in the choroid plexus by intraventricular application of bumetanide results in an ~50% reduction in both CSF secretion (Javaheri & Wagner, 1993) and apical $Cl^-$ efflux (Johanson, Sweeney, Parmelee, & Epstein, 1990), as well as an ~50% reduction $Na^+$, $K^+$, and $Cl^-$ uptake (Bairamian, Johanson, Parmelee, & Epstein, 1991; Johnson, Singer, S., Hoop, B., Kazemi, H., 1987; Preston, Dyas, & Johanson, 1993). Bumetanide also causes a reduction in CPEC water volume (Bairamian et al., 1991; Wu et al., 1998). Equal reduction of both $Cl^-$ influx and efflux in the presence of bumetanide suggests that NKCC1-mediated ion and associated water fluxes in CPECs are inwardly directed under basal conditions and function to maintain the cell water volume required for CSF secretion. Additionally, it is hypothesized that NKCC1 is working near to its flux reversal point in CPECs, thus permitting the cotransporter to function in both directions (Keep et al., 1994). The flux reversal point, or chemical equilibrium, of NKCC1 is where the net chemical potential free energy driving NKCC1 cotransport ($\Delta\mu_{NKCC1}$) is equal to zero, given by the following equation 1 for this <u>electroneutral</u> cotransporter:

(equation 1) $$\Delta\mu_{NKCC1} = RT \cdot \ln \frac{([Na^+]_i \cdot [K^+]_i \cdot [Cl^-]_i^2)}{([Na^+]_o \cdot [K^+]_o \cdot [Cl^-]_o^2)},$$

where R is the Gas Constant (8.314 Joules/ Kelvin/ mole) and T is temperature in degrees Kelvin. Reported values for the intracellular $Na^+$ concentration of CPECs has

varied widely over the past few decades, and it is impossible to calculate the flux reversal point for NKCC1 without knowing this concentration. Measurements using ion-selective microelectrodes in amphibian CPECs report a $[Na^+]_i$ =10.5 mM (Saito & Wright, 1987), in contrast to mammalian measurements, using ion tracers and flame photometry, that asserted that CPECs have $[Na^+]_i$ as high as 48 mM (Johanson & Murphy, 1990). It should be noted that the latter measurement technique damages cells, they are whole tissue measurements of total ion content where extra- and intracellular water contents are subject to significant errors, usually yielding erroneously high ion concentrations. Thus, these techniques measure total $Na^+$ (free plus bound) and the thermodynamically relevant parameter is the free $Na^+$ ion (Harootunian, Kao, Eckert, & Tsien, 1989). Most animal cells have a low $[Na^+]_i$ of approximately 10 mM that is maintained by NKATP, and other ion cotransporters, including NKCC1, utilize the chemical potential energy stored in the $Na^+$ gradient across the plasma membrane to cotransport ions and molecules into the cell. An $[Na^+]_i$ as high as that reported by Johanson and Murphey (1990) may significantly alter the driving force of cotransporters on CPECs. Measurements and predictions of high $[Na^+]_i$ have been cited as evidence to support NKCC1 working in the outward direction, however the validity of these measurements is questionable for the reasons given above. Having a clear comprehension of the biophysical characteristics of CPECs, especially ion transport, is fundamental to the knowledge of CSF secretion and homeostasis. This knowledge is key to develop treatment strategies in which the control of CSF production or its regulation is needed, such as with primary or secondary intracranial hypertension, because NKCC1 is a potential

pharmacological target for controlling CSF secretion (Kahle et al., 2009; Karimy et al., 2016; Lu et al., 2006).

# *Chapter 2: General Methods*

## *Animals*

NKCC1 -/- mouse breeders, developed from C57/129 Swiss mouse strains on a mixed background (a generous gift from Dr. Gary Shull, University of Cincinnati), were used to develop our NKCC1 -/- colony. All experiments were performed with NKCC1 -/- mice derived from this colony or their WT littermates. The Wright State University Laboratory Animal Care and Use Committee approved the housing, handling, and use of all mice in accordance with National Institutes of Health guidelines.

In every experiment in which NKCC1 -/- mice were used, the animal's genotype and phenotype were tested to ensure that it was a homozygous knockout. NKCC1 -/- mice have slowed growth and are smaller than their +/- and +/+ littermates, they are deaf, and they display shaker/ waltzer behavior that manifests as the mouse shaking and spinning in circles (Delpire, Lu, England, Dull, & Thorne, 1999; Flagella et al., 1999). An NKCC1 -/- mouse had to display these three phenotypes to be used for experiments. The imbalance seen in NKCC1 -/- mice is the result of a collapsed cochlear duct containing a $K^+$-rich endolymph generated by NKCC1 (Delpire et al.,

1999; Flagella et al., 1999). NKCC1 -/- mice also have reduced blood pressure, severely impaired saliva production, and a 28% incident of death by weaning at postnatal age (P) 21 days (Evans et al., 2000; Flagella et al., 1999). Due to the latter phenotypes, all NKCC1 -/- mice were euthanized at P21, if they were not used for an experiment.

### *Genotyping*

The procedure used to genotype NKCC1 -/- mice was performed using 1 –3 mm of tissue obtained from mouse-tail clips performed during postnatal days 3 –6. Tail clips were processed and the DNA extracted using Qiagen DNeasy Blood and Tissue Kit for Spin-columns. Polymerase chain reaction (PCR) amplification was performed in 21 μL and containing: 13.4 μL ultra-pure water, 0.4 μL Taq DNA Polymerase (GenScript), 4 μL 10x Taq Buffer (Invitrogen), 1 μL dNTP (10 μM, USB/Affimetrix), 1.2 μL mouse NKCC1 (mNKCC1) custom primers (see Table 2.1, Integrated DNA Technologies), and 0.5 μL mouse DNA. The PCR reaction was performed using a thermocycler (BioRad) under the following protocol: 4 min 95° C; 34 cycles (30 sec 95° C, 30 sec 60° C, 50 sec 72° C); 10 min 72° C; hold at 0° C. PCR products weights were separated using a gel electrophoresis bath in a 2% agarose gel.

***Table 2.1: mNKCC1 custom PCR Primers***

| Primer | Sequence |
|---|---|
| mNKCC1 5' | G G A A C A T T C C A T A C T T A T G A T A G A T G |
| mNKCC1 3' | C T C A C C T T T G C T T C C C A C T C C A T T C C |
| mNKCC1 neo | G A C A A T A G C A G G C A T G C T G G |

*Lists the custom mNKCC1 primers used for genotyping NKCC1 -/- mice.*

## *Isolation of single CPECs*

Mice, P10-P21, were anesthetized using $CO_2$ then euthanized by rapid decapitation. As detailed in Figure 2.1, the brain was removed and immediately submersed into room temperature Dulbecco's Phosphate Buffered Saline (DPBS, Life Technologies, no $Ca^{2+}$ & no $Mg^{2+}$), pH 7.1, and the CP of the fourth ventricle was visualized and dissected-out under a 20X microscope. The dissected CP was incubated for 1 hour in 1 mL of dissociation media that was composed of culture media supplemented with protease XIV (0.5 mg/ mL, Sigma Aldrich) and collagenase IV (0.5 mg/ mL, Sigma Aldrich). Culture media was prepared the day of the experiment, and the following ingredients were brought to room temperature, combined into, and pass through a 10 mL lauer-lock syringe attached to a sterile filter (33 mm Millex -GP Express PES 0.22 μm, Merck Millipore) before use: DMEM/ F12 (HyClone-Fisher), 10% heat-inactivated FBS (Gibco-Fisher), penicillin/

streptavidin (HyClone-Fisher, 10 U/ mL: 10 μg/ mL), and hEGF (40 ng/ mL). Following the incubation, the dissociation media was aspirated off and the CP was rinsed 3X with culture media before the final volume of 500 μL of culture media was added. To dissociate the cells, the CP in culture media was vigorously shaken with a vortex shaker for 3 seconds, after which the cells were gently triturated with fire-polished glass Pasteur pipettes of two different bore diameters that were equivalent to 23 and 32 gauge needles (used in that order), 20X per bore size. Cells were plated on laminin (Sigma Aldrich, No. L-2020, 5 μg /ml) and poly-D-lysine (BD Bioscience, No. 354210, 100 μg /ml) coated 25-mm sterile and de-greased cover slips (Electron Microscopy Sciences, No. 72196-25). Degreased cover slips were soaked for 24-72 hours in acetone (Fisher) then rinsed 3x first in 70% ethanol (Fisher, diluted with double distilled water ($ddH_2O$)) followed by a 3x rinse in ddH2O prior to being sterilized to remove any manufacturing residues. Plated cells were incubated at 5% $CO_2$ –95% air atmosphere /85 –95% humidity /37° C for 2 –6 hours prior to use for experimentation.

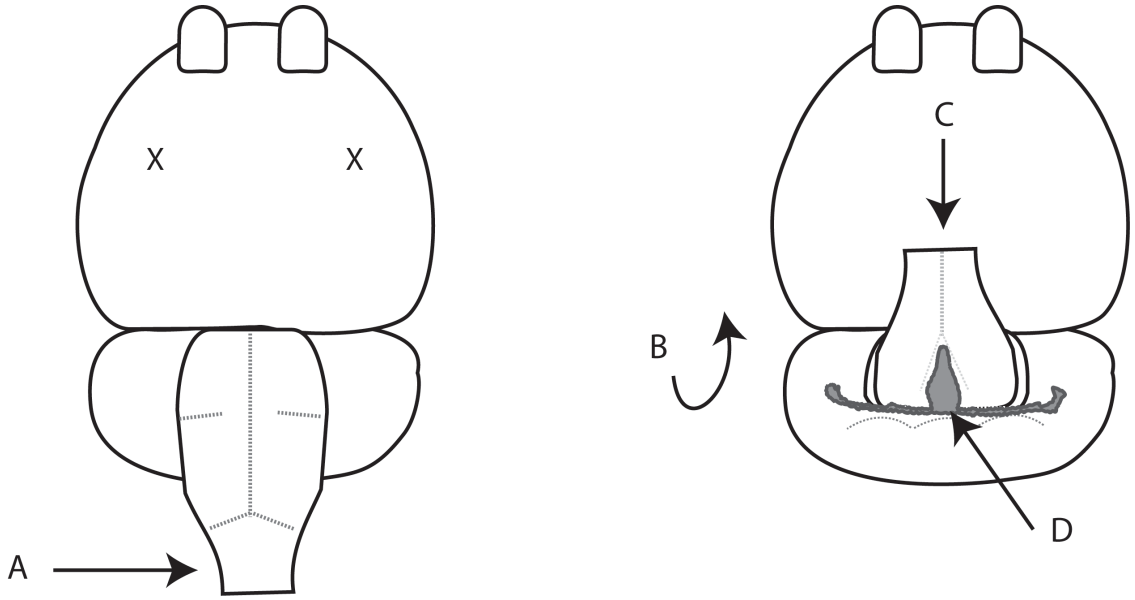


***Figure 2.1: Dissection of the CP of the 4th ventricle in mouse.*** *The dissected mouse brain was immediately submerged into a silicone lined dissection plate that contained sterile room temperature DPBS. Two 23 gauge needles were used to secure the brain ventral-side-up in the silicone at the points marked with* ***X****. The tissue was illuminated and visualized under a 20X dissection microscope. A pair of #4 micro-forceps was used to gently pick-up the brain stem (at point* ***A****) and fold it upwards so that the ventral surface of the brain was in contact with the ventral surface of the brain stem* ***(B)****. The CP* ***(D)*** *was located by following the dorsal mid-line* ***(C)*** *in the posterior direction towards the cerebellum. The CP of the 4th ventricle is Y-shaped, and, with a second pair of #4 forceps, each "arm" of the CP was first freed from the connective tissue and vasculature before the entire CP was dissected-out in one piece.*

## *Saline Solutions*

### *HEPES-buffered solutions*

The isosmotic (ISO) physiological control solution, herein referred to as artificial CSF (aCSF), contained 123.5 mM NaCl, 3 mM KCl, 1 mM $CaCl_2$, 1.25 mM $MgCl_2$, 5 mM HEPES, and 10 mM glucose. The pH adjusted to 7.3 at 25° C with 1 M NaOH, and the osmolality adjusted to 290 ± 1% mOsm with sucrose. Isosmotic nominally chloride free (0Cl) and isosmotic nominally sodium free (0Na) solutions were made by mole-for-mole replacement of $Cl^-$ with gluconate and $Na^+$ with NMDG (N-methyl-D-glucamine) + HCl, respectively. Solutions with various $[K^+]_o$ were made by adding the corresponding volume of 3 M KCl prior to adjusting the osmolality with sucrose. Osmotic calibration solutions were created by adjusting the amount of sucrose in the ISO to 261 ± 1% mOsm for the 10% hyposmotic solution and 319 ± 1% mOsm for the 10% hyperosmotic solution. The osmolality of all solutions was measured with a Wescor osmometer.

### *Bicarbonate-buffered solutions*

Bicarbonate buffered aCSF solutions contained 105.2 mM NaCl, 2 mM $NaH_2PO_4$, 1 mM $CaCl_2$, 1.25 mM $MgCl_2$, 3 mM KCl, 10.5 mM Glucose, and 24.8 mM $NaHCO_3$. The pH adjusted to 7.3 by slowly adding the $NaHCO_3$ after the solution has been bubbled for 20 min with 5% $CO_2$ balanced with air, and the osmolality adjusted to 290 ± 1% mOsm with sucrose. Osmotic calibration solutions and isosmotic

solutions with variations in $[K^+]_o$ were made in the same manner as with the HEPES buffered solutions.

### *Drug and Chemical Preparation*

Stock solutions of chemicals were prepared using dimethyl sulfoxide (DMSO) or water as the initial solvent, and then diluted using aCSF. When DMSO was used as the solvent, care was taken to ensure that the final amount of total DMSO in the solution was less than 1%. This preparation was used for Bumetanide, Ouabain, Verapamil, Calcein-AM, Asante Natrium Green-2 (ANG-2), and N-(Ethoxycarbonylmethyl)-6-Methoxyquinolinium Bromide (MQAE).

## *Fluorescence imaging microscopy*

Cover slips with attached CPECs were mounted into a fluid perfusion imaging chamber (~300 μL volume) that rested on the stage of an epifluorescence inverted microscope (Olympus IX-81, Olympus America, Center Valley, PA) equipped with an oil-immersion lens (Olympus, 40X, NA 1.35) and differential interference contrast (DIC) optics (Figure 2.2). Physiological solutions were perfused over the cells at a rate of 6 mL/ min at 25° C, and changes in fluorescence intensity of individual cells were measured through a digital pinhole (15 x 15 pixels for calcein and MQAE, and 20 x 20 pixels for ANG-2) using MetaSeries Software (Alvarez-Leefmans, Herrera-Perez, Marquez, & Blanco, 2006). Light originating from a xenon arc lamp was

directed through the input slit of a monochromator (Optoscan, Cairn Research Limited, UK) that allowed independent control of both the wavelength of light and the output slit width of the beam of light emitted. The light beam then passed through a liquid guide and neutral density filter to reduce photodynamic damage and photo-bleaching prior to entering the optical path of the microscope. To use Calcein as an example, the excitation wavelength for calcein is 495 ± 3 nm and the peak emission occurs at 535 nm, thus a 515 nm dichroic mirror/ 535 emissions filter cube (Chroma Technology) was used to reflect excitation wavelengths below 515 nm into the inverted objective where it excited the fluorophores within the cells. Any wavelengths above 515 nm, calcein emissions, were able to pass back down through the dichroic mirror and reached the 535 nm emissions filter below. The emission filter prevented stray light, outside the emission filter wavelength of 535 ± 13 nm, from reaching the cooled CCD camera (Hamamatsu ORCA-ER C4742-95). To further reduce photodynamic damage to CPECs, the shutter speed was kept between 40 –80 ms and fluorescence acquisition frequency was 0.1 –0.25 Hz.

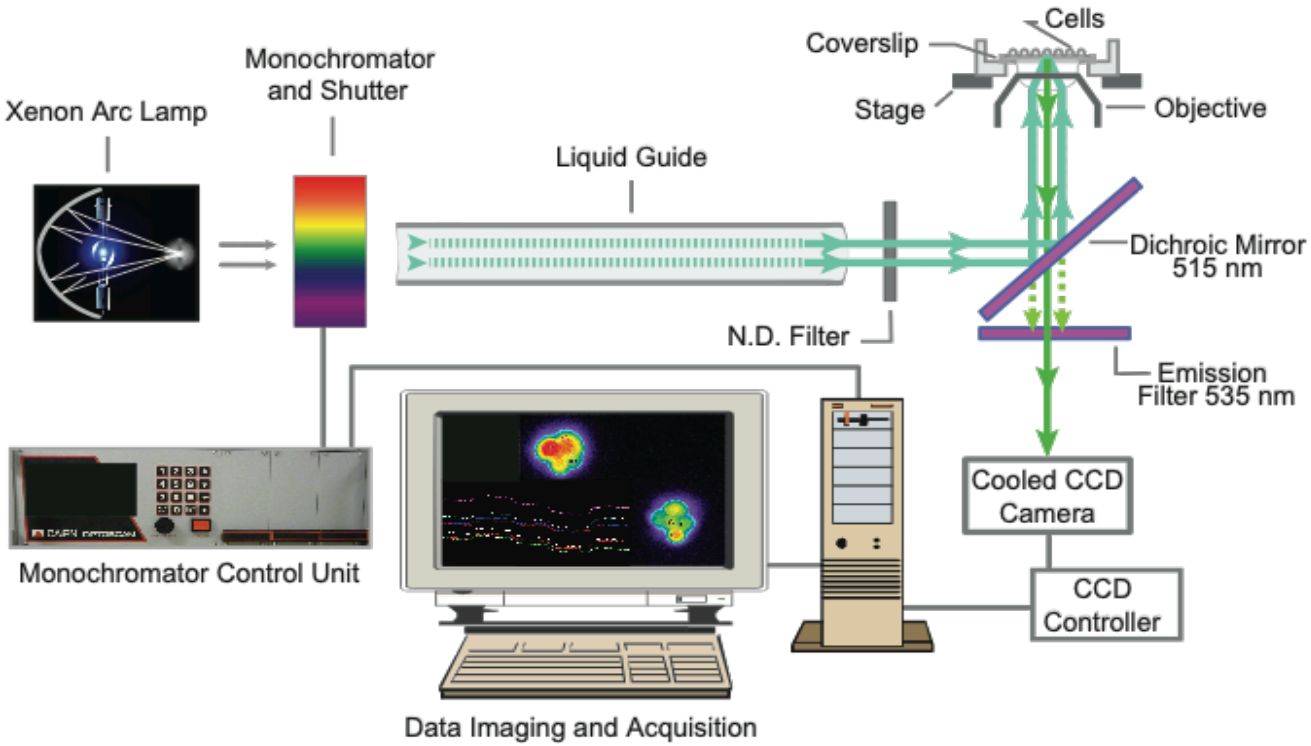


***Figure 2.2: Microscope set-up for quantitative fluorescence imaging microscopy.*** *Imaging setup used to record CWV changes and/or intracellular $Na^+$ and $Cl^-$ in single CPECs loaded with calcein or ion-indicator. The filter's wavelengths are shown for Calcein. This figure is modified from Alvarez-Leefmans, F. J., Herrera-Perez, J. J., Marquez, M. S., & Blanco, V. M. (2006). Simultaneous measurement of water volume and pH in single cells using BCECF and fluorescence imaging microscopy. Biophysical Journal, 90(2), 608-618, and is reproduced with permission.*

A

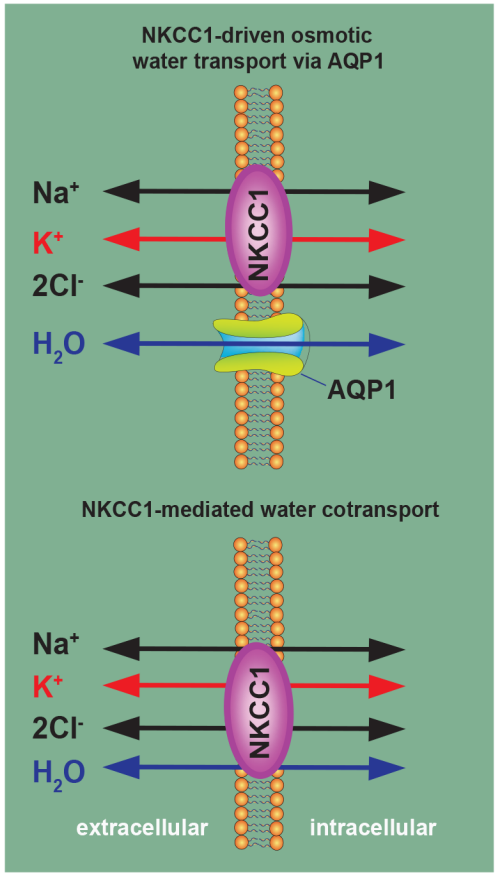


B

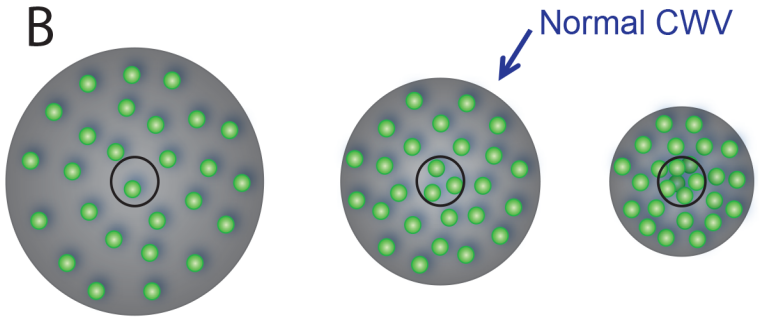


$$CWV = \frac{Qm}{Cm}$$

CWV = relative cell water volume

Qm = total intracellular content of the probe (m),(Qm must be constant).

Cm = relative change in concentration of m. (By measuring changes in Cm, i.e., calcein fluoresence, it is possible to determine CWV.)

***Figure 2.3: Basic principles and methods for measuring changes in CWV.*** *NKCC1-mediated ion transport is tightly linked to water transport (Hamann et al., 2010), thus the direction and relative magnitude of NKCC1-mediated fluxes can be inferred by measuring changes in relative CWV in single CPECs.* ***A)*** *from Alvarez-Leefmans, F.J. (unpublished), reproduced with permission. Two models explaining how NKCC1-mediated ion transport is tightly linked to water transport.* ***B)*** *This figure is modified from Alvarez-Leefmans et al., (2006). Simultaneous measurement of water volume and pH in single cells using BCECF and fluorescence imaging microscopy. Biophysical Journal, 90(2), 608 -618. Basic principle for measuring relative CWV through a pinhole in CPECs using live-cell imaging fluorescence microscopy in dissociated CPECs loaded with the fluorescent probe calcein (Alvarez-Leefmans et al., 2006), and reproduced with permission.*

### *Measurement of cross-sectional area of in vitro CPECs*

Using the microscope set-up described above, freshly dissociated CPECs from WT and NKCC1 KO mice were visualized and imaged using differential interference contrast (DIC) microscopy. The perimeter of each living cell imaged with DIC was digitally outlined offline using a mouse, and cross-sectional areas of individual cells calculated using MATLAB (Math Works), using algorithms developed by Mr. Aaron Madaris. Cells were loaded with Calcein-AM, which was used for subsequent parts of the experiments to measure CWV changes, but also indicated cell viability. Only cells that were loaded with Calcein were measured using DIC imaging. Each cell within the field was identified with a color-coded pinhole and a number.

### *Method to measure cell water volume changes in single CPECs*

NKCC1-mediated ion fluxes are tightly linked to water fluxes that occur either through the cotransporter or through aquaporins (Figure 2.3A) (Alvarez-Leefmans, 2012; Hamann et al., 2005; Hamann et al., 2010; Macaulay & Zeuthen, 2012). Therefore, changes in cell volume can be measured as a surrogate for NKCC1-mediated fluxes (Alvarez-Leefmans et al., 2006; Hamann et al., 2010). Changes in the fluorescence intensity of intracellular free Calcein are inversely proportional to changes in cell water volume (Figure 2.3B), according to the following equation 2 from Alvarez-Leefmans et al., (2006):

(equation 2) $$CWV = \frac{Q_m}{C_m},$$

where CWV is relative cell water volume, $Q_m$ is total intracellular content of the dye (m), and $C_m$ is the relative change in concentration of m. CWV can be determined by measuring changes in Calcein fluorescence ($C_m$) as long as $Q_m$ is constant (Alvarez-Leefmans et al., 2006). Calcein was loaded by exposing the cells to a solution containing of 2 μM of Calcein-AM (Invitrogen) along with 20 μM Verapamil (Invitrogen). Verapamil was added to inhibit the multi-drug resistant P-glycoprotein that is expressed in CPECs and can remove fluorescent dyes from the cell (Rao et al., 1999 Snyder, Finch, Sartorelli, Piwnica-Worms, 1999; Robertson, 1995; Valverde et al., 1996). Calcein was excited at 495 ± 3 nm for 80 ms at a frequency of 0.25 Hz and the emission recorded above 515 nm. Volume calibration was performed for each cell with ± 10% anisosmotic solutions.

Data analysis was performed using SigmaPlot versions 9 & 12, and Microsoft Excel. When required, drift correction of the Calcein transient was performed using a linear regression. Calcein fluorescence was converted to CWV using the following equation 3 (Alvarez-Leefmans, 1995):

(equation 3) $$\frac{V_t}{V_o} = \frac{(\frac{F_t}{F_o} - F_{Background})}{(1 - F_{Background})},$$

where $V_t$ is cell water volume with respect to time of the entire transient, $V_o$ is $V_t$ at t

= 0, $F_t$ is the measured fluorescence intensity with respect to time, $F_o$ is the steady-state fluorescence intensity at baseline (during ISO), and $F_{Background}$ is the background fluorescence of the cell that is insensitive to changes in CWV.

### *Measurement of intracellular chloride in single CPECs*

The $[Cl^-]_i$ of CPECs was measured using the fluorescent indicator MQAE (N-(Ethoxycarbonylmethyl)-6-Methoxyquinolinium Bromide, Invitrogen). MQAE is a single wavelength indicator that detects $Cl^-$ through collisional quenching (Verkman, Sellers, Chao, Leung, & Ketcham, 1989). The method for measuring $[Cl^-]_i$ in CPECs follows the procedure used in other cell types (Mao et al., 2012; Rocha-Gonzalez, Mao, & Alvarez-Leefmans, 2008). MQAE was applied to the chamber containing CPECs at a concentration of 5 mM and with 20 μM Verapamil. The dye was excited at 350 ± 5 nm for 20 ms at a frequency of 0.1 Hz; the peak emission wavelength was 460 nm captured every 10 seconds. CPECs were equilibrated in isosmotic aCSF prior to $Cl^-$ depletion by exposing the cells to an isosmotic 0Cl solution. Once a new steady state was reached in the 0Cl solution, the CPECs were considered fully depleted of intracellular $Cl^-$, and external $Cl^-$ was replaced with isosmotic aCSF. At the end of the experiment MQAE was calibrated against $[Cl^-]_i$ using the double ionophore technique (Koncz & Daugirdas, 1994; Krapf, Berry, & Verkman, 1988; Mao et al., 2012; Rocha-Gonzalez et al., 2008). CPECs were permeabilized with the $K^+/H^+$ ionophore Nigericin (5 μM, Sigma Aldrich) and the $Cl^-/ OH^-$ ionophore Tributyltin Acetate (10 μM, Sigma Aldrich). Calibration solutions contained 10 mM Glucose, 5 mM HEPES, 120 mM $K^+$, and $[Cl^-] + [NO_3^-] = 120$ mM. The calibration

steps were 0, 20, 40, and 60 mM $Cl^-$ and then MQAE was quenched with a final solution of 150 mM KSCN to set the background.

MQAE signal drift correction was performed offline by fitting the entire data transient to a straight line (Mao et al., 2012; Rocha-Gonzalez et al., 2008). The correlation coefficient of the fit was ≥ 0.99 for the cell to be included in the analysis. MQAE fluorescence data was then converted to $[Cl^-]$ using the Stern-Volmer equation:

(equation 4) $$[Cl^-]_i = \frac{((\frac{F_o}{F_t})-1)}{K_{sv}}$$

where $F_o$ = the steady-state fluorescence during chloride depletion using the 0Cl solution, $F_t$ = fluorescence measurements with respect to time, and $K_{sv}$ = Stern-Volmer Constant. $K_{sv}$ was obtained by plotting the mean fluorescence measurements of the calibration steps to the Stern-Volmer Graph $(F_o/F_t) - 1$ vs. $[Cl^-]$ and taking the slope as $K_{sv}$. The mean $K_{sv}$ for the intracellular calibration of MQAE in WT CPECs was within the normal range at 17.0 ± 0.6 $M^{-1}$ (mean ± SEM, n = 5 animals) and the mean $K_{SV}$ of KO CPECs was 10.4 ± 1.2 $M^{-1}$ (n = 7 animals). In other cell types the reported values for intracellular $K_{sv}$ is 5 –25 $M^{-1}$ (Kaneko, Putzier, Frings, Kaupp, & Gensch, 2004; Mao et al., 2012). Further, the MQAE analysis followed three constraints described in Mao et al., 2012. Briefly, for a cell to be included in the analysis 1) the correlation coefficient for the line fitting the

calibration plot ≥ 0.99, 2) MQAE fluorescence in each calibration solution reached steady state, and 3) MQAE fluorescence in the both the isosmotic aCSF and 0Cl solutions reached steady state (Mao et al., 2012). The $Cl^-$ equilibrium potential ($E_{Cl}$) was calculated from the Nernst equation:

(equation 5) $$E_{Cl} = \frac{RT}{zF} \ln \frac{[Cl^-]_i}{[Cl^-]_o}$$

where z (= -1) is the valence of $Cl^-$, R is the gas constant, T is temperature, and F is the Faraday constant.

### *Measurement of intracellular sodium in single CPECs*

Measurements of $[Na^+]_i$ were done with the fluorescent sodium indicator dye Asante Natrium Green 2 (ANG-2) (TEFLabs, 2012). CPEC $[Na^+]_i$ measurements were first attempted with SBFI, but the cells could not be successfully loaded with the indicator. ANG-2 has a similar $Na^+$ binding affinity as SBFI, and was developed as an alternative $Na^+$ indicator (Lamy & Chatton, 2011; Roder & Hille, 2014). Unlike SBFI, ANG-2 is a single wavelength dye with excitation and emission wavelengths at 488 –517 nm (peak excitation at 517 nm) and 540 nm, respectively (Lamy & Chatton, 2011; TEFLabs, 2012). The benefit of ANG-2 is that it is easier to load into cells and the excitation wavelength is less damaging compared to the near ultraviolet excitation wavelengths of SBFI. ANG-2 was applied to the cover slip at concentration 5 μM, along with an equal volume of the nonionic detergent Pluronic

F-127 (20% weight/ volume) and verapamil (20 μM). During the data acquisition the excitation wavelength was set at 500 ± 10 nm for 80 ms at a frequency of 0.1 Hz. The fluorescence intensity of each cell was sampled every 10 seconds until a steady-state was achieved, and then calibration of the dye was done at the end of each experiment to determine $[Na^+]_i$. At the start of calibration cells were treated with a nonselective monovalent cation ionophore, Gramicidin D (7 μM, Sigma Aldrich), to collapse the $Na^+$ and $K^+$ gradients across the cell membrane (Robertson, 1995). Calibration solutions contained 10 mM HEPES, 1.2 mM $Ca^{2+}$, 57.4 mM $Cl^-$, 65 mM gluconic acid, with $[Na^+] + [K^+] = 120$ mM, pH= 7.3, and 290 mOsm, adjusted with sucrose. The calibration points were 120, 90, 60, 30, 12, and 6 mM $Na^+$.

To analyze the fluorescence measurements, the data transient was first normalized to the 0Na calibration steady-state measurements using the equation 6:

(equation 6) $$1-F_o/F_t,$$

where $F_o$ = mean fluorescence measurements during the 0Na calibration at steady-state, $F_t$ = the fluorescence measurements with respect to time of the entire transient, and it was subtracted from 1 so that the data was not inverted. The mean measurement for each $Na^+$ Calibration solution was then used to plot the graph $1-F_o/F_t$ vs. $[Na^+]$ (mM). From this graph, a regression curve was fitted using the Michaelis-Menton equation,

(equation 7) $$y = \frac{(F_{max} \cdot [Na^+])}{(K_d + [Na^+])}$$

and a report was created giving the $F_{max}$ and $K_d$ values for each individual cell. The normalized data ($1-F_o/F_t$) was then converted into $[Na^+]$ using the following equation 8 that was based on the $Ca^{2+}$ indicator FURA-2 and modified here for ANG-2 (Grynkiewicz, Poenie, & Tsien, 1985):

(equation 8) $$[Na^+] = K_d \cdot \frac{(F - F_{min})}{(F_{max} - F)}$$

Where F = the normalized data $1-F_o/F_t$, $F_{min} = 0$, $F_{max}$ and $K_d$ were taken from the report.

### *Method for immunofluorescence labeling of NKATPα1 and aquaporin 1 (AQP1)*

Brain and kidney tissues of WT and NKCC1 KO mice, P17-19, were used to verify the polarized expression of NKATP and AQP1 in the CPECs NKCC1 KO mice. After animal fixation, tissue was post-fixed using 4% Paraformaldehyde for 1 -2 hours prior to cryoprotecting in 15% sucrose. Cryostat sectioning of tissue (10 μm) was mounted directly onto slides to protect the CP.

AQP1: Sections were permeabilized using 0.1% Triton-X and blocked for 30 minutes with 10% goat serum before overnight incubation in a humidity chamber at

4° C using rabbit polyclonal antibody against rat AQP1 (5 µg/ mL, Alpha Diagnostics). The sections were washed 3x 5 min in 0.01 M PBS both before and after a 1.5-hour incubation with goat anti-rabbit Alexa 594 (1:200, Jackson ImmunoResearch). The coverslip was mounted using ProLong Gold Anti-fade reagent with DAPI (Invitrogen).

NKATPα1: Tissue was stained using Vector Mouse on Mouse (M.O.M.) Antibody Kit. Briefly, sections were permeabilized in ice-cold acetone at -20° C for 5-10 minutes and were allowed to air dry. Sections were washed 2x 2 minute in 0.01M PBS prior to the application of each solution. To start, there was a 1-hour incubation in M.O.M. Mouse Ig Blocking Reagent solution. The sections were then incubated for 30 minutes in M.O.M. Diluent solution that contained the mouse monoclonal NKATP-α1 subunit antibody (4 µg/ml, Millipore), followed by a 10-minute incubation in M.O.M. Biotinylated Anti-Mouse IgG Reagent solution, and a 5-min incubation in Fluorescein Avidin DCS solution. Sections received a final 3x 3 minute PBS wash before they were mounted on coverslips with either ProLong Gold w/ DAPI or VectaShield Anti-Fade Reagent.

### *Statistics*

Data is presented as the mean ± standard error of the mean (SEM), n = number of animals. Individual animal means were calculated by taking the mean of the cells obtained from that animal, then those means were averaged and the SEM calculated using Microsoft Excel. Comparison of ion concentrations between CPECs

from WT and NKCC1 KO was performed using an unpaired Student's t-test for independent samples in Sigma Plot version 9.

## *Chapter 3: Specific Aims*

The overall objective this research is to understand how CPECs secrete CSF and regulate its ionic composition in order to find safe and more effective treatment strategies to control CSF secretion, **The Central Thesis:** NKCC1 functions as a sensor and regulator of CSF [$K^+$] in the apical membrane of CPECs by working near to its flux reversal point and in the inward direction under basal physiological conditions. The $K_m$ for external $K^+$ and the thermodynamic features of NKCC1 enables it to reverse net flux direction in response to small (± 2 mM) changes in external [$K^+$]. To prove this thesis the two following aims have been developed:

**1) Determine the direction NKCC1-mediated ion and associated water net fluxes in CPECs under basal conditions.** ***Hypothesis:*** A function of NKCC1 in CPECs is maintenance of both normal and constant cell water volume. Under basal physiological conditions NKCC1 is constitutively active, inwardly transporting ions and associated water. Epithelial cell volume maintenance requires equal rates of solute and water entry and exit across the apical and basolateral membranes, respectively (Ruess, 1988). Hence, we predict that NKCC1 inactivation results in CPEC shrinkage due to unbalanced solute and water fluxes.

The direction of NKCC1 activity can be inferred by measuring cell water volume in the presence and absence of NKCC1 transport activity. NKCC1 activity is inhibited in this research using a three-pronged approach that includes pharmacological inhibition of the cotransporter, genetic ablation of the NKCC1 protein, and ion-substitution experiments. Pharmacological inhibition of NKCC1 is performed using the loop-diuretic bumetanide and genetic ablation via the global NKCC1 knockout (KO) mouse. Using these approaches controls for any unknown variables, such as a compensatory mechanism, that may be present with the NKCC1 global KO mouse model (Eisener-Dorman, Lawrence, & Bolivar, 2009; Nelson, 1997). Additionally, the extracellular ion dependence of changes in CWV is examined to determine whether the apical location of NKCC1 impacts the function of this cotransporter as a $Cl^-$ loader, given that the CP is considered a $Cl^-$ secretory epithelium.

**2) Test the hypothesis that NKCC1 functions as a sensor and regulator of CSF $[K^+]$ in CPECs.** ***Hypothesis:*** NKCC1 is working near to its chemical equilibrium in CPECs, therefore small changes in $[K^+]_o$ are sufficient to alter both the direction and magnitude of NKCC1-mediated ion and associated water fluxes.

Experiments will test the sensitivity of NKCC1 to small changes in $[K^+]_o$ in CPECs by comparing the responses of cells from NKCC1 KOs to those from WT mice. The flux reversal point of NKCC1 in CPECs is calculated by modeling the net free energy driving NKCC1 cotransport with respect to $[K^+]_o$. Our model predicts that

apical NKCC1 is working in the net inward mode under basal conditions, and near to chemical equilibrium, i.e., its flux reversal point. Consequently, CPECs can utilize NKCC1 to sense and control the $K^+$ uptake and/or secretion in response to the $[K^+]_{CSF}$.

## *Chapter 4: Specific Aim 1 Results*

Testing the hypothesis of Specific Aim 1 requires that the following questions be answered:

1) What is the direction of NKCC1-mediated fluxes in CPECs under physiological conditions?
2) Is NKCC1 constitutively active and functioning to maintain normal and constant cell water volume in CPECs?

Knowing the direction of NKCC1-mediated fluxes under basal physiological conditions is critical to understanding how this cotransporter functions on the apical membrane of CPECs, and whether NKCC1 contributes to CSF secretion directly vs indirectly. If NKCC1 is constitutively active and functions in the maintenance of CPEC water volume, then NKCC1-mediated fluxes contribute indirectly to CSF secretion, as opposed to a direct contribution to CSF secretion via ion efflux. Given that NKCC1 is phosphorylated and activated in response to cell shrinkage or a decrease in $[Cl^-]_i$, we predict that in CPECs the NKCC1-mediated fluxes are inwardly directed under basal physiological conditions, and indirectly contribute to CSF secretion by maintaining both normal and constant cell water

volume needed for sustained activation of volume-sensitive transporters and channels.

### *Morphometric comparison of the cross-sectional areas of CPECs from NKCC1 KO and WT mice*

Cell water volume is maintained by balancing the net influx and the net efflux of solute and water across the plasma membrane. Removing NKCC1-mediated ion fluxes will unbalance the net trans-epithelial solute and water fluxes and reveal the direction of cotransport (Figure 4.1), because epithelial cell volume maintenance requires equal rates of solute and water influx and efflux across the apical and basolateral membranes (Ruess, 1988). CPECs are reported to shrink when NKCC1 is blocked with bumetanide, suggesting that the cotransporter is constitutively active and inwardly directed in these cells (Bairamian et al., 1991; Wu et al., 1998). Bairamian et al., (1991) found that 10 μM bumetanide reduced CP water weight by 20 mg H2O/ g tissue, and Wu et al., (1998) observed a ~9% reduction in the CSA of dissociated rodent CPECs after exposure to both 10 and 100 μM bumetanide, although they only showed data for the highest bumetanide concentration. Later studies challenged these findings and interpretations based on the observations that bumetanide at concentrations of 100 μM caused a reduction in CPEC volume, but not at concentrations of 10 μM (Brown, Davies, and Millar, 2009; Hughes, Pakhomova, & Brown, 2010). Both groups of researchers used DIC microscopy that yields total cell volume and have relatively low-resolution due to edge/ hallow

effect, needing a large number of cells to increase the signal to noise ratio to reach reliable conclusions. We addressed this controversy by measuring changes in CWV of CPECs from NKCC1+/+ exposed to 10 μM bumetanide, and ruled out unspecific effects of this compound by using CPECs from NKCC1-/-. Changes in CWV were assessed by intracellular Calcein dilution, a live-cell imaging microscopy method that can resolve changes in CWV of ~1% with time resolution of 0.25 Hz, and allows osmotic calibration of each cell (Crowe, Altamirano, Huerto, & Alvarez-Leefmans, 1995; Alvarez-Leefmans, 1995; Rocha-Gonzalez et al., 2008). We also used DIC live-cell imaging microcopy to measure CSAs of isolated CPECs. The rational is that if NKCC1 is constitutively active (i.e., it is always on), and works in the net ion and water influx mode under basal conditions, then CPECs from NKCC1 KO mice should also be shrunken compared with those from WT mice. Thus, shrinkage occurs because the net influx of solute and water will be reduced compared to the net efflux of solute and water.

A morphometric comparison of the CSA of individual dissociated CPECs revealed that CPECs from NKCC1 -/- mice were smaller than those from WT mice. The mean CSA measurements from both groups were normally distributed. Measurements of the cross-sectional area of CPECs (Figure 4.2) revealed that CPECs from WT mice had a mean cross-sectional area of 155 ± 4.1 $\mu m^2$ (n = 44 animals), whereas those from NKCC1 KO mice had a mean cross-sectional area of 137 ± 4.8 $\mu m^2$, p = 0.0106 (n = 22 animals). Therefore, CPECs from NKCC1 KO animals were ~18 $\mu m^2$ smaller than those from WT. DIC images of dissociated CPECs from sibling WT and NKCC1 KO showed some additional subtle morphological differences

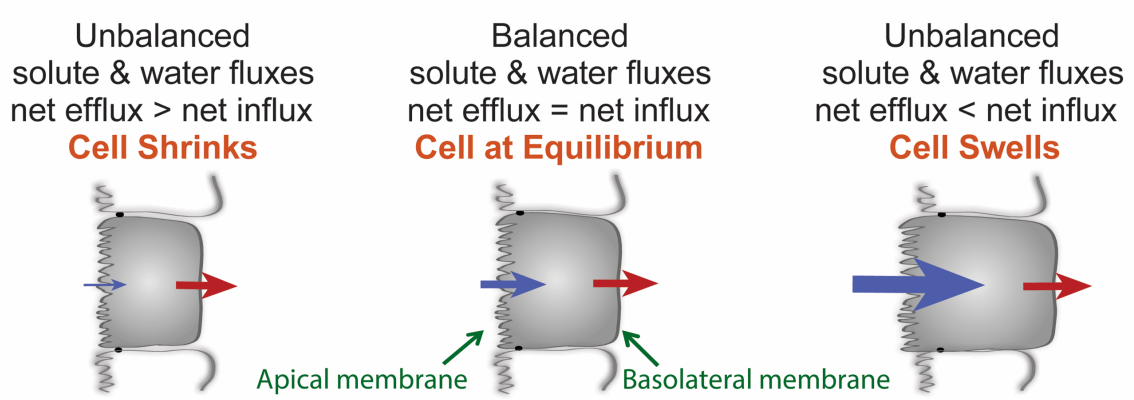


***Figure 4.1: Balance of net solute and water fluxes determines choroidal epithelial cell volume.*** *A function of NKCC1 in CPECs is maintenance of both normal and constant CWV. Under normal physiological conditions NKCC1 is constitutively active, inwardly transporting ions and associated water. Hence, we predict that NKCC1 inactivation results in CPEC shrinkage due to unbalanced solute and water effluxes.*

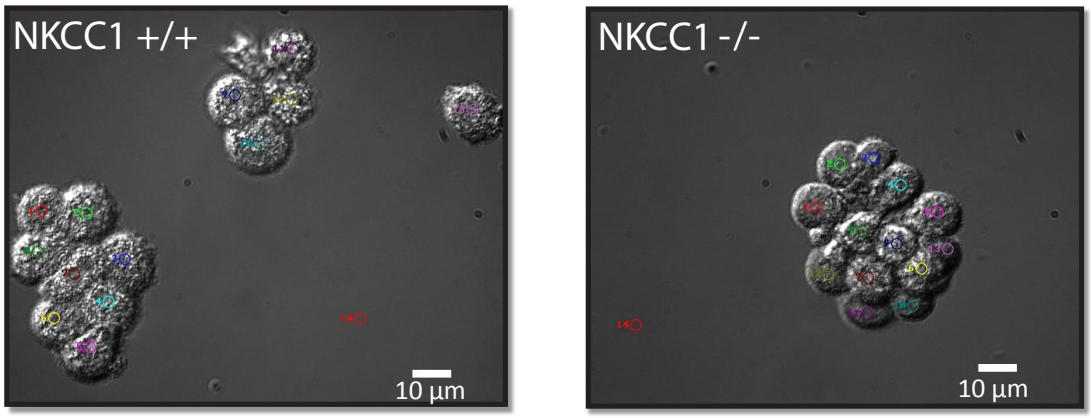


***Figure 4.2: CPECs from NKCC1 -/- mice are significantly smaller than CPECs from WT mice.*** ***Top)*** *In vitro CPECs from WT (left) and NKCC1 KO (right) sibling animals. CPECs from NKCC1 KO mice were visually smaller than those from WT*

*mice.* ***Bottom)*** *CPECs from WT mice had a mean cross-sectional area of 155 ± 4.1 μm$^2$ (dotted line in box plot), n = 44 animals. CPECs from NKCC1 KO mice were -11.5% smaller than those of the WT and had a mean cross-sectional area of 137 ± 4.8 μm$^2$, p = 0.0106, n = 22 animals. Boxplot illustrates the spread of CSA measurements with median CSA denoted as a black line, the box represents the 1st and 3rd quartiles, stems represent quartiles 0 and 4, and the dots are those values beyond the quartile spread. Both groups of measurements were fitted to a Gaussian distribution.*

between the two groups. In the image from NKCC1 +/+, the dense microvilli of the apical membrane were observed by the bumpy texture of the CPECs. In comparison, the CPECs from the NKCC1 -/- animal appeared slightly smaller and smoother suggesting that these cells were shrunken.

### *Effect of Bumetanide on cell water volume of CPECs from NKCC1 -/- and NKCC1 +/+ mice*

Using the pharmacological approach to verify our measurements, we also measured the change in CWV of dissociated CPECs loaded with Calcein and exposed to bumetanide (Figure 4.3). When 10 μM bumetanide was applied to CPECs from WT mice the cells shrunk an average of -15.9 ± 9.1% (n = 3 animals), at an initial rate of -5.4 ± 0.6 %/ min. CPECs from NKCC1 KO mice did not respond to 10 μM bumetanide, mean volume change was equivalent to noise at < ± 1% (-0.5 ± 0.7 %, n = 3 animals). By treating CPECs attached to the cover slips as hemispherical domes, we used the measurements of CSA to estimate the predicted reduction in CWV of NKCC1 -/- CPECS and compared it to that resulting from 10 μM bumetanide exposure (Table 4.1). What we found was that NKCC1 -/- CPECs had a predicted difference in CWV of approximately -16%, which corresponded to the 15.9% loss in CWV in WT CPECs that followed exposure to 10 μM bumetanide. This similarity in CWV loss suggested that 10 μM bumetanide produced nearly complete inhibition of the NKCC1 cotransporter in CPECs. In conclusion, blocking NKCC1-mediated ion and associated water fluxes in CPECs by either pharmacological blockade by bumetanide

or genetic ablation of NKCC1 resulted in CPEC shrinkage. These results strongly suggest that on the apical membrane of CPECs NKCC1 is constitutively active and functions in the inward mode.

### *External ion dependence of cell water volume in CPECs*

We also examined the external $Cl^-$ and $Na^+$ dependence of CWV in CPECs. By examining the changes in CWV that occurred during $Cl^-$ uptake in the presence and absence of NKCC1, we could infer the contribution of NKCC1 to $Cl^-$ loading. This inference is possible given that ion transport mediated by NKCC1 is tightly linked to water transport in epithelial and non-epithelial cells (Hamann et al., 2010; Rocha-Gonzalez et al., 2008; Zeuthen & Macaulay, 2012). The removal of extracellular $Cl^-$ (replaced with gluconate) depleted WT CPECs of $Cl^-$ and water, and resulted in a mean cell shrinkage of -20.3 ± 1.8% (n = 10 animals), with an initial rate of -43.9 ± 8.0 %/min (Figure 4.4, A). This shrinkage reversed when $Cl^-$ was reintroduced. In contrast to cells obtained from WT animals, CPECs from NKCC1 KO mice only shrank by -7.7 ± 2.1% (n = 4 animals), during isosmotic removal of $Cl^-$, with an initial rate of cell shrinkage of -12.7 ± 3.9 %/min (Figure 4.4, B). These results support our hypothesis that NKCC1-mediated ion and associated water fluxes are constitutively active, inwardly directed, and function to maintain normal CWV under basal conditions.

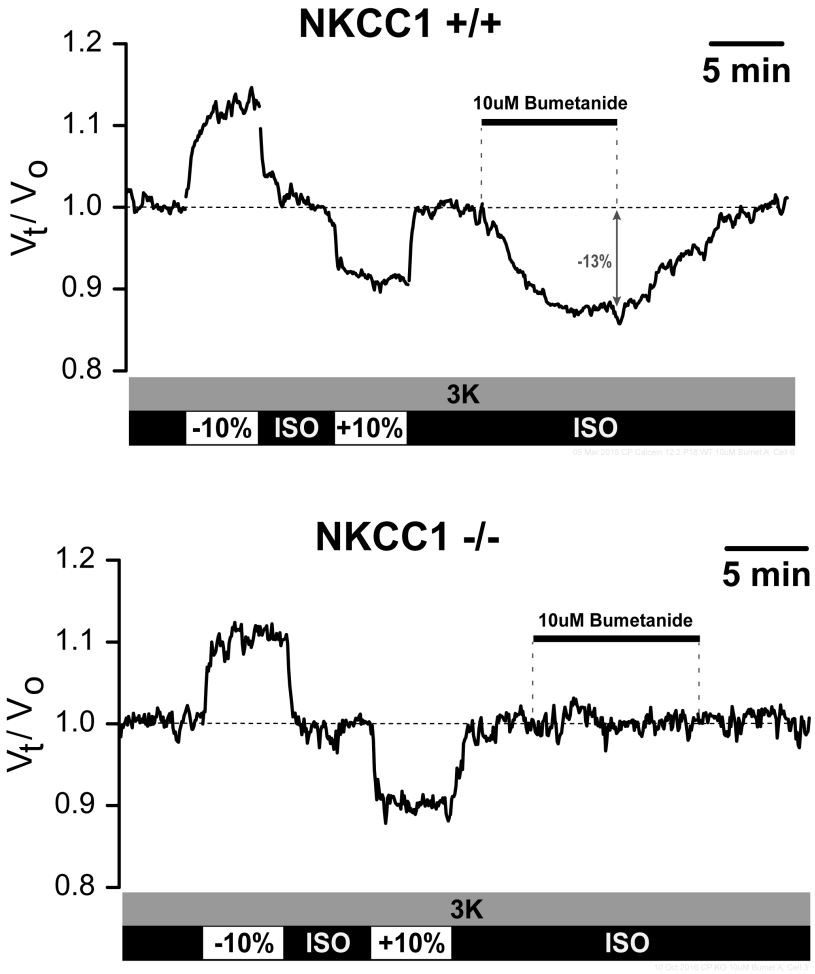


***Figure 4.3. Blocking NKCC1 with bumetanide causes NKCC1 +/+ CPEC shrinkage.*** ***Top)*** *volume recording of an individual CPEC from a WT mouse. The trace began with the two ± 10% hypo- / hyperosmotic calibration pulses, prior to the application of bumetanide. In this particular cell, bumetanide caused ~ 13% decrease in CWV, which was recovered during the drug wash out.* ***Bottom)*** *The same experiment was repeated in a CPEC from an NKCC1 -/- mouse. NKCC1 -/- CPECs responded well to the calibration pulses, but failed to respond to bumetanide due to the loss of NKCC1-mediated fluxes.*

***Table 4.1: Predicted difference in CPEC volume using CPEC CSA's***

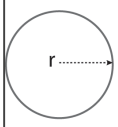


$CSA = \pi r^2$

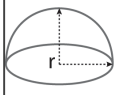


$V_{hemisphere} = (2/3)\,\pi r^3$

| | WT | KO |
|---|---|---|
| **mean CSA** | 155µm$^2$ | 137µm$^2$ |
| **r** | 7.0µm | 6.6µm |
| **$V_{1/2sphere}$** | 722µm$^3$ | 605µm$^3$ |
| **predicted difference** | | -16% |

*Using the mean CSA (from Figure 4.2), the radius was calculated and inserted into the formula for the volume of a hemisphere. The predicted difference in volume between the WT and NKCC1 -/- CPECs was very close to mean volume difference found by inhibiting the cotransporter with 10 µM bumetanide.*

Once CPECs were depleted of $Cl^-$, we observed the external $Na^+$ dependence of CWV recovery by the simultaneous replacement of extracellular $Cl^-$ and removal of extracellular $Na^+$ (replaced with N-methyl-D-glucamine). By removing external $Na^+$, we inhibited all $Na^+/Cl^-$ co-transport into the cell. CWV recovery was partially inhibited in the absence of $Na^+$, and the volume recovered to -15.8 ± 4.0% (n = 3 animals) during the $Na^+$-free recovery. About 75 —80% of this CWV recovery was $Na^+$-dependent. The rate of volume recovery during the sodium-independent component (SIC) was slower, 2.6 ± 0.1%/min, compared to the rate during sodium-dependent component (SDC), 30.2 ± 12.6%/min (n = 3 animals) (Figure 4.4, D). Given that NKCC1 functions as an active $Cl^-$ uptake mechanism in other $Cl^-$ secreting epithelia, it is likely that the SDC of CWV recovery that followed CPEC $Cl^-$ depletion was mediated by apical NKCC1, and the SIC likely resulted from the combined effects of the Anion Exchanger 2, NKATP, and osmotically committed water (Brown et al., 2004).

To test the hypothesis that NKCC1 was contributing to the CWV recovery that followed $Cl^-$ depletion, CWV recovery was examined in the presence of bumetanide. Volume recovery following CPEC shrinkage with 0Cl in the presence of bumetanide (10 μM) produced a small bumetanide-independent volume recovery to -13.0 ± 1.2 %, with an initial rate of 8.3 ± 0.1 %/min, followed by a very slow bumetanide-dependent volume recovery when the drug was washed off 2.6 ± 0.003 %/min (n = 3 animals) (Figure 4.4, C). The bumetanide-insensitive (BIC) and $Na^+$-independent

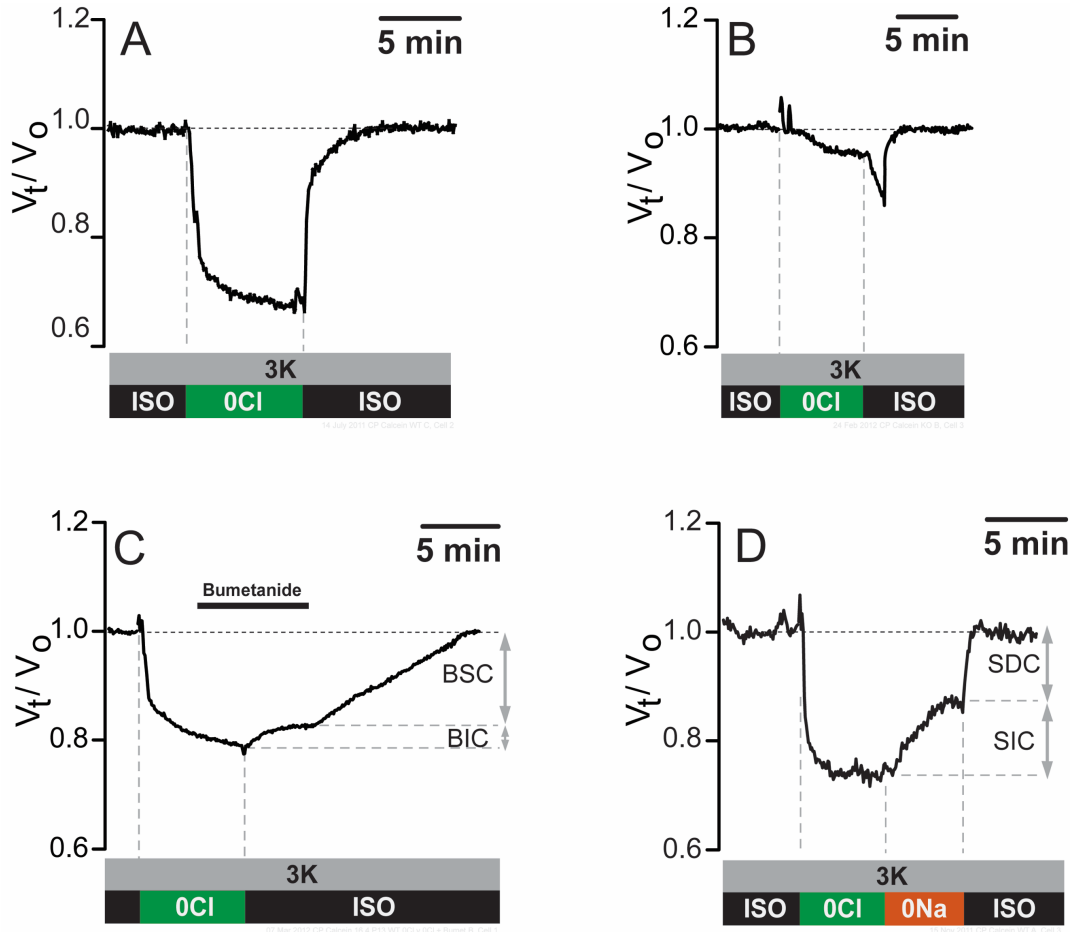


***Figure 4.4: External Chloride and Sodium dependence of CPEC CWV.*** *Gregoriades, Madaris, Alvarez, and Alvarez-Leefmans (2017, manuscript in preparation).* ***A & B)*** *Isosmotic removal of aCSF $Cl^-$ (0Cl) resulted in CPEC shrinkage that reversed upon readmission of isosmotic solution (ISO), and indicated that external $Cl^-$ was required for CWV maintenance.* ***A)*** *Volume recording of a CPEC from a WT that shrank -32.4% compared to a CPEC from a NKCC1 -/- mouse* ***(B)*** *where the cell shrank -4.8%.* ***C)*** *CWV recovery was reduced in the presence of 10 $\mu$M bumetanide. During the bumetanide-*

*insensitive component of the volume recovery (BIC), the volume in this cell only recovered 1.3%, while most volume was restored during the bumetanide-sensitive component of the volume recovery (BSC) after the drug was removed.* ***D)*** *In the absence of external $Na^+$ there was also incomplete CWV recovery. The BIC and $Na^+$-independent (SIC) components indicated the expression of mechanisms other than NKCC1 in this volume recovery. BIC mean rate of volume recovery was much faster than the BSC mean rate of volume recovery at 8.3% / min vs 2.6% / min, respectively. The $Na^+$-dependent component (SDC) of the recovery proceeded at a rate that was one order of magnitude faster than in $0Na^+$ (SIC mean rate of volume recovery was 2.5% / min vs. 30.2% / min during SDC). Thus, most of the $Cl^-$ fluxes were mediated by $Na^+$-dependent and bumetanide-sensitive mechanisms, most likely NKCC1.*

(SIC) components indicated the expression of mechanisms other than NKCC1 in this volume recovery. However, most of the water fluxes (and inferred $Cl^-$ fluxes) were mediated by $Na^+$-dependent and bumetanide-sensitive mechanisms, most likely NKCC1.

## *Conclusion*

The data presented above demonstrate that basal NKCC1-mediated fluxes are inwardly directed in CPECs. When NKCC1 was genetically ablated in the KO mouse and/or when NKCC1 was inhibited with bumetanide, CPECs lost CWV due to an imbalance in the net solute and water fluxes across the cell. Additionally, full recovery from a loss of cell water and intracellular $Cl^-$ required the presence of external $Na^+$ and was bumetanide sensitive. This supports the hypothesis that NKCC1 is constitutively active and functions in the maintenance of both normal and constant CWV in CPECs.

## *Chapter 5: Specific Aim 2 Results*

The experiments in this chapter focus on answering the following questions:

1) What are the $[Na^+]_i$ and $[Cl^-]_i$ of mammalian CPECs?
2) Do the $[Na^+]_i$ and $[Cl^-]_i$ change in CPECs from NKCC1 -/-?
3) Can apical NKCC1 act as a sensor and regulator of CSF $[K^+]$ in CPECs?

The link between these questions became evident while attempting to create a predictive model of NKCC1 cotransport in relation to CSF $[K^+]$. At that time, we came across very different values for the intracellular ion concentrations of CPECs, and quickly realized the necessity to measure these concentrations ourselves (see next section). Without these data, it would have been impossible to make our model realistic. Answering the first question involved using the ion-sensitive dyes ANG-2 and MQAE to determine the intracellular $Na^+$ and $Cl^-$ concentrations, respectively. To answer the second question, we examined the sensitivity of CPECs to small changes in external $[K^+]$ within a physiological plausible range.

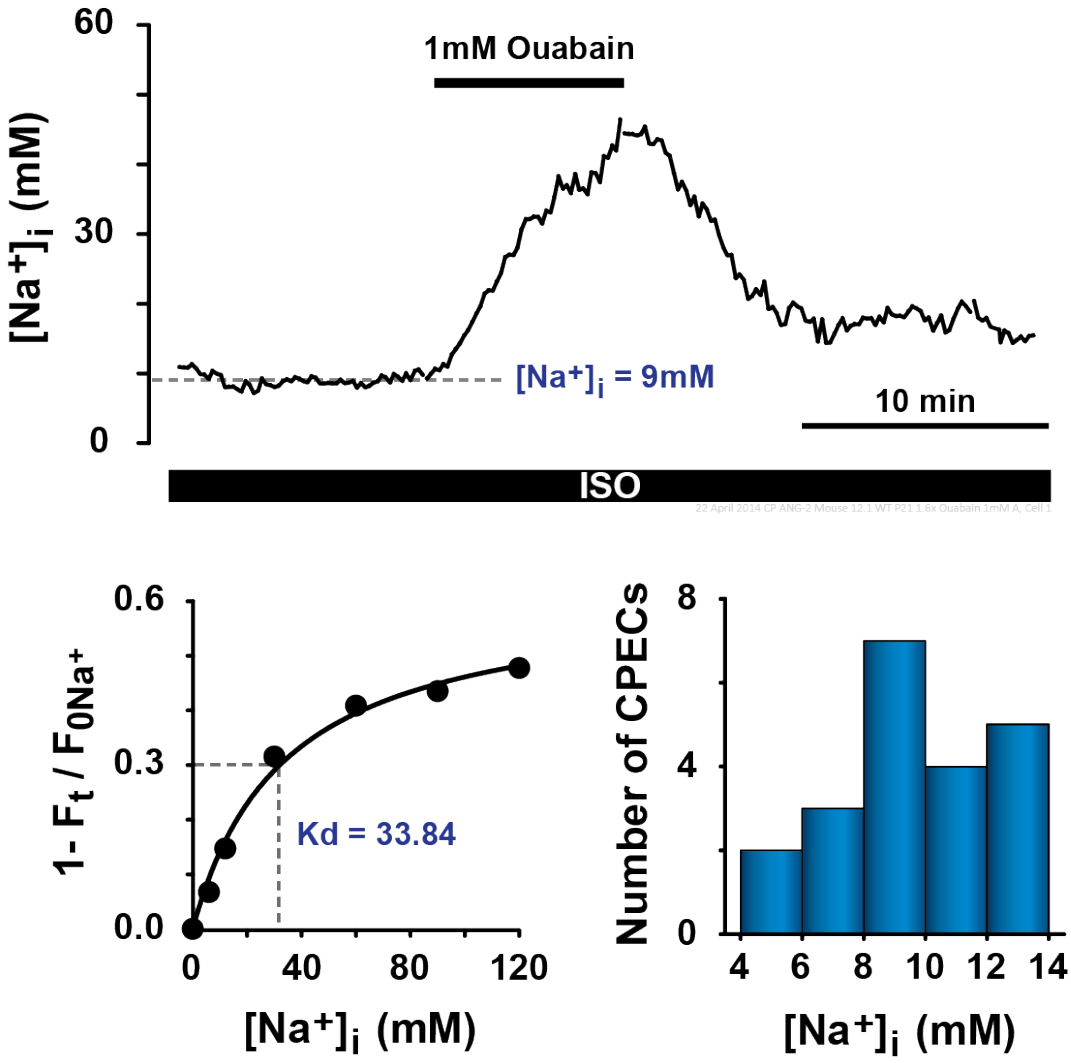


***Figure 5.1: Measuring $[Na^+]_i$ in single CPECs using ANG- 2. Top)*** *Measurement of basal $[Na^+]_i$ in a NKCC1 +/+ CPEC loaded with ANG-2. The basal $[Na^+]_i$ of this CPEC was 9 mM. After taking the basal $[Na^+]_i$ measurement, NKATP was inhibited with ouabain (1 mM) to test that the dye responded to changes in $[Na^+]_i$. In this CPEC, ouabain exposure resulted in an increase in $[Na^+]_i$ to ~45 mM, which was reversible upon the removal of ouabain.* ***Bottom Left)*** *Fitting the*

*Michaelis-Menton equation to the plot of the relative fluorescence (1-Fo/Ft) of ANG-2 vs [$Na^+$] provided Kd and Fmax values for each cell. These values were used to convert fluorescence intensities into [$Na^+$].* ***Bottom Right)*** *Histogram showing the distribution of $[Na^+]_i$ in the 21 individual CPECs. The mean $[Na^+]_i$ of CPECs was 8.4 ± 1.0 mM, n = 3 animals.*

### *Intracellular $Na^+$ and $Cl^-$ concentrations of mouse CPECs*

Using ANG-2, we found that $[Na^+]_i$ of WT CPECs was 8.4 ± 1.0 mM (n = 3 animals), as shown in Figure 5.1. This $Na^+$ concentration was closer to the values of 10 –15 mM measured in amphibians (Saito & Wright, 1987; Zeuthen, 1994) using ion-selective microelectrodes, but differed greatly to the $[Na^+]_i$ measured by Johanson and Murphey (1990) and Smith and Johanson (1985) using whole tissue/ flame photometry, or that by Keep et al., (1994) in their calculations to determine the direction of cotransport. The average values of $[Na^+]_i$ obtained or assumed by Johanson, Keep, and coworkers ranged between 30 -48 mM. Our measured $[Na^+]_i$ was consistent with $[Na^+]_i$ measured in a number of epithelial and non-epithelial cells using fluorescent dyes or microelectrodes (Donoso, Mill, O'Neill, & Eisner, 1992; Rose & Ransom, 1996; Zeuthen, 1978, 1994; Zhao & Muallem, 1995). In Figure 5.2, a comparison of the ion concentrations presented by Johanson and Murphey (1990), Keep et al., (1994), Saito and Wright (1987), and our measured intracellular $Na^+$ and $Cl^-$ concentrations was made. We were unable to measure the $[K^+]_i$ in CPECs because so far there are no reliable dyes for this cation, so we used an $[K^+]_i$ = 110 mM based on the range of values obtained by Zeuthen et al., (1987) using ion-selective microelectrodes in amphibian CP of 100-120mM (Zeuthen, Christensen, Baerentsen, & la Cour, 1987).

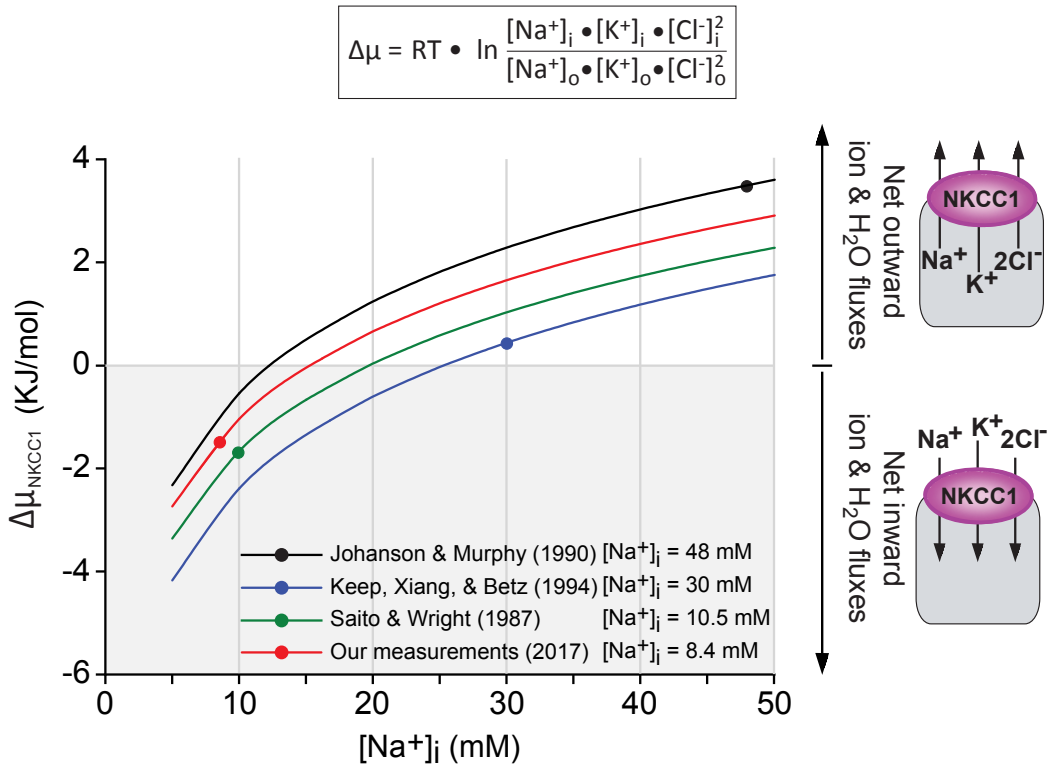


***Figure 5.2: Effect of $[Na^+]_i$ on the net free energy driving NKCC1 transport in CPECs***. *Measurements using the fluorescent indicator dye ANG-2 revealed that mouse CPECs had an $[Na^+]_i$ = 8.4 ± 1.0 mM, similar to that of amphibian CPECs, 10.5 mM, measured by Dr. Zeuthen using ion-selective microelectrodes and reported by Saito & Wright (1987). Using the measured values for $[Na^+]_i$ and $[Cl^-]_i$ in equation 1, we found $\Delta\mu_{NKCC1}$ was negative, indicating that under basal conditions the cotransporter is working in the inward direction.*

***Table 5.1: CPEC intracellular ion concentrations used to calculate $\Delta\mu_{NKCC1}$.***

| | $[Na^+]_i$ (mM) | $[Cl^-]_i$ (mM) | $[K^+]_i$ (mM) | $[Na^+]_o$ (mM) | $[Cl^-]_o$ (mM) | $[K^+]_o$ (mM) |
|---|---|---|---|---|---|---|
| *Johanson & Murphy (1990)* | 48 | 65 | 145 | 154 | 128 | 3 |
| *Keep et al., (1994)* | 30 | 50 | 120 | 150 | 130 | 3 |
| *Saito & Wright (1987)* | 10.5 | 31.6 | 90 | 110 | 89 | 2 |
| *Our Measured Values* | 8.4 | 62.1 | 110* | 126 | 131 | 3 |

*The top two rows represent values for mammalian CPECs, while Saito & Wright used amphibian CPECs. The values for $[Na^+]_i$ reported for mammalian CPEC are very large compared to the value for amphibian CPEC. *estimate value based on the range of values obtained by using ion-selective microelectrodes in amphibian CP of 100 -120 mM (Zeuthen et al., 1987). The same value has been obtained in glioma cells using the fluorescent indicator PBFI-AM (Zhu et al., 2014).*

Using MQAE we found $[Cl^-]_i$ of NKCC1 WT CPECs was 62.1 ± 3.5 mM (n = 5 animals), a concentration that was close to that reported for other mammalian CPEC (Johanson & Murphy, 1990). Both mammalian $[Cl^-]_i$ measurements were about 1.5X greater than those of amphibian CPECs using ion-selective microelectrodes, which were approximately 40 mM (Saito & Wright, 1987; Zeuthen, 1987).

We used the same methodological approach to measure $[Na^+]_i$ and $[Cl^-]_i$ in CPECs from NKCC1 -/- mice. The results show that $[Na^+]_i$ was 12.2 ± 1.2 mM (n = 3 animals), a value that was not significantly different to that in WT CPECs (p = 0.07). In contrast, the $[Cl^-]_i$ of NKCC1 -/- CPECs was significantly less than that of WT cells; $[Cl^-]_i$ of NKCC1 -/- CPECs was 31.5 ± 4.8 (n = 7 animals), which was significantly different (p <0.001) to that of WT (Figure 5.3). This decrease in intracellular $[Cl^-]$ by about -50% is consistent with NKCC1 being a major $Cl^-$ uptake system that maintains $[Cl^-]_i$ and cell volume at a level needed for the cells to work. Knowing both the intra- and extracellular $[Cl^-]$, it was possible to estimate the chloride equilibrium potential ($E_{Cl}$) in WT and KO CPECs using equation 5. The $E_{Cl}$ was then be compared to the membrane potential ($E_m$) of -53 mV, a value recorded in rat CPECs (Kotera & Brown, 1994), to determine whether $Cl^-$ was passively distributed across the membrane or actively maintained above chemical equilibrium in CPECs. The estimated mean $E_{Cl}$ of NKCC1 +/+ CPECs was -19.71 ± 1.4 mV (assuming all the cells had the same $E_m$, which obviously renders this calculation as a valid, but rough estimate). All of the WT CPEC had estimated $E_{Cl}$ values that were less negative than expected if $Cl^-$ was maintained above electrochemical equilibrium in CPECs. The estimated mean $E_{Cl}$ in NKCC1 -/- CPECs was -38.9 ± 4.2 mV (n= 7 animals), a value

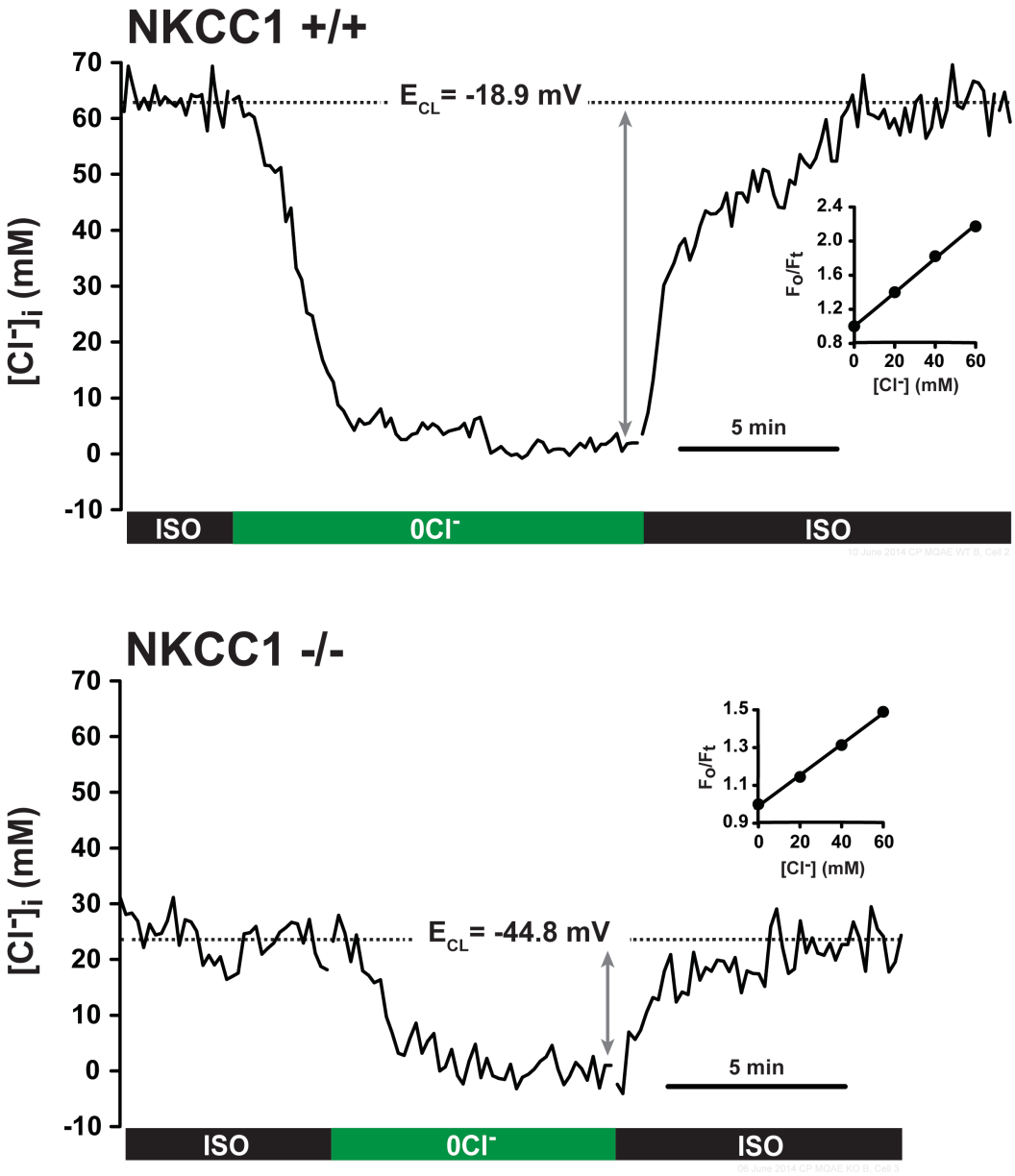


***Figure 5.3: Measuring $[Cl^-]_i$ in single CPECs.*** *Representative examples of NKCC1 +/+ and NKCC1 -/- $Cl^-$ transients that measured the $[Cl^-]_i$ and $E_{Cl}$ of single CPECs loaded with MQAE. CPECs became depleted of their internal $Cl^-$ stores when*

*the external $Cl^-$ was removed (0$Cl^-$), and were able to recover to initial values when external $Cl^-$ was replaced. The difference between the ISO and 0Cl- steady-states (gray arrow) was used to calculate the $[Cl^-]_i$. The inset is the calibration plot of the relative MQAE fluorescence (Fo/Ft) as a function of $[Cl^-]$ in the calibration solutions, and the slope of this relationship is the Stern-Volmer constant ($K_{SV}$).* ***Top)*** *$Cl^-$ transient from NKCC1 +/+ CPEC. The $[Cl^-]_i$ measured in this cell was 62.9 mM, the $K_{SV}$ = 19.7 $M^{-1}$, and $E_{Cl}$ was calculated at -18.9 mV.* ***Bottom)*** *$Cl^-$ transient from NKCC1 -/- CPEC. The $[Cl^-]_i$ in this was measured to be 22.9 mM, $K_{SV}$ = 8 $M^{-1}$, and $E_{Cl}$ was calculated at -44.8 mV. NKCC1 -/- CPECs had a reduction in $[Cl^-]_i$ by 50% compared to WT. NKCC1 -/- CPECs also had a reduced $K_{SV}$, which may have been a consequence of the reduced CWV, however further investigation on this matter is necessary.*

that was more negative than that of the WT, but still more positive than $E_m$ by about 10 mV. These estimates must be taken with caution because the actual $E_m$ was not measured in the present study. However, it is worth mentioning that of the 7 NKCC1 -/- animals in this study, 2 had an estimated mean $E_{Cl}$ more negative than -50 mV. Meaning that in some animals, $Cl^-$ was passively distributed across the CPEC plasma membrane.

### *Testing the sensitivity of NKCC1 in CPECs to small changes in $[K^+]_o$.*

The net free energy driving NKCC1 depends on the extracellular and intracellular concentrations of the cotransported ions ($Na^+$, $K^+$, and $Cl^-$), and the stoichiometry (see equation 1). Equation 1 predicts that relatively modest changes in $[K^+]_o$ have a big impact on $\Delta\mu_{NKCC1}$ (Figure 5.4). Figure 5.4 illustrates how the $[K^+]_{CSF}$ of 2.9 –3 mM resulted in the cotransporter working nearer to its flux reversal point (FRP), where the chemical potential driving force of NKCC1 ($\Delta\mu_{NKCC1}$) is equal to zero, as compared to the more negative value of $\Delta\mu_{NKCC1}$ when $[K^+]_o$ is 4.7 –5 mM, as in the plasma. Specifically, the FRP of NKCC1 in CPECs occurred between 1.4 – 1.6 mM $[K^+]_o$ when using the measured $[Na^+]_i$ and $[Cl^-]_i$, and the estimate of $[K^+]_i$ of 110 mM reported by Zeuthen et al., (1987). When $[K^+]_o$ dropped below the FRP, the model predicted that NKCC1 would reverse direction and ion cotransport would occur in the outward mode. We can think of this thermodynamic model in vector terms, with each point on the graph representing both a direction of cotransport and magnitude of the driving force. The farther away a point is from zero, the

greater the driving force of NKCC1 cotransport. Additionally, the curve of $\Delta\mu_{NKCC1}$ vs $[K^+]_o$ became increasingly steep as $[K^+]_o$ decreased. This is due to the stoichiometry of NKCC1. Cotransport mediated by NKCC1 requires the binding of 2 $Cl^-$, which results in the internal and external $[Cl^-]$ to be raised to the power of 2 in equation 1. As $[K^+]_o$ decreases to 1 mM, the influence of $[Cl^-]_o$ on NKCC1 transport increases. When $[K^+]_o$ becomes less than 1 mM, the product of the denominator in equation 1 approaches zero. A small change in the $[K^+]_o$ of ± 2 mM $K^+$ with respect to the basal level of 3 mM, is sufficient to reverse the sign of $\Delta\mu_{NKCC1}$ indicating a change in the direction of cotransport. In the experiments that follow, we tested the sensitivity of dissociated CPECs in vitro to ± 2 mM changes in $[K^+]_o$. We used measured changes in the CWV of CPECs that occurred in response to changes in $[K^+]_o$, as an indicator of the net flux direction and magnitude, and utilized the two-prong approach to NKCC1 transport inactivation as in Chapter 4.

One of the central hypotheses of this work is that apical NKCC1 of CPECs is highly sensitive to changes in $[K^+]_{CSF}$. This is predictable given that the cotransporter is in the apical membrane, which is in direct contact with the CSF, and because of the net free energy driving the cotransporter, as discussed above (equation 1), and the $K_m$ for $K^+$ of NKCC1 (Payne & Forbush, 1995). An isosmotic decrease in $[K^+]_o$ by 2 mM (i.e., from baseline 3 mM to 1 mM) produced a mean CPEC shrinkage of -11.8 ± 1.7% (n = 11 animals), that proceeded at an initial rate of -12.0 ± 1.4% / min. An isosmotic increase in $[K^+]_o$ by 2 mM (i.e., from 3 mM to 5 mM), caused CPECs to swell by 10.4 ± 1.6% (n = 8 animals), and the initial rate of that swelling was 8.3 ± 1.0% / min. CPECs from NKCC1 KO mice had no change in CWV in response to

Both direction and magnitude of the overall net free energy driving NKCC1 transport (Δμ) can be predicted using the ion concentrations shown in the table below. For an electroneutral stoichiometry of $1Na^+:1K^+:2Cl^-$,

$$\Delta\mu = RT \bullet \ln \frac{[Na^+]_i \bullet [K^+]_i \bullet [Cl^-]_i^2}{[Na^+]_o \bullet [K^+]_o \bullet [Cl^-]_o^2}$$

| Ion | CSF (mM) | aCSF (mM) | Intracellular (mM) |
|---|---|---|---|
| $Na^+$ | 148 | 126 | 8.4† |
| $K^+$ | 3 | 3 | 110* |
| $Cl^-$ | 130 | 131 | 62.1‡ |

*estimate based on other mammalian epithelial cells.
†,‡ mean concentrations of CPECs measured using ion-sensitive fluorescent indicators, ANG-2 and MQAE.
CSF = cerebrospinal fluid
aCSF = artificial cerebrospinal fluid

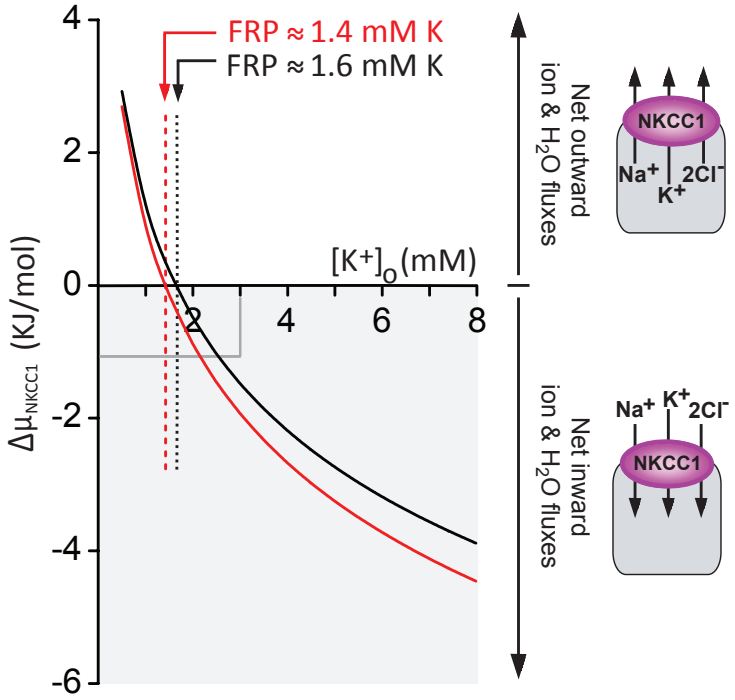


***Figure 5.4: Modeling the FRP of NKCC1 as a function of $[K^+]_o$ in CSF and artificial CSF (aCSF).*** *Plot of $\Delta\mu$ of NKCC1 as a function of $[K^+]_o$ in CSF (red) or in aCSF (black). The NKCC1 mediated fluxes reverse when $\Delta\mu$=0 (FRP), which occurs in this model when $[K^+]_o$ is 1.4 mM (CSF) or 1.6 mM (aCSF). This indicates that under physiological $[K^+]_o$ (2.9-3 mM) NKCC1 works in the inward mode, near thermodynamic equilibrium. $\Delta\mu$ is calculated at T= 295 K for aCSF and T= 310 K for CSF. The FRP is unchanged for temperatures between 295 -310 K.*

± 2 mM changes in $[K^+]_o$, which indicated that they lost this "$K^+$-sensitivity." Specifically, after 5 minutes of exposure to 1 mM $K^+$ and 5 mM $K^+$, the mean CWV change in NKCC1 -/-cells was within the noise level of < 1% (n = 3 animals for each). Figure 5.5 provides a comparison between the traces obtained from single WT CPECs vs NKCC1 -/- CPECs. There was a striking difference in the volume response to changes in $[K^+]_o$ between the two representative cells. In the top trace, the WT CPEC showed a robust shrinkage in response to lowering the $[K^+]_o$ just 2 mM, that reversed upon exposure to baseline 3 mM $K^+$. The cells swelled in response to increasing $[K^+]_o$ from 3 mM to 5 mM. These responses were absent in NKCC1 -/- CPECs, as shown in the lower panel of Fig. 5.5. To further prove that the previous results were due to specific inactivation of NKCC1-mediated fluxes and not to some unknown change related to the genetic mutant, such as a change in the location or a functional alteration of other membrane proteins (e.g., NKATP or aquaporin 1 (AQP1)), the changes in CPE CWV in response to ± 2 mM $K^+$ were repeated in cells from NKCC1 +/+ in the presence of 10 μM bumetanide, a concentration expected to block NKCC1 (Alvarez-Leefmans, 2012; Russell, 2000). As illustrated in Figure 5.6, CPECs responded to two sequential changes in external $[K^+]$. Pharmacologic inhibition of NKCC1 with 10 μM bumetanide resulted in CPEC shrinkage, as expected from halting constitutively active NKCC1, that blocked the "sensitivity" to the changes in $[K^+]_o$ which was clearly mediated by NKCC1. Bumetanide produced CPEC shrinkage and blocked the cell's ability to swell in response to a second exposure of 5 mM $K^+$ (Figure 5.6C). Similarly, in the presence of bumetanide CPEC shrinkage when $[K^+]_o$ was decreased to 1 mM $K^+$ did not occur (Fig. 5.6D). However,

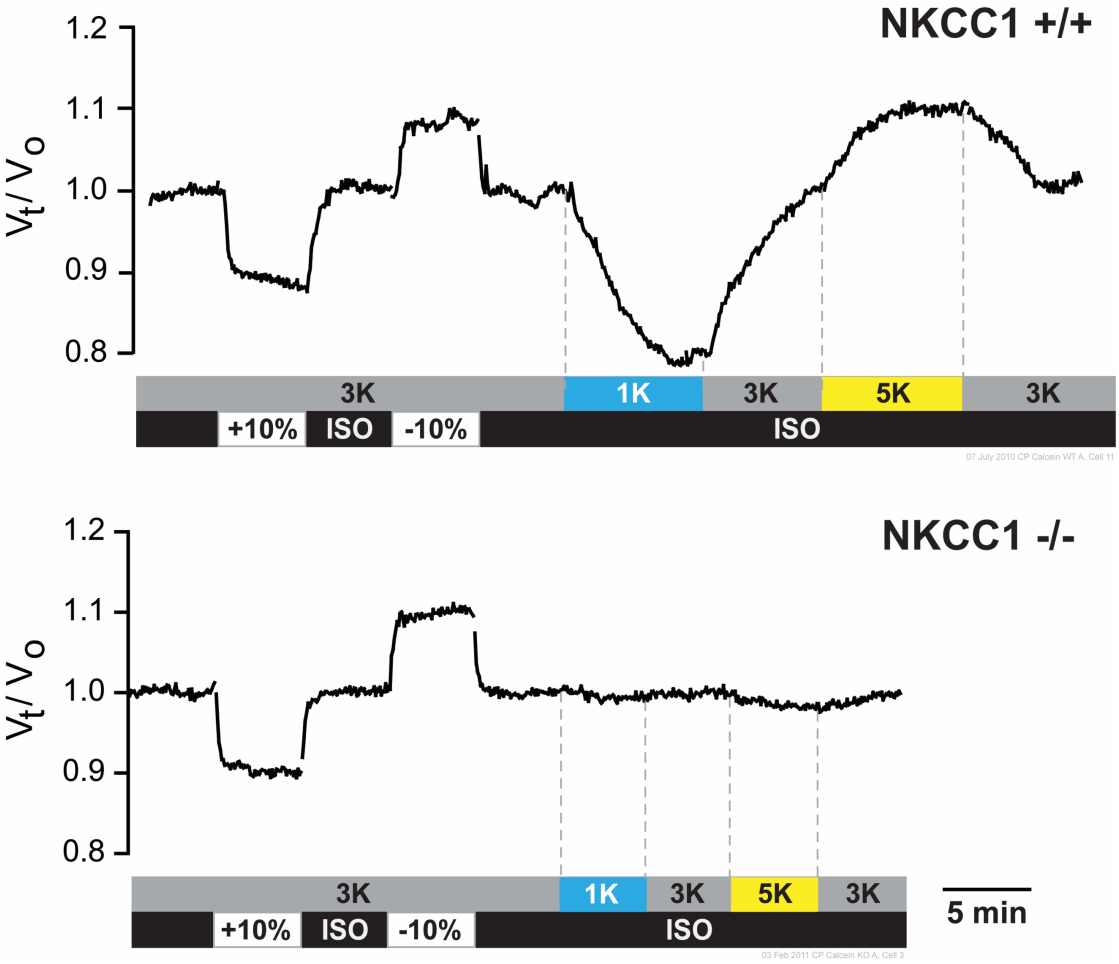


***Figure 5.5: Comparison of the changes in relative cell volume of CPECs in response to various $[K^+]_o$ in cells dissociated from NKCC1 +/+ and NKCC1 -/- animals.*** *Top trace illustrates the CPEC volume sensitivity to ± 2 mM changes in $[K^+]_o$, and the bottom trace the experiment was repeated in an NKCC1 -/- CPEC.* ***Top)*** *WT CPEC shrank by -20.6% when $K^+$ was lowered to 1 mM, and swelled 10.0% above its basal volume when $K^+$ was increased to 5 mM.* ***Bottom)*** *NKCC1 -/- CPEC does not respond to± 2 mM changes in $[K^+]_o$. Both cells were able to respond to the ± 10% anisosmotic calibrations. Thus, in the absence of NKCC1, CPECs lose the ability to respond to ± 2 mM changes in external $[K^+]$.*

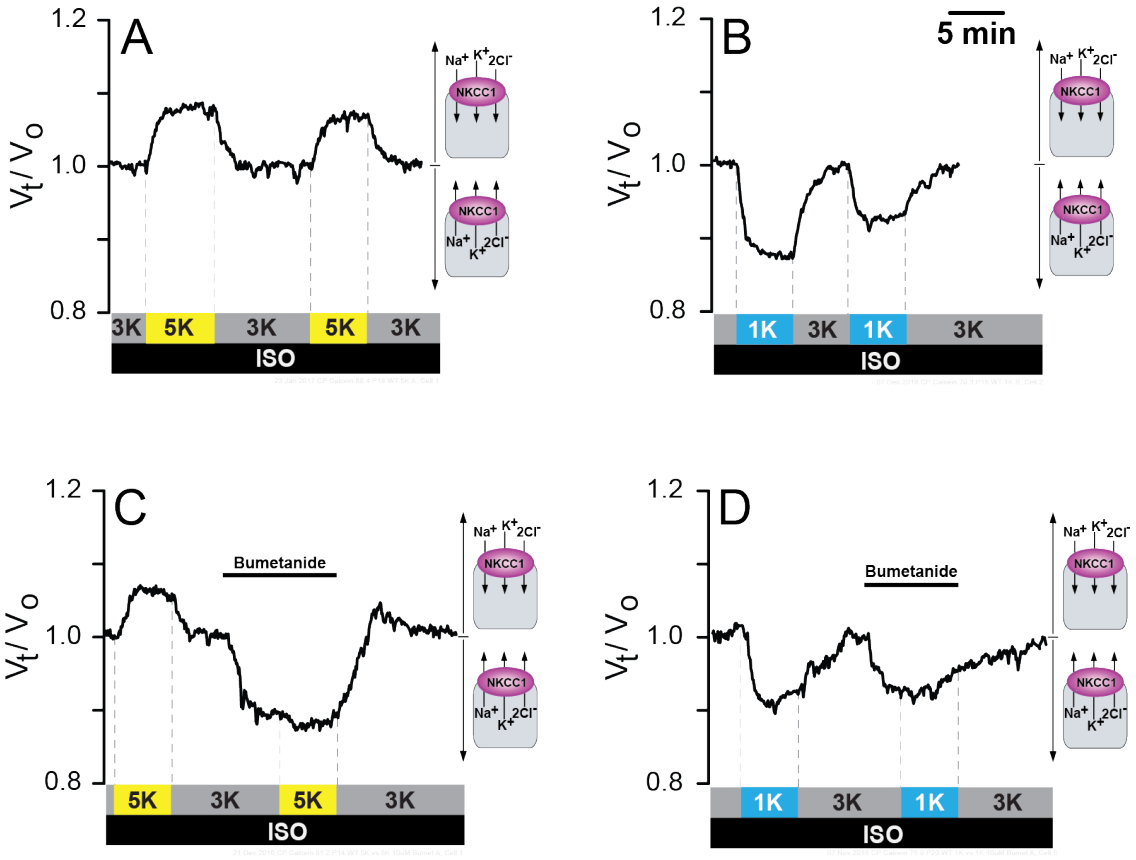


***Figure 5.6. CPEC sensitivity to changes in $[K^+]_o$ was blocked by bumetanide. A & B) Isosmotic*** *changes in cell water volume induced in CPECs by altering $[K^+]_o \pm 2$ mM $K^+$ were blocked by bumetanide.* ***(A)*** *CWV changes in response to two sequential 5K pulses (from 3 to 5 mM $K^+$)* ***(B)*** *Similar to A, but the sequential pulses were 1K (from 3 to 1 mM $K^+$). There was a slight decrease in the amplitude of the second $K^+$ pulse compared to the first, but the effect of the second $K^+$ pulse was reproducible and of sufficient amplitude to be used as test pulse in the experiments shown in the second part of this figure to probe the effect of bumetanide. In trace* ***A****, the first 5 mM $K^+$ pulse produced a swelling of*

*8.0% compared to a swelling of 6.8% in the second pulse. Differences between the first and second 1 mM $K^+$ pulses **(B)** were larger. The shrinkage during the first 1 mM $K^+$ pulse was -12.4% verses -7.9% during the second 1 mM $K^+$ pulse. **C & D)** Inhibition of NKCC1 with 10 µM bumetanide resulted in CPEC shrinkage and loss of the response to small changes in $[K^+]_o$. Following a control pulse of 5 mM $K^+$ **(C)** or 1 mM $K^+$ **(D)**, the application of bumetanide produced CPEC shrinkage and blocked the cell's ability to response to a second ± 2 mM change in $[K^+]_o$.*

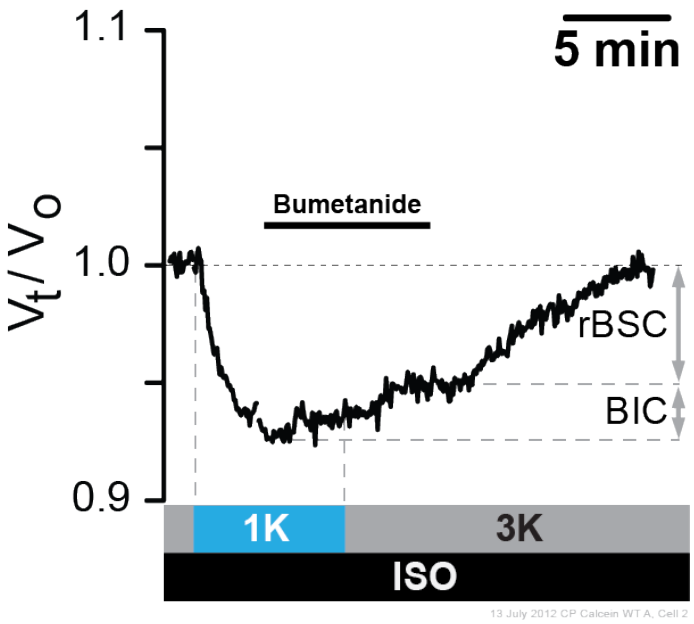


***Figure 5.7: Cell water volume recovery following 1 mM $K^+$ isosmotic shrinkage was bumetanide-sensitive in CPECs from NKCC1 +/+.*** *CWV recovery from shrinkage produced by exposure to 1K was blunted in the presence of 10 μM bumetanide. However, there was a small bumetanide-insensitive component (BIC) of the recovery. During the BIC, the volume in this cell recovered from -7.2 to -5.1 %, and the remaining volume recovery occurred during the relative bumetanide-sensitive component (rBSC) after the drug was removed. The BIC indicates the possibility of mechanisms other than NKCC1 in this volume recovery. BIC mean rate of volume recovery is 0.71 % / min compared to the rBSC mean rate of volume recovery at 1.3 % / min.*

CPECs presented a modest volume recovery from shrinkage in the presence of bumetanide to a mean volume of -5.2 ± 0.1% (n = 3 animals) (Figure 5.7). The bumetanide-insensitive (BIC) component of the CWV suggested either incomplete block of NKCC1, or the expression of mechanisms other than NKCC1 in this volume recovery. BIC mean rate of volume recovery was the same as the relative bumetanide-sensitive component (rBSC) mean rate of volume recovery at 1.2%/min, indicating that possibly the same mechanism was responsible for both components of the recovery. These results are consistent with our data using NKCC1 KO mice, and reveal that the $[K^+]_o$ sensitivity of CPECs was dependent on NKCC1-mediated fluxes.

### *Testing the sensitivity of NKCC1 to various $[K^+]_o$ with solutions buffered with $CO_2/HCO^-_3$*

The previous experiments were performed using HEPES buffered solutions equilibrated in air. Under these conditions, atmospheric $CO_2$ is able to dissolve into the solutions, leading to $CO_2$ hydration and consequent formation of $H_2CO_3$, which dissociates to form $H^+$ and $HCO_3^-$ (Praetorius & Damkier, 2017). Further, cell metabolism results in the production of intracellular $CO_2$ which reacts with intracellular water also forming $HCO_3^-$. Given the presence of extracellular and intracellular membrane bound carbonic anhydrases (CA) in CPECs (reviewed in Praetorius & Damkier, 2017), the $CO_2$ hydration reactions are catalyzed both in the intra- and extra-cellular membrane domains. Thus, HEPES solutions equilibrated

with air do have sufficient bicarbonate to drive bicarbonate-dependent transporters. This effect is enhanced because the major bicarbonate transporters physically or functionally interact with the various intra- or extra-cellular CAs isoforms, forming supramolecular complexes known as "metabolons" (Deitmer & Becker, 2013; Deitmer, Theparambil, Ruminot, & Becker, 2014; McMurtrie et al., 2004). CPECs have a high concentration of CA's that catalyze the hydration of $CO_2$ thereby forming $H^+$ and $HCO_3^-$ (Fisher & Copenhaver, 1959; Giacobini, 1961, 1962; Maren, 1967; Masuzawa, Shimabukuro, Sato, & Saito, 1981). A reason for performing experiments using HEPES-buffered solutions equilibrated with air is that it is easier to maintain a constant pH compared to $CO_2/HCO_3^-$, when running the solutions through perfusion lines. Further, experiments using $HCO_3^-$ buffered aCSF showed that WT CPECs responded similarly to changes in $[K^+]_o$ in either HEPES or $HCO_3^-$ buffered solutions (Figure 5.8). In $HCO_3^-$ buffered solutions the mean shrinkage in response to 1 mM $K^+$ was -13.1 $\pm$ 2.3 % (n = 4 animals) and the mean swelling in response to 5 mM $K^+$ was 16.6 $\pm$ 2.9 % (n = 4 animals), with p = 0.69 and 0.07, respectively, when compared to their corresponding responses in HEPES buffered solutions. Table 5.2 summarizes the data below. It is important to mention that $K^+$ induced responses showed considerable variability between cells, possibly due to variations in the content of intracellular ions affecting NKCC1 transport.

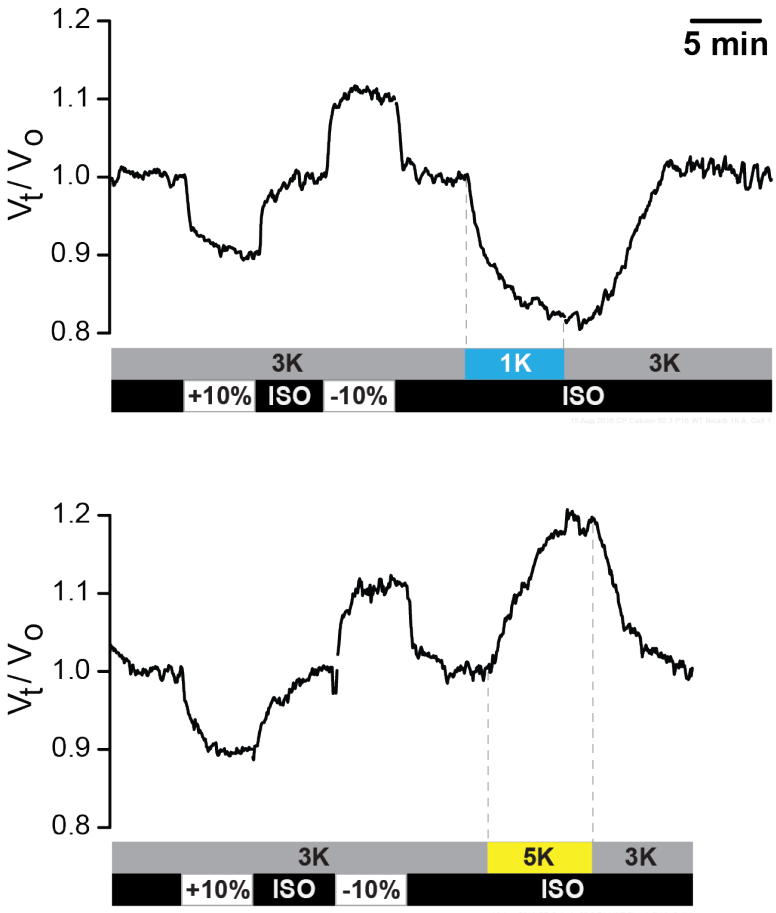


***Figure 5.8: CPEC $K^+$ sensitivity was unchanged in the presence of added $HCO_3^-$ to the bathing solutions.*** *Two representative cells showing the CWV response to ± 2 mM $K^+$ in $CO_2$/ $HCO_3^-$ buffered bathing solutions. No significant differences were found between the $K^+$ sensitivity of CPECs in bicarbonate buffered solutions vs HEPES buffered solutions.* ***Top)*** *A WT CPEC was exposed to 1 mM $K^+$ and this particular cell shrank -18.1 %.* ***Bottom)*** *This WT CPEC was exposed to 5 mM $K^+$ and swelled 19.1 %.*

***Table 5.2: Comparing the changes in CWV in response to ± 2 mM $K^+$ when the bathing solutions are buffered with HEPES vs $CO_2/HCO_3^-$.***

| *Buffer* | *1 mM $K^+$* *ΔVolume* | *5 mM $K^+$* *ΔVolume* |
|---|---|---|
| *HEPES* | -11.8 ± 1.7% | 10.4 ± 1.6% |
| | n = 11 animals | n = 8 animals |
| *$CO_2/HCO_3^-$* | -13.1 ± 2.3 % | 16.6 ± 2.9 % |
| | n = 4 animals | n = 4 animals |
| *Significance* | P = 0.69 | P =0.07 |

*A comparison of the $K^+$-induced changes in CWV in differently buffered bathing solutions.*

## *Conclusion*

CPECs had an $[Na^+]_i$ = 8.4 mM and an $[Cl^-]_i$ = 62.1 mM. These concentrations support the hypothesis that in CPECs NKCC1 functions near to its FRP. CPECs were exquisitely sensitive to small changes in $[K^+]_o$ in the physiological range of ± 2 mM. In the absence of NKCC1-mediated fluxes, either by pharmacological inhibition or genetic ablation using the NKCC1 -/- mouse, CPECs lost this $[K^+]_o$ sensitivity. This loss in sensitivity was not the result of altered NKATP or AQP1 expression on the apical membrane of NKCC1 -/- CPECs (see Appendix A). Thus, we propose that the CPECs use NKCC1 as a sensor and regulator of CSF $[K^+]$.

## *Chapter 6: Discussion*

The results in this dissertation contribute to elucidating the function of the apical NKCC1 cotransporter in CPECs, with a focus on determining 1) the direction of NKCC1 cotransport under basal conditions; and 2) whether NKCC1 works near to its FRP, thus permitting it to function as a sensor and regulator of CSF [$K^+$]. These data include a three-pronged approach to NKCC1 inactivation, utilizing NKCC1 -/- mouse, pharmacological inhibition of NKCC1 with bumetanide, and ion-substitution experiments.

NKCC1 inactivation by either genetic ablation or pharmacological inhibition reduces CPEC water volume by ~16% (Figure 4.2, 4.3, and Table 4.1). Ion-substitution experiments demonstrate that maintenance of normal CPEC water volume requires the presence of external $Cl^-$ and $Na^+$, and is bumetanide-sensitive (Fig. 4.4). These data prove that NKCC1 is constitutively active and inwardly directed in CPECs under basal physiological conditions, solving a long-standing controversy in the field. Further, the results of the present study establish that a critical function of NKCC1 in CPECs is the maintenance of both normal and constant CWV, that we propose is needed for CSF secretion.

Reported $[Na^+]_i$ of CPECs range from 10 –15 mM in amphibians, and 30 –50 mM in mammals (Figure 5.2 and Table 5.1) (Johanson & Murphy, 1990; Keep et al., 1994; Saito & Wright, 1987; Zeuthen et al., 1987). Using the non-invasive $Na^+$-indicator, ANG-2, the $[Na^+]_i$ measurement of mouse CPECs is 8.4 ± 1.0 mM (Figure 5.1), a value much less than is reported for mammalian CPECs (30 -50 mM) from whole tissue, but closer to the 10 –15 mM measured in single CPECs of amphibian using ion-selective microelectrodes. The ANG-2 $[Na^+]_i$ measurements require the calibration of every cell in order to determine the individual Kd of each cell. The verifies that the calibration solutions of permeabilized cells do not give spurious values due to changes in cell volume, a very important control for a single excitation/emission dye.

NKCC1 -/- CPECs have ~50% reduction in $[Cl^-]_i$ (31.5 ± 4.8, n = 7 animals, $p < 0.001$) compared to WT (62.1 ± 3.5 mM, n = 5 animals), and in both WT and KO CPECs, intracellular $Cl^-$ is maintained above chemical equilibrium (Figure 5.3). Estimates of $E_{Cl}$ were made using measured $[Cl^-]_i$ but assuming a constant $E_m$, and are consequently considered preliminary. Nevertheless, the results suggest that in the absence of NKCC1, these cells are endowed with other $Cl^-$ uptake mechanisms, a situation similar to that reported for NKCC1-/- olfactory neurons and DRG neurons (Alvarez-Leefmans & Mao, 2015; Nickell, Kleene, & Kleene, 2007).

Using these measurements for intracellular $[Na^+]$ and $[Cl^-]$, a model of the net free energy driving NKCC1 cotransport can be created (Figure 5.4). This model is consistent with the hypothesis that NKCC1 is working in the inward direction and

relatively near to thermodynamic equilibrium, or its FRP, when $[K^+]_o$ is 3 mM, which is the physiological concentration in CSF. Since NKCC1-mediated fluxes are tightly linked to water fluxes (Figure 2.2), changes in CWV act as a surrogate for measuring NKCC1-mediated $K^+$ fluxes in CPECs (Alvarez-Leefmans, 2012; Hamann et al., 2005; Hamann et al., 2010; Rocha-Gonzalez et al., 2008; Zeuthen & Macaulay, 2012). Results show that CPECs are exquisitely sensitive to changes in $[K^+]_o$; varying $[K^+]_o$ as little as $\pm$ 2 mM, keeping the osmolality constant i.e., isosmotic with respect to the control solution, is sufficient to produce changes in CWV of $\pm$ 10 % or greater (Figure 5.5), indicating that NKCC1 reverses transport direction. Although this reversibility is predicted on thermodynamic grounds (Alvarez-Leefmans, 2012; Russell, 2000), to our knowledge, this is the first demonstration of this property of NKCC1. That the changes in CWV are specifically mediated by NKCC1, is evident given that NKCC1 -/- CPECs do not respond these changes in $[K^+]_o$, thus these cells lose their external "$K^+$ sensitivity". As expected from the NKCC1 -/- experiments, pharmacologic inhibition of NKCC1 with 10 μM bumetanide blocks the response to changing $[K^+]_o$ in WT CPECs. These results not only prove the reversibility of NKCC1 transport, but strongly suggest that NKCC1 can function as a sensor and regulator of $[K^+]_o$ in CPECs.

### *The direction of NKCC1 cotransport in CPECs*

To understand the functional role of apical NKCC1 in CPECs, it is critical to determine the direction of NKCC1 transport under basal physiological conditions.

Outwardly directed NKCC1 transport, operating in the net efflux mode, would function solely as a CSF secretion mechanism. Conversely, an inwardly directed NKCC1 transport would have an absorptive function and contribute to maintenance of CWV. The direction of NKCC1 cotransport has been debated since it was first hypothesized that the cotransporter is located to the apical membrane of CPECs by Keep et al., (1994), which was later demonstrated by Plotkin et al., (1997) using immunofluorescence microscopy with NKCC1 specific antibodies (Plotkin et al., 1997). The apical location generates a debate because NKCC1 expression usually occurs in the basolateral membrane of secretory epithelia. In 1998, Wu et al. provided evidence in individual CPECs that contradicts the claims made by Keep et al., (1994), and supports NKCC1 functioning in the inward direction (Wu et al., 1998). The present findings confirm and extend those of Wu and colleagues.

CPECs maintain normal cell volume through a balance of net solute and water influx to efflux. As illustrated in Figure 6.1, basolateral $Na^+$ and $HCO_3^-$ influx occurs through the $Na^+$/ $HCO_3^-$ $Cl^-$ exchanger (NBCE) and the electroneutral $Na^+/HCO_3^-$ cotransporter (NBCn1), and $Cl^-$ uptake occurs via the anion exchanger 2 (AE2) (Praetorius & Damkier, 2017). There is basolateral efflux of $HCO_3^-$ via AE2 and $Cl^-$ via NCBE, with the additional K-Cl efflux through KCC3a (Praetorius & Damkier, 2017). On the apical membrane, $K^+$ influx occurs mostly through NKATP and NKCC1. Apical $Na^+$ influx by the $Na^+$/ $H^+$ exchanger (NHE1), and $Na^+$ and $Cl^-$ influx through NKCC1 (Praetorius & Damkier, 2017). Both outward and inward rectifying $K^+$ channels (Kv 1.1, Kv 1.3, Kir 7.1, KCNQ1, and KCNE2) are present on the apical membrane to facilitate $K^+$ recycling to the lumen, in addition to volume activated K-

$Cl^-$ efflux through KCC4 (Praetorius & Damkier, 2017). While most of the $Cl^-$ efflux is carried by the volume activated and inward rectifying $Cl^-$ channels (Clir and VRAC) (Praetorius & Damkier, 2017). Apical $Na^+$ efflux by NKATP and the electrogenic $Na^+$/ $HCO_3^-$ cotransporter (NBCe2), along with $HCO_3^-$ efflux via NBCe2 and $H^+$ efflux via NHE1 (Praetorius & Damkier, 2017). Carbonic anhydrases are located on the basolateral membrane (CAXII & CAIX) and in the cytosol (CAII), and aquaporin 1 (AQP1) is expressed on the apical membrane (Praetorius & Damkier, 2017). By inactivating NKCC1 on the apical membrane, there is a decrease in $Na^+$, $K^+$, and $Cl^-$ influx, along with associated water. This imbalance in the net solute and water fluxes results in CPECs shrinking until the net solute and water efflux is once again balanced with the net influx, and the new steady-state is obtained. Measurements of CSA of freshly dissociated CPECs from NKCC1 -/- mice shows they are ~18 $\mu m^2$ smaller than those from WT (Figure 4.2); additionally, inhibiting NKCC1-mediated fluxes with bumetanide (10 μM) causes a decrease in CPEC water volume by -15.9 ± 9.1%, (n = 3 animals) (Figure 4.3). Using live-cell imaging microscopy the research presented here extends the results of Wu et al., (1998) by resolving the precise change in CWV that occurs when NKCC1 is inhibited with bumetanide. Further, these measurements include the CSA of NKCC1 -/- CPECs (137 ± 4.9 $\mu m^2$, n = 22 animals), and by extrapolating the radii and treating the cells as hemispherical domes, NKCC1 -/- CPECs have a predicted volume reduction of ~16% (Table 4.1). In comparison with the -15.9% mean CWV reduction observed in bumetanide exposed WT CPECs, one can conclude a near complete inhibition of NKCC1 occurs using 10 μM bumetanide. Wu et al., (1998) used bumetanide concentrations as high as 100

μM to ensure complete inhibition of NKCC1, which can lead to non-specific inhibition of other cation cotransporters expressed in CPECs such as apical KCC4 and basolateral KCC3a (Alvarez-Leefmans, 2012).

NKCC1-mediated ion and associated water fluxes are essential contributors to CWV regulation in both polarized and symmetrical cell types (Hamann et al., 2010; Rocha-Gonzalez et al., 2008; Russell, 2000). The findings presented here demonstrate that NKCC1-mediated fluxes not only contribute to maintaining the normal and constant CWV of CPECS, but also support the hypothesis that under basal conditions NKCC1 is constitutively active in CPECs. When a cotransporter is constitutively active, it is always "on", constantly working. Almost immediately upon the application of 10 μM bumetanide WT CPECs begin to shrink (Figure 4.3), indicating that NKCC1 is actively co-transporting in the inward direction under basal isosmotic conditions. This response is in contrast to what is found some other cell types, including human pigmented retinal epithelial cells and dorsal root ganglion cells (Hamann et al., 2010; Rocha-Gonzalez et al., 2008; Russell, 2000). Thus, NKCC1 is constitutively active in CPECs. Evidence of a constitutively active NKCC1 suggests that in certain cell types, such as CPECs, the cotransporter has a background or persistent phosphorylation state that contributes to cell volume maintenance. In $Cl^-$ transporting secretory epithelial cells of exocrine glands (e.g., salivary, lacrimal, airway epithelium, intestinal crypts, and corneal epithelium), the direction of basolateral NKCC1 cotransport occurs in the same direction as epithelial secretion and NKCC1 participates in trans-cellular $Cl^-$ transport and CWV maintenance (Haas & Forbush, 2000; Hamann et al., 2010; Nakamoto et al., 2007;

Silva et al., 1977; Walcott, Birzgalis, Moore, & Brink, 2005). Interestingly, apical NKCC1 cotransports in the direction opposite to that expected for epithelial secretion in CPECs. In the absence of external $Cl^-$, CPECs experienced a large decrease in CWV, -20.3 ± 1.8% (n = 10 animals), presumably due to cell $Cl^-$ depletion (Figure 4.4A). NKCC1 -/- CPECs responded to external $Cl^-$ removal with a more modest decrease in CWV of -7.7 ± 2.1% (n = 4 animals) (Figure 4.4B), which supports NKCC1 -/- CPECs having less CWV than WT (because they have significantly less $Cl^-$ and $K^+$). The recovery of CWV that followed $Cl^-$ depletion was 55 - 78 % (n = 3 animals) $Na^+$-dependent and 70 – 85 % (n = 3 animals) bumetanide-sensitive in CPECs (Figure 4.4C, D, and APPENDIX B), strengthening the notion that NKCC1 contributes to cell $Cl^-$, water accumulation, and CWV maintenance and it behaves as an absorbing epithelium. Taken together, this evidence supports the hypothesis of Specific Aim 1: A function of NKCC1 in CPECs is the maintenance of both normal and constant CWV. Under physiological conditions NKCC1 is constitutively active, inwardly transporting ions and associated water.

### *Measurements of $[Cl^-]_i$ in single CPECS*

Inhibiting NKCC1 in CPECs with bumetanide is shown to reduce both $Cl^-$ uptake by the cells and $Cl^-$ efflux into the CSF (Johanson et al., 1990; Johnson, Singer, Hoop, & Kazemi, 1987; Preston et al., 1993). NKCC1 -/- CPECs shrink 62% less, $p < 0.01$, in response to $Cl^-$ depletion compared to WT CPECs (Figure 4.4 A-B). These results suggest NKCC1 -/- CPECs have less intracellular $[Cl^-]$ than WT cells. To test

this hypothesis, we measured the $[Cl^-]_i$ of individual CPECs isolated from both WT and NKCC1 -/- mice using the $Cl^-$ indicator MQAE, and find that NKCC1 -/- CPECs have approximately half the $[Cl^-]_i$ as WT CPECs, $p < 0.001$ (Figure 5.3). CPECs from WT have a mean $[Cl^-]_i$ equal to 62.1 ± 3.5 mM (n = 5 animals) and NKCC1 -/- CPECs have a mean $[Cl^-]_i$ of 31.5 ± 4.8 (n = 7 animals). This decrease in $[Cl^-]_i$ of NKCC1 -/- CPECs is in agreement with the findings of Johanson et al., (1990) who report that (10 –100 μM) bumetanide reduces CPEC $Cl^-$ uptake by ~45% (Johanson et al., 1990). They conclude that bumetanide and DIDS (4,4-diisothiocyanatostilbene-2,2'-disulfonic acid, an inhibitor of $Cl^-/HCO3^-$ exchange) equally contribute >90% of $Cl^-$ uptake in CPECs (Johanson et al., 1990). Thus, although NKCC1 is the main $Cl^-$ loader, it is not the only $Cl^-$ loader. For instance, anion exchangers known to be expressed in CPECs (Lindsey et al., 1990; Wu et al., 1998) may contribute to uphill intracellular $Cl^-$ accumulation.

There are three reported values of CPEC $E_m$: Rabbit CPEC have a $E_m$ of -64 mV across the ventricular membrane and an $E_m$ of -50 mV across the basolateral membrane (Welch & Sadler, 1965); bullfrog CPECs have a $E_m$ of -47 mV when $[K^+]_o$ = 2 mM (Zeuthen & Wright, 1981); and rat CPECs have an $E_m$ of -53 mV (Kotera & Brown, 1994). We chose $E_m$ = -53 mV, measured in rat CPECs (Kotera & Brown, 1994) to calculate $E_{Cl}$ from our measurements of $[Cl^-]_i$. The mean estimate $E_{Cl}$ of NKCC1 +/+ CPECs is about -19.71 ± 1.4 mV, which is more depolarized (less negative) than the reported $E_m$ of -53 mV, suggesting that $Cl^-$ is maintained above electrochemical equilibrium in CPECs. The difference between $E_{Cl} - E_m$ (i.e., the

driving force for $Cl^-$) is ~33 mV. The mean $E_{Cl}$ in NKCC1 -/- CPECs is -38.9 ± 4.2 mV (n= 7 animals), therefore $[Cl^-]_i$ appears to be maintained above equilibrium in NKCC1 KO cells as well; but the difference $E_{Cl} - E_m$ is about 13 mV, one third of that estimated in WT cells. Although these are rough estimates, given that we did not measure $E_m$, they suggest that that NKCC1 -/- CPECs have a mechanism of $Cl^-$ uptake other than NKCC1. Whether or not this mechanism is expressed in the NKCC1 -/- due to a compensatory change remains to be determined. In their most recent review, Praetorius and Damkier propose that the two primary $Cl^-$ uptake paths in CPECs are apical NKCC1 and basolateral anion exchanger 2 (AE2) (Praetorius & Damkier, 2017), so this would point to AE2 being the other $Cl^-$ uptake mechanism observed in the NKCC1 -/-.

Assuming that the hypothesis of Praetorius and Damkier (2017) is correct, then CPECs uptake $Cl^-$ on both the apical and basolateral membranes (Figure 6.1). AE2 interacts with plasma membrane bound carbonic anhydrases, and AE2 activity is affected by the $[HCO_3^-]$ localized near the basolateral membrane (Jeong & Hong, 2016). NKCC1 activity is regulated by the phosphorylation of SPAK, which is abundantly expressed in the apical membrane of CPECs (Piechotta, Lu, & Delpire, 2002). SPAK phosphorylation occurs by phosphorylated WNK kinases, and $Cl^-$ can competitively bind to the catalytic domain of WNKs to inhibit their auto-phosphorylation, and consequently inhibit WNK kinase activity (Piala et al., 2014; Shekarabi et al., 2017). There are four WNKs (WNK1 – 4) which are believed to act as $[Cl^-]_i$ and/ or volume sensors that can subsequently modulate the activity of the slc12 family of cation-chloride cotransporters (Gagnon & Delpire, 2012; Hadchouel,

Ellison, & Gamba, 2016; Mercado et al., 2016; Piala et al., 2014; Shekarabi et al., 2017; Terker et al., 2016). In the kidney, Terker and colleagues (2016) find that WNK4 is inhibited when $[Cl^-]_i$ is 0 -40 mM, WNK1 is inhibited when $[Cl^-]_i$ is 60 – 150 mM, and WNK3 is inhibited when $[Cl^-]_i$ is 100 -150 mM (Terker et al., 2016). WNK2 is not included in this list because it is only found in the brain (Terker et al., 2016), and it is not currently known if WNK2 kinase is expressed in CPECs. Given the CPEC $[Cl^-]_i$ of 62 mM, one would hypothesize that WNK1 and WNK3 could control the set-point for NKCC1-mediated $Cl^-$ uptake and KCC3-mediate K-Cl efflux, since WNK1 and WNK3 are known to interact with both NKCC1 and KCC3 (Hadchouel et al., 2016). Additionally, changes in $[K^+]_o$ lead to changes in $Cl^-$ efflux and $[Cl^-]_i$, which can modulate the phosphorylation of WNKs (Shekarabi et al., 2017), supporting NKCC1 functioning as $[K^+]_o$ regulator.

### *Measured $[Na^+]_i$ in single CPECs*

Keep et al., (1994) hypothesize that NKCC1 works in the outward under basal conditions, but near to its FRP, when $[Na^+]_i$ is estimated at ~30 mM (Figure 5.2) (Keep et al., 1994). Wu et al., (1998) estimate a similar value of 32.5 mM using "volume calculations", but it is unclear how the value of 32.5 mM is obtained. Smith and Johanson (1985) report that CPEC $[Na^+]_i$ = 34 –52 mM and Amin et al., (2009) report a value of 35 mM, it should be noted that both measurements were taken using pieces of choroid plexus tissue, Smith and Johanson use flame photometry and Amin et al. use Sodium Green fluorescence of choroidal epithelia containing

several cells (Amin et al., 2009; Smith & Johanson, 1985). As pointed out by Minta and Tsein (1989), measuring $[Na^+]_i$ using methods that measure the $Na^+$ content in whole tissue will produce erroneously high $[Na^+]$, because 1) both intracellular and extracellular fluid is present in whole tissue making it difficult to assess the exact value of extra and intracellular water, particularly in a tissue composed of many cell types like the CP; and 2) methods such as flame photometry measure the total $[Na^+]$, i.e., free plus bound, a value that is greater than the intracellular concentration of *free* $Na^+$ (Minta & Tsien, 1989). The major downside to the methods employed by Johanson's group is that they use an estimate of percent cell water (Murphy & Johanson, 1990; Smith & Johanson, 1985) and cannot accurately determine the ratio of bound vs free $Na^+$ in their measurements, nor can they differentiate between intra- vs extracellular $Na^+$ in the whole tissue. Similarly, Amin et al., (2009) loaded pieces of choroid plexus tissue with Sodium Green to obtain the $[Na^+]$ of the epithelium and assume its equivalence to CPEC $[Na^+]_i$ without controlling for the presence extracellular fluid or the vasculature.

Using the recently developed Asante Natrium Green 2 indicator from TEFLabs, Inc., we successfully performed the first $[Na^+]_i$ measurements in individual mammalian CPECs. Our measurement of free intracellular $[Na^+]_i$ in CPECs is 8.4 ± 1.0 mM (n = 3 animals) under basal conditions (Figure 5.1). With this $[Na^+]_i$ the net free energy driving NKCC1 transport is inwardly directed in CPECs (Figure 5.2). Additionally, there is no significant difference between the $[Na^+]_i$ of WT verses NKCC1 -/- CPECs (12.2 ± 1.2 mM, n = 3 animals, p = 0.07).

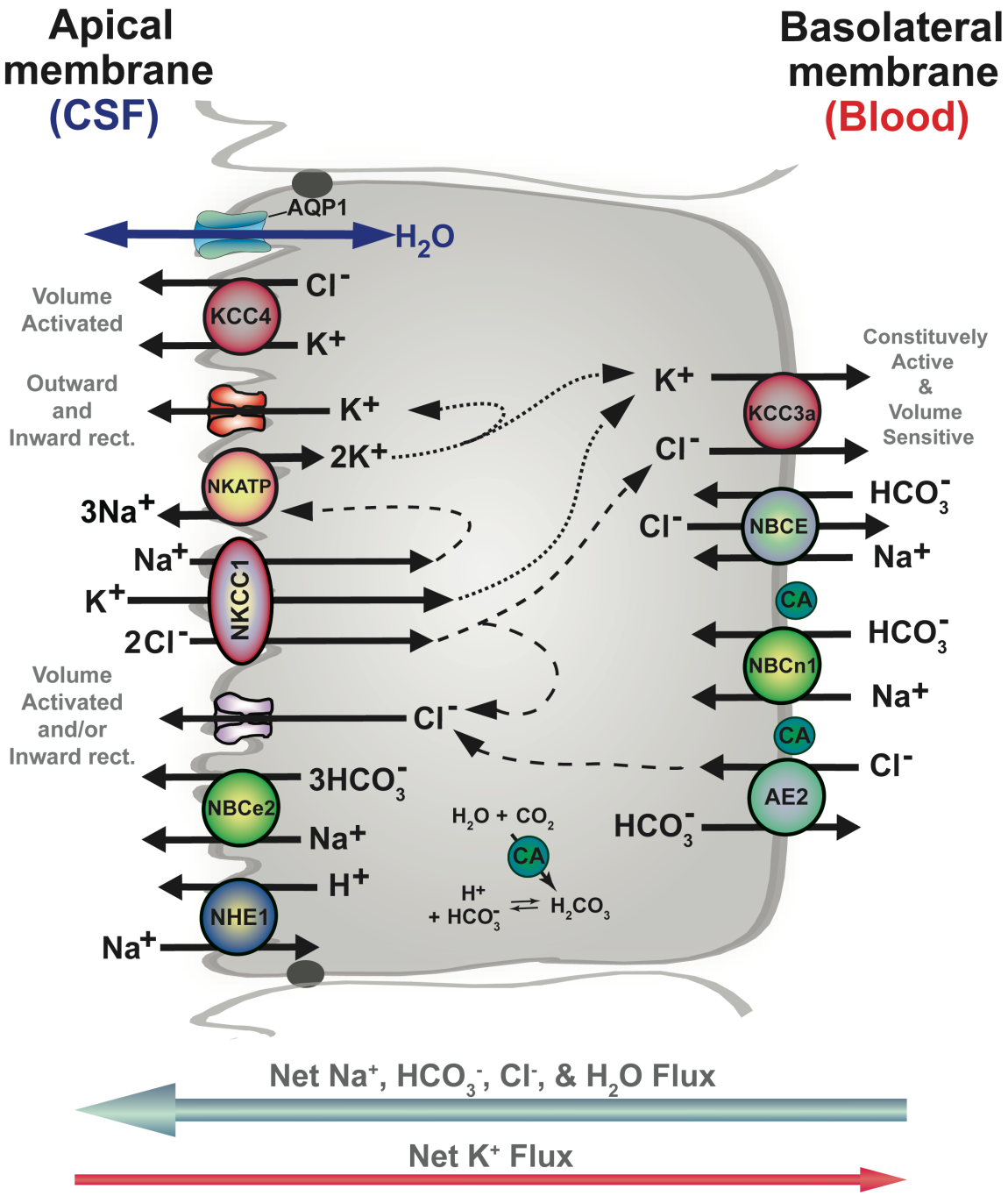


***Figure 6.1: Proposed model of NKCC1 function in CPECs under basal conditions.*** *CPECs not only secrete CSF but also regulate CSF [$K^+$] using NKCC1. This homeostatic mechanism is crucial for normal brain function*

*because $K^+$ freely diffuses between CSF and interstitial brain fluid. Modest elevations in CSF [$K^+$] increases net inward ion and water transport mediated by NKCC1. CSF $K^+$ is taken up into CPECs via NKCC1 & NKATP and either exits through basolateral KCC3a or is recycled back into the lumen by $K^+$ channels (Brown et al., 2004; Praetorius & Damkier, 2017). $Na^+$ is recycled by the apical NKATP, and $Cl^-$ is partly recycled via apical $Cl^-$ channels and KCCs. Apical KCC4 is only activated upon osmotic cell swelling, whereas basolateral KCC3a is constitutively active (Alvarez-Leefmans, 2012). This model is consistent with the notion that apical NKCC1 plays a key role in the reabsorption of $K^+$ from CSF to blood and in the regulation of brain extracellular [$K^+$].*

### *NKCC1 functions as a sensor and regulator of CSF [$K^+$]*

It is known that CSF $K^+$ is tightly regulated given its constant concentration in spite of variations in plasma and intraventricular $K^+$ (Ames et al., 1965; Bekaert & Demeester, 1954; Bradbury & Kleeman, 1967; Cserr, 1965; Husted & Reed, 1976). This $K^+$ regulation occurs independently and in parallel to CSF secretion (Ames et al., 1965; Cserr, 1965; Husted & Reed, 1976). CPECs actively uptake $K^+$ through the combined actions of NKATP and NKCC1, both located on the apical membrane (see Figure 6.1) (Bairamian et al., 1991; Parmelee & Johanson, 1989; Saito & Wright, 1987; Wu et al., 1998). Husted and Reed (1976) propose the existence of a mechanism in the CP that is capable of regulating CSF [$K^+$]. This mechanism enables CPECs to substantially decrease the amount of $K^+$ secreted when CSF $K^+$ is high (6.56 mEq. /l), and also slightly increase the amount of $K^+$ secreted when CSF $K^+$ is very low (0.15 mEq. /l) (Husted & Reed, 1976). However, the identity of this CSF [$K^+$] regulation mechanism remained to be determined. Our results demonstrate that freshly dissociated CPECs are exquisitely sensitive to small changes in $[K^+]_o$, and CPECs lose this $K^+$ sensitivity when NKCC1-mediated fluxes are removed by either pharmacological inhibition or genetic ablation. By modeling the net free energy driving NKCC1 transport ($\Delta\mu_{NKCC1}$) with respect to $[K^+]_o$, we find $\Delta\mu_{NKCC1}$ to be negative. Thus, apical NKCC1 works near to its FRP for basal $K^+$ (2.9 mM) but in the net inward mode, FRP occurs $[K^+]_o \approx 1.4$ -1.6 mM, in CPECs (Figure 5.4). NKCC1 has

a $K_m$ for $K^+$ of 2.7 mM (Payne & Forbush, 1995), thus $\Delta\mu_{NKCC1}$ is in the steep part of the relation in the range near basal $[K^+]_o$ (Figure 5.4).

Using the model as our guide, we tested the CPEC sensitivity to $\pm$ 2 mM $K^+$ with respect to baseline $K^+$ (3 mM), and keeping the osmolality of the solutions constant (Figure 5.5). When we increase $[K^+]_o$ from 3 to 5 mM CPECs swell, increasing their volume by 10.4 ± 1.6% (n = 8 animals). When we decrease $[K^+]_o$ from 3 to 1mM CPECs shrink, decreasing their volume by -11.8 ± 1.7% (n = 11 animals). When we repeat these experiments using NKCC1 -/- CPECs, there is no statistically significant response to either 1 or 5 mM $K^+$ (Figure 5.5). Similarly, WT CPECs lose their ability to respond to $\pm$ 2 mM changes in $[K^+]_o$ when NKCC1 activity is blocked with 10 μM bumetanide (Figure 5.6). CPECs maintain $HCO_3^-$ above chemical equilibrium, and $HCO_3^-$ is important for CSF secretion as inhibiting carbonic anhydrase (CA) decreases the rate of CSF production by 30 –80 % (Saito & Wright, 1983, 1984; Vogh & Langham, 1981). $Cl^-/HCO_3^-$ exchange (AE2) is modulated by plasma membrane bound CA, therefore inhibiting $HCO_3^-$ production decreases $Cl^-$ uptake on the basolateral membrane (Jeong & Hong, 2016). The physiological saline solutions used in our experiments are buffered with HEPES and equilibrated with air. Atmospheric $CO_2$ is able to dissolve into the solutions where it can readily enter the cell and convert to $HCO_3^-$ by carbonic anhydrases present inside the cell and on the plasma membrane (Wright, 1978). To test the hypothesis that using HEPES buffered solutions does not alter the ability of CPECs to respond to

changes in $[K^+]_o$, the $K^+$ experiments are repeated using $CO_2/HCO_3^-$ buffered saline solutions.

In the presence of added $HCO_3^-$ the CWV responses to $\pm$ 2 mM $[K^+]_o$ are slightly larger (Table 5.2) but not statistically different. During exposure to 1 mM $K^+$ CPECs shrink -13.1 $\pm$ 2.3 % (n = 4 animals), and during exposure to 5 mM $K^+$ CPECs swell 16.6 $\pm$ 2.9 % (n = 4 animals). A t-test finds no difference in the 1 mM $K^+$ responses between either buffer, p = 0.69, and no significant difference in the 5 mM $K^+$ responses, p = 0.07. Altogether, these results suggests that NKCC1 is the $K^+$ sensor described by Husted and Reed (1976) and supports the hypothesis of Specific Aim 2: <u>NKCC1 is working near to its chemical equilibrium in CPECs, therefore small changes in $[K^+]_o$ are sufficient to alter both the direction and magnitude of NKCC1-mediated ion and associated water fluxes.</u>

In summary, on the apical membrane of CPECs, NKATP and NKCC1 work in concert to maintain the low CSF $K^+$ concentration (Figure 6.1). However, NKATP activity alone cannot account for the CSF $K^+$ sensing and regulating abilities of CPECs. NKATP$\alpha 1\beta 1/\beta 2$ has a high affinity for $K^+$, bring in two $K^+$ ions per cycle with a $K_m$ for external $K^+$ of 0.92 –1.16 mM; whereas NKCC1 has a lower affinity for external $K^+$, $K_m \approx 2.7$mM, and uptakes one $K^+$ ion along with a $Na^+$ and two $Cl^-$ ions (Brown et al., 2004; Crambert et al., 2000; Payne & Forbush, 1995; Russell, 2000; Watts et al., 1991). So, when CSF $[K^+]$ is ~ 3 mM, NKATP is transporting more $K^+$ into the CPECs than NKCC1, but NKCC1 has a greater response rate to fluctuations in CSF $[K^+]$. Together, NKATP and NKCC1 bring in the $K^+$ and $Cl^-$ that is required for

basolateral K-Cl efflux via KCC3a, the sole $K^+$ transporter mechanism on the basolateral membrane of CPECs known thus far (Praetorius & Damkier, 2017). NKATP and NKCC1 may also work in concert to regulate CPEC $Na^+$ secretion, with NKATP acting as the major $Na^+$ secretion mechanism and $Na^+$ efflux regulation occurring through the inward transport of NKCC1 (Gagnon & Delpire, 2012). Both $[K^+]_o$ and $[Na^+]_i$ are limited in their respective compartments and prone to fluctuations that can subsequently alter the direction of net ion and associated water fluxes mediated by NKCC1. Increases in $[Na^+]_i$ occur with increases in $[HCO3^-]_i$ (Zeuthen & Wright, 1981), and fluctuations in the intracellular ion concentrations may occur during normal CSF secretion. Figure 6.2 illustrates how both $[K^+]_o$ and $[Na^+]_i$ impact the direction of NKCC1 cotransport in CPECs. The graph illustrates that both low $[Na^+]_i$ and high $[K^+]_o$ promote inwardly directed NKCC1 cotransport in CPECs. In the physiological range, when $[K^+]_o$ is 2 – 4 mM and $[Na^+]_i$ is 10 – 20 mM, $\Delta\mu_{NKCC1}$ is working very near to its FRP and has the ability to reverse the direction of transport outwards if either $[Na^+]_i$ becomes too high or $[K^+]_o$ becomes too low. Therefore, the $[Na^+]_i$ that is maintained by NKATP can influence the FRP of NKCC1 with respect to $[K^+]_o$ and can modulate $\Delta\mu_{NKCC1}$. The NKATP $Na^+$ efflux is a major driver of CSF secretion, as ouabain reduces CSF production, and this points to the essential roles of NKATP in maintaining both the osmotic and electrochemical gradients necessary for CSF secretion (Karimy et al., 2016). It is clear that both NKATP and NKCC1 are important contributors to CSF secretion and regulation. Their expression on the apical membrane ensures that there is no $K^+$ uptake by

CPECs from the blood (Figure 6.1). The ability of CPECs to recycle $K^+$ at the apical membrane is one way in which the CSF $[K^+]$ is maintained at 2.9 mM.

Under basal conditions NKCC1 is working in the net influx mode but near to its FRP for external $K^+$, which Russell (2000) describes as under $\pm$ 1 KJ/ mol. NKCC1 working near its FRP is normal in some cells types, such as Ehrlich ascites tumor cells and bovine aortic endothelial cells, and is not an indication that the cotransporter reverses transport direction (Russell, 2000). It is unlikely that $[K^+]_{CSF}$ would ever become low enough to support NKCC1 outward transport. Rare cases of lower CSF $[K^+]$ do occur in some people with concomitant presentation of hypokalemia schizophrenic-like psychiatric disorders (Hatta et al., 1999; Lam, Chau, & Wing, 2009; Plum, 1958). However, measured CSF $[K^+]$ in psychiatric patients does not lower more than 3% (Plum, 1958), and so is insufficient to reverse the direction of NKCC1 transport. Therefore, we propose that in CPECs, the cotransporter functions as a $K^+$ absorption mechanism under basal conditions, similar to how it functions in glia (Lu et al., 2006; Macaulay & Zeuthen, 2012). Going back to the work of Keep and colleagues (1994), we find a few retrospective issues in their conclusions. First, Keep et al., inhibited K-Cl cotransport with R(+)-butylindazone (DOIA), a good inhibitor of KCC3 and poor inhibitor of KCC4 (Alvarez-Leefmans, 2012; Keep et al., 1994). Additionally, as our work demonstrates, blocking NKCC1-mediated inward ion fluxes decreases $[Cl^-]_i$ that consequently reduces the amount of $Cl^-$ efflux. If CPECs rely on KCCs for $K^+$ efflux, then reducing the $[Cl^-]_i$ would both reduce the available cell $Cl^-$ and promote WNKs,

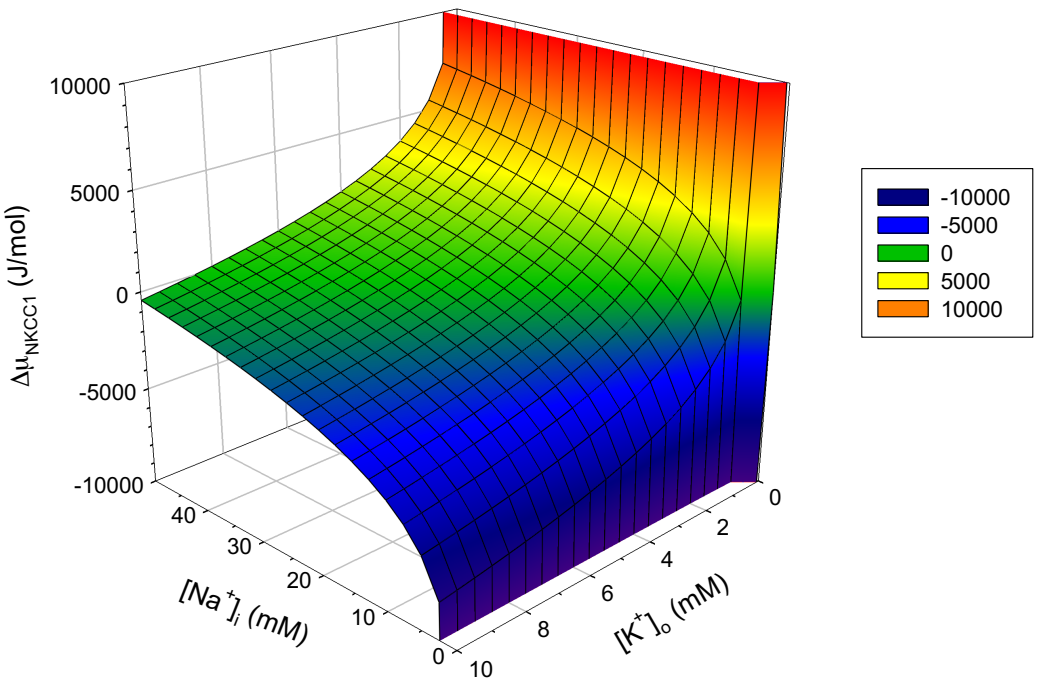


***Figure 6.2: 3D Model of the FRP of NKCC1 in CPECs***

*3-dimensional model of the direction of NKCC1 cotransport with respect to intracellular $[Na^+]$ and CSF $[K^+]$. $\Delta\mu_{NKCC1}$ was calculated at 310 K, with $[Na^+]_o$ = 148 mM, $[Cl^-]_o$ = 130 mM, $[K^+]_o$ = 0 – 10 mM, $[Na^+]_i$ = 0 – 50 mM, $[Cl^-]_i$ = 62.1 mM, and $[K^+]_i$ = 110 mM. Modeling FRP of NKCC1 with respect to $[K^+]_o$ and $[Na^+]_i$ , and on the right is a color guide for values of $\Delta\mu_{NKCC1}$. The dark green areas are when NKCC1 is working very near to its FRP. As the color becomes blue, NKCC1 is working in the inward direction and farther away from its FRP. Areas where the graph is yellow and red indicate that NKCC1 is working in the outward direction and away from its FRP—acting solely in the ion secretion mode.*

and subsequently SPAK and KCC, phosphorylation that deactivates KCC $K^+$ efflux. Keep et al., (1994) proposed NKCC1 working near flux reversal as an explanation of their results and those of Javaheri and Wagner (1993), who demonstrate that intraventricular bumetanide decreases CSF secretion. We propose that the explanation is that the constitutively active apical NKCC1 cotransporter on CPECs functions to maintain both $[Cl^-]_i$ and CWV that is necessary for normal CSF secretion and $K^+$ absorption. NKCC1 is likely able to sense and regulate the $[K^+]_o$ through $[Cl^-]_i$, similarly to the $Na^+$/ $Cl^-$ symporter (Shekarabi et al., 2017). The low $[K^+]_o$ of the CSF promotes apical $Cl^-$ efflux by maintaining a hyperpolarized membrane potential that is more negative than $E_{Cl}$ (Frizzell & Hanrahan, 2012; Russell, 2000). Changes in $[K^+]_o$ lead to changes in $[Cl^-]_i$ and cell volume, thereby modulating the reciprocal phosphorylation states of WNKs, SPAK, NKCC1, KCC3, and KCC4 (Shekarabi et al., 2017).

### *Future Directions*

NKCC1 inhibition is currently under investigation as a treatment strategy to reduce cytotoxic edema/ glial swelling and promote neurogenesis following brain injuries (Begum et al., 2015; Glykys et al., 2017; Hertz & Chen, 2016; Hui et al., 2016; Jantzie et al., 2015; Jayakumar et al., 2011; Kahle et al., 2009; Wang, Huang, He, Ruan, & Huang, 2014; Zhang, Pu, et al., 2017). Recent research points to WNK3 and SPAK as excellent drug targets to reduce cytotoxic edema and improve recovery (Zhao et al., 2017). In a focal ischemic stroke model WNK3 -/-, SPAK -/-, and SPAK

+/- mice have a > 50% reduction in lesion size and improved recovery compared to WT mice (Zhao et al., 2017). While it appears that inhibition of NKCC1 or its regulatory kinases improves brain injury outcome and recovery, this NKCC1 inactivation means there will be an increase in brain $[K^+]_o$ that will have to be removed. It is critical to understand how NKCC1/SPAK/WNKs inhibition in the brain parenchyma can affect the ability of the choroid plexus to absorb excess $K^+$ and secrete CSF. NKCC1 contributes indirectly to CSF secretion and can be a drug target to reduce CSF production. Further work is also needed to develop a drug capable of crossing the blood-brain and blood-CSF barriers to inhibit NKCC1 directly or inactivate SPAK or WNKs (Zhang, Karimy, Delpire, & Kahle, 2017). By analyzing the CSF composition and neuronal function of the NKCC1 -/- mouse, the consequence of NKCC1 inhibition in the brain will be better understood. Also, it would then be possible to test how NKCC1 -/- respond to increases in CSF $K^+$ from injury, and whether the decrease in CSF production helps with brain edema. The use of knockout animals is increasingly more common and it is critical to have a thorough understanding of the physiology of these animals. Preliminary work verifies the expression of NKATP$\alpha$1 and AQP1 on the apical membrane of NKCC1 -/- CPECs (see Appendix A), and more work is needed to complete the screening by including all $K^+$ cotransporters, and performing a quantitative fluorescence intensity analysis. Further, measuring the CPEC $[K^+]_i$ using Asante Potassium Green (TEFLabs) is necessary to complete the model of NKCC1 cotransport so that computer models of NKCC1 transport can be used in place of animals. All intracellular ion measurements need repeating using bicarbonate-buffered aCSF as

control, as well as test solutions which are buffered using a combination of both HEPES and bicarbonate.

## *References*


Alvarez-Leefmans, F. J. (2012). Intracellular Chloride Regulation. In N. Sperelakis (Ed.), *Cell Physiology Source Book: Essentials of Membrane Biophysics* (4th ed., pp. 221- 260). London: Academic Press.

Alvarez-Leefmans, F. J., and Mao, S. (2015). Higher than Equilibrium Intracellular Cl- Concentration in Dorsal Root Ganglion Neurons of NKCC1 Knockout Mice. . *The FASEB Journal, 29*(1), Supplement 845.822.

Alvarez-Leefmans, F. J., Herrera-Perez, J. J., Marquez, M. S., & Blanco, V. M. (2006). Simultaneous measurement of water volume and pH in single cells using BCECF and fluorescence imaging microscopy. *Biophys J, 90*(2), 608-618. doi:10.1529/biophysj.105.069450

Ames, A., 3rd, Higashi, K., & Nesbett, F. B. (1965). Relation of potassium concentration in choroidplexus fluid to that in plasma. *J Physiol, 181*(3), 506-515.

Amin, M. S., Reza, E., Wang, H., & Leenen, F. H. (2009). Sodium transport in the choroid plexus and salt-sensitive hypertension. *Hypertension, 54*(4), 860-867. doi:10.1161/HYPERTENSIONAHA.108.125807

Bairamian, D., Johanson, C. E., Parmelee, J. T., & Epstein, M. H. (1991). Potassium cotransport with sodium and chloride in the choroid plexus. *J Neurochem, 56*(5), 1623-1629.

Begum, G., Yuan, H., Kahle, K. T., Li, L., Wang, S., Shi, Y., . . . Sun, D. (2015). Inhibition of WNK3 Kinase Signaling Reduces Brain Damage and Accelerates Neurological Recovery After Stroke. *Stroke, 46*(7), 1956-1965. doi:10.1161/STROKEAHA.115.008939

Bekaert, J., & Demeester, G. (1954). Influence of the potassium concentration of the blood on the potassium level of the cerebrospinal fluid. *Exp Med Surg, 12*(4), 480-501.

Bradbury, M. W., & Kleeman, C. R. (1967). Stability of the potassium content of cerebrospinal fluid and brain. *Am J Physiol, 213*(2), 519-528.

Brown, P. D., Davies, S. L., Speake, T., & Millar, I. D. (2004). Molecular mechanisms of cerebrospinal fluid production. *Neuroscience, 129*(4), 957-970. doi:10.1016/j.neuroscience.2004.07.003

Brown, P. D., Davies, S. L., and Millar, I. D. (2009). Ion Transport in Choroid Plexus. In F. J. a. D. Alvarez-Leefmans, E. (Ed.), *Physiology and Pathology of Chloride Transporters and Channels in the Nervous System* (pp. 569-584): Elsevier Inc.

Bulat, M., & Klarica, M. (2011). Recent insights into a new hydrodynamics of the cerebrospinal fluid. *Brain Res Rev, 65*(2), 99-112. doi:10.1016/j.brainresrev.2010.08.002

Conrad E. Johanson, E. G. S., and Paul N. McMillan. (2011). The Blood–Cerebrospinal Fluid Barrier: Structure

and Functional Significance. In S. Nag (Ed.), The Blood-Brain and Other Neural Barriers: Reviews and ProtocolsMethods in Molecular Biology (Vol. 686, pp. 101- 131): Springer Science+Business Media, LLC. doi:10.1007/978-1-60761-938-3_4

Crambert, G., Hasler, U., Beggah, A. T., Yu, C., Modyanov, N. N., Horisberger, J. D., . . . Geering, K. (2000). Transport and pharmacological properties of nine different human Na, K-ATPase isozymes. *J Biol Chem, 275*(3), 1976-1986.

Crowe, W. E., Altamirano, J., Huerto, L., & Alvarez-Leefmans, F. J. (1995). Volume changes in single N1E-115 neuroblastoma cells measured with a fluorescent probe. *Neuroscience, 69*(1), 283-296.

Cserr, H. (1965). Potassium exchange between cerebrospinal fluid, plasma, and brain. *American Journal of Physiology, 209*(6), 1219-1226.

Damkier, H. H., Brown, P. D., & Praetorius, J. (2010). Epithelial pathways in choroid plexus electrolyte transport. *Physiology (Bethesda), 25*(4), 239-249. doi:10.1152/physiol.00011.2010

Deitmer, J. W., & Becker, H. M. (2013). Transport metabolons with carbonic anhydrases. *Front Physiol, 4*, 291. doi:10.3389/fphys.2013.00291

Deitmer, J. W., Theparambil, S. M., Ruminot, I., & Becker, H. M. (2014). The role of membrane acid/base transporters and carbonic anhydrases for cellular pH and metabolic processes. *Front Neurosci, 8*, 430. doi:10.3389/fnins.2014.00430

Delpire, E., & Gagnon, K. B. (2006). SPAK and OSR1, key kinases involved in the regulation of chloride transport. *Acta Physiol (Oxf), 187*(1-2), 103-113. doi:10.1111/j.1748-1716.2006.01565.x

Delpire, E., Lu, J., England, R., Dull, C., & Thorne, T. (1999). Deafness and imbalance associated with inactivation of the secretory Na-K-2Cl co-transporter. *Nat Genet, 22*(2), 192-195. doi:10.1038/9713

Donoso, P., Mill, J. G., O'Neill, S. C., & Eisner, D. A. (1992). Fluorescence measurements of cytoplasmic and mitochondrial sodium concentration in rat ventricular myocytes. *J Physiol, 448*, 493-509.

Eisener-Dorman, A. F., Lawrence, D. A., & Bolivar, V. J. (2009). Cautionary insights on knockout mouse studies: the gene or not the gene? *Brain Behav Immun, 23*(3), 318-324. doi:10.1016/j.bbi.2008.09.001

Evans, R. L., Park, K., Turner, R. J., Watson, G. E., Nguyen, H. V., Dennett, M. R., . . . Melvin, J. E. (2000). Severe impairment of salivation in Na+/K+/2Cl-cotransporter (NKCC1)-deficient mice. *J Biol Chem, 275*(35), 26720-26726. doi:10.1074/jbc.M003753200

Fisher, R. G., & Copenhaver, J. H. (1959). The metabolic activity in the choroid plexus. *J Neurosurg, 16*(2), 167-176. doi:10.3171/jns.1959.16.2.0167

Flagella, M., Clarke, L. L., Miller, M. L., Erway, L. C., Giannella, R. A., Andringa, A., . . . Shull, G. E. (1999). Mice lacking the basolateral Na-K-2Cl cotransporter have impaired epithelial chloride secretion and are profoundly deaf. *J Biol Chem, 274*(38), 26946-26955.

Francisco J. Alvarez-Leefmans, J. A., & William E. Crowe. (1995). Use of ion-selective microelectrodes and fluorescent probes to measure cell volume. In J. K. S. J. Dixon (Ed.), *Methods in Neurosciences: Measurement and Manipulation of Intracellular Ions* (Vol. 27, pp. Chapter 19;361-391). San Diego: Academic Press.

Frizzell, R. A., & Hanrahan, J. W. (2012). Physiology of epithelial chloride and fluid secretion. *Cold Spring Harb Perspect Med, 2*(6), a009563. doi:10.1101/cshperspect.a009563

Gagnon, K. B., & Delpire, E. (2012). Molecular physiology of SPAK and OSR1: two Ste20-related protein kinases regulating ion transport. *Physiol Rev, 92*(4), 1577-1617. doi:10.1152/physrev.00009.2012

Gagnon, K. B., England, R., & Delpire, E. (2006). Characterization of SPAK and OSR1, regulatory kinases of the Na-K-2Cl cotransporter. *Mol Cell Biol, 26*(2), 689-698. doi:26/2/689 [pii]

10.1128/MCB.26.2.689-698.2006

Gagnon, K. B., England, R., & Delpire, E. (2007). A single binding motif is required for SPAK activation of the Na-K-2Cl cotransporter. *Cell Physiol Biochem, 20*(1-4), 131-142. doi:10.1159/000104161

Giacobini, E. (1961). Localization of carbonic anhydrase in the nervous system. *Science, 134*(3489), 1524-1525.

Giacobini, E. (1962). A cytochemical study of the localization of carbonic anhydrase in the nervous system. *J Neurochem, 9*, 169-177.

Glykys, J., Dzhala, V., Egawa, K., Kahle, K. T., Delpire, E., & Staley, K. (2017). Chloride Dysregulation, Seizures, and Cerebral Edema: A Relationship with Therapeutic Potential. *Trends Neurosci, 40*(5), 276-294. doi:10.1016/j.tins.2017.03.006

Grimm, P. R., Taneja, T. K., Liu, J., Coleman, R., Chen, Y. Y., Delpire, E., . . . Welling, P. A. (2012). SPAK Isoforms and OSR1 Regulate Sodium-Chloride Co-transporters in a Nephron-specific Manner. *J Biol Chem, 287*(45), 37673-37690. doi:10.1074/jbc.M112.402800

Grynkiewicz, G., Poenie, M., & Tsien, R. Y. (1985). A new generation of Ca2+ indicators with greatly improved fluorescence properties. *J Biol Chem, 260*(6), 3440-3450.

Haas, M., & Forbush, B., 3rd. (2000). The Na-K-Cl cotransporter of secretory epithelia. *Annu Rev Physiol, 62*, 515-534. doi:10.1146/annurev.physiol.62.1.515

Hadchouel, J., Ellison, D. H., & Gamba, G. (2016). Regulation of Renal Electrolyte Transport by WNK and SPAK-OSR1 Kinases. *Annu Rev Physiol, 78*, 367-389. doi:10.1146/annurev-physiol-021115-105431

Hamann, S., Herrera-Perez, J. J., Bundgaard, M., Alvarez-Leefmans, F. J., & Zeuthen, T. (2005). Water permeability of Na+-K+-2Cl- cotransporters in mammalian epithelial cells. *J Physiol, 568*(Pt 1), 123-135. doi:jphysiol.2005.093526 [pii]

10.1113/jphysiol.2005.093526

Hamann, S., Herrera-Perez, J. J., Zeuthen, T., & Alvarez-Leefmans, F. J. (2010). Cotransport of water by the Na+-K+-2Cl(-) cotransporter NKCC1 in

mammalian epithelial cells. *J Physiol, 588*(Pt 21), 4089-4101. doi:10.1113/jphysiol.2010.194738

Harootunian, A. T., Kao, J. P., Eckert, B. K., & Tsien, R. Y. (1989). Fluorescence ratio imaging of cytosolic free Na+ in individual fibroblasts and lymphocytes. *J Biol Chem, 264*(32), 19458-19467.

Hatta, K., Takahashi, T., Nakamura, H., Yamashiro, H., Asukai, N., & Yonezawa, Y. (1999). Hypokalemia and agitation in acute psychotic patients. *Psychiatry Res, 86*(1), 85-88.

Hertz, L., & Chen, Y. (2016). Importance of astrocytes for potassium ion (K+) homeostasis in brain and glial effects of K+ and its transporters on learning. *Neurosci Biobehav Rev, 71*, 484-505. doi:10.1016/j.neubiorev.2016.09.018

Hughes, A. L., Pakhomova, A., & Brown, P. D. (2010). Regulatory volume increase in epithelial cells isolated from the mouse fourth ventricle choroid plexus involves Na(+)-H(+) exchange but not Na(+)-K(+)-2Cl(-) cotransport. *Brain Res, 1323*, 1-10. doi:10.1016/j.brainres.2009.12.094

Hui, H., Rao, W., Zhang, L., Xie, Z., Peng, C., Su, N., . . . Fei, Z. (2016). Inhibition of Na(+)-K(+)-2Cl(-) Cotransporter-1 attenuates traumatic brain injury-induced neuronal apoptosis via regulation of Erk signaling. *Neurochem Int, 94*, 23-31. doi:10.1016/j.neuint.2016.02.002

Husted, R. F., & Reed, D. J. (1976). Regulation of cerebrospinal fluid potassium by the cat choroid plexus. *J Physiol, 259*(1), 213-221.

Jantzie, L. L., Hu, M. Y., Park, H. K., Jackson, M. C., Yu, J., Maxwell, J. R., & Jensen, F. E. (2015). Chloride cotransporter NKCC1 inhibitor bumetanide protects against

white matter injury in a rodent model of periventricular leukomalacia. *Pediatr Res, 77*(4), 554-562. doi:10.1038/pr.2015.9

Javaheri, S., & Wagner, K. R. (1993). Bumetanide decreases canine cerebrospinal fluid production. In vivo evidence for NaCl cotransport in the central nervous system. *J Clin Invest, 92*(5), 2257-2261. doi:10.1172/JCI116829

Jayakumar, A. R., Panickar, K. S., Curtis, K. M., Tong, X. Y., Moriyama, M., & Norenberg, M. D. (2011). Na-K-Cl cotransporter-1 in the mechanism of cell swelling in cultured astrocytes after fluid percussion injury. *J Neurochem, 117*(3), 437-448. doi:10.1111/j.1471-4159.2011.07211.x

Jeong, Y. S., & Hong, J. H. (2016). Governing effect of regulatory proteins for Cl(-)/HCO3(-) exchanger 2 activity. *Channels (Austin), 10*(3), 214-224. doi:10.1080/19336950.2015.1134068

Johanson, C. E., Duncan, J. A., 3rd, Klinge, P. M., Brinker, T., Stopa, E. G., & Silverberg, G. D. (2008). Multiplicity of cerebrospinal fluid functions: New challenges in health and disease. *Cerebrospinal Fluid Res, 5*, 10. doi:10.1186/1743-8454-5-10

Johanson, C. E., & Murphy, V. A. (1990). Acetazolamide and insulin alter choroid plexus epithelial cell [Na+], pH, and volume. *Am J Physiol, 258*(6 Pt 2), F1538-1546.

Johanson, C. E., Stopa, E. G., & McMillan, P. N. (2011). The blood-cerebrospinal fluid barrier: structure and functional significance. *Methods Mol Biol, 686*, 101-131. doi:10.1007/978-1-60761-938-3_4

Johanson, C. E., Sweeney, S. M., Parmelee, J. T., & Epstein, M. H. (1990). Cotransport of sodium and chloride by the adult mammalian choroid plexus. *Am J Physiol, 258*(2 Pt 1), C211-216.

Johnson, D. C., Singer, S., Hoop, B., & Kazemi, H. (1987). Chloride flux from blood to CSF: inhibition by furosemide and bumetanide. *J Appl Physiol (1985), 63*(4), 1591-1600.

Johnson, D. C., Singer, S., Hoop, B., Kazemi, H. (1987). Chloride flux from blood to CSF: inhibition by furosemide and bumetanide. *J Appl Physiol (1985), 63*, 1591-1600.

Jones, H. C., & Keep, R. F. (1987). The control of potassium concentration in the cerebrospinal fluid and brain interstitial fluid of developing rats. *J Physiol, 383*, 441-453.

Kahle, K. T., Simard, J. M., Staley, K. J., Nahed, B. V., Jones, P. S., & Sun, D. (2009). Molecular mechanisms of ischemic cerebral edema: role of electroneutral ion transport. *Physiology (Bethesda), 24*, 257-265. doi:10.1152/physiol.00015.2009

Kaneko, H., Putzier, I., Frings, S., Kaupp, U. B., & Gensch, T. (2004). Chloride accumulation in mammalian olfactory sensory neurons. *J Neurosci, 24*(36), 7931-7938. doi:10.1523/JNEUROSCI.2115-04.2004

Karimy, J. K., Duran, D., Hu, J. K., Gavankar, C., Gaillard, J. R., Bayri, Y., . . . Kahle, K. T. (2016). Cerebrospinal fluid hypersecretion in pediatric hydrocephalus. *Neurosurg Focus, 41*(5), E10. doi:10.3171/2016.8.FOCUS16278

Keep, R. F., & Xiang, J. (1995). Choroid plexus potassium cotransport: modulation by osmotic stress and external potassium. *J Neurochem, 64*(6), 2747-2754.

Keep, R. F., Xiang, J., & Betz, A. L. (1994). Potassium cotransport at the rat choroid plexus. *Am J Physiol, 267*(6 Pt 1), C1616-1622.

Koncz, C., & Daugirdas, J. T. (1994). Use of MQAE for measurement of intracellular [Cl-] in cultured aortic smooth muscle cells. *Am J Physiol, 267*(6 Pt 2), H2114-2123.

Kotera, T., & Brown, P. D. (1994). Evidence for two types of potassium current in rat choroid plexus epithelial cells. *Pflugers Arch, 427*(3-4), 317-324.

Krapf, R., Berry, C. A., & Verkman, A. S. (1988). Estimation of intracellular chloride activity in isolated perfused rabbit proximal convoluted tubules using a fluorescent indicator. *Biophys J, 53*(6), 955-962. doi:10.1016/S0006-3495(88)83176-X

Lam, M. H., Chau, S. W., & Wing, Y. K. (2009). High prevalence of hypokalemia in acute psychiatric inpatients. *Gen Hosp Psychiatry, 31*(3), 262-265. doi:10.1016/j.genhosppsych.2009.02.007

Lamy, C. M., & Chatton, J. Y. (2011). Optical probing of sodium dynamics in neurons and astrocytes. *Neuroimage, 58*(2), 572-578. doi:10.1016/j.neuroimage.2011.06.074

Lindsey, A. E., Schneider, K., Simmons, D. M., Baron, R., Lee, B. S., & Kopito, R. R. (1990). Functional expression and subcellular localization of an anion exchanger cloned from choroid plexus. *Proc Natl Acad Sci U S A, 87*(14), 5278-5282.

Lu, K. T., Wu, C. Y., Cheng, N. C., Wo, Y. Y., Yang, J. T., Yen, H. H., & Yang, Y. L. (2006). Inhibition of the Na+ -K+ -2Cl- -cotransporter in choroid plexus attenuates traumatic brain injury-induced brain edema and neuronal damage. *Eur J Pharmacol, 548*(1-3), 99-105. doi:10.1016/j.ejphar.2006.07.048

Lytle, C., McManus, T. J., & Haas, M. (1998). A model of Na-K-2Cl cotransport based on ordered ion binding and glide symmetry. *Am J Physiol, 274*(2 Pt 1), C299-309.

Macaulay, N., & Zeuthen, T. (2012). Glial k(+) clearance and cell swelling: key roles for cotransporters and pumps. *Neurochem Res, 37*(11), 2299-2309. doi:10.1007/s11064-012-0731-3

Mao, S., Garzon-Muvdi, T., Di Fulvio, M., Chen, Y., Delpire, E., Alvarez, F. J., & Alvarez-Leefmans, F. J. (2012). Molecular and functional expression of cation-chloride cotransporters in dorsal root ganglion neurons during postnatal maturation. *J Neurophysiol, 108*(3), 834-852. doi:10.1152/jn.00970.2011

Maren, T. H. (1967). Carbonic anhydrase: chemistry, physiology, and inhibition. *Physiol Rev, 47*(4), 595-781.

Masuzawa, T., Shimabukuro, H., Sato, F., & Saito, T. (1981). Ultrastructural localization of carbonic anhydrase activity in the rat choroid plexus epithelial cell. *Histochemistry, 73*(2), 201-209.

McMurtrie, H. L., Cleary, H. J., Alvarez, B. V., Loiselle, F. B., Sterling, D., Morgan, P. E., . . . Casey, J. R. (2004). The bicarbonate transport metabolon. *J Enzyme Inhib Med Chem, 19*(3), 231-236. doi:10.1080/14756360410001704443

Mercado, A., de Los Heros, P., Melo, Z., Chavez-Canales, M., Murillo-de-Ozores, A. R., Moreno, E., . . . Gamba, G. (2016). With no lysine L-WNK1 isoforms are negative regulators of the K+-Cl- cotransporters. *Am J Physiol Cell Physiol, 311*(1), C54-66. doi:10.1152/ajpcell.00193.2015

Minta, A., & Tsien, R. Y. (1989). Fluorescent indicators for cytosolic sodium. *J Biol Chem, 264*(32), 19449-19457.

Murphy, V. A., & Johanson, C. E. (1990). Na(+)-H+ exchange in choroid plexus and CSF in acute metabolic acidosis or alkalosis. *Am J Physiol, 258*(6 Pt 2), F1528-1537.

Nakamoto, T., Srivastava, A., Romanenko, V. G., Ovitt, C. E., Perez-Cornejo, P., Arreola, J., . . . Melvin, J. E. (2007). Functional and molecular characterization of the fluid secretion mechanism in human parotid acinar cells. *Am J Physiol Regul Integr Comp Physiol, 292*(6), R2380-2390. doi:10.1152/ajpregu.00591.2006

Nelson, R. J. (1997). The use of genetic "knockout" mice in behavioral endocrinology research. *Horm Behav, 31*(3), 188-196. doi:10.1006/hbeh.1997.1381

Nickell, W. T., Kleene, N. K., & Kleene, S. J. (2007). Mechanisms of neuronal chloride accumulation in intact mouse olfactory epithelium. *J Physiol, 583*(Pt 3), 1005-1020. doi:10.1113/jphysiol.2007.129601

Parmelee, J. T., Bairamian, D., & Johanson, C. E. (1991). Response of infant and adult rat choroid plexus potassium transporters to increased extracellular potassium. *Brain Res Dev Brain Res, 60*(2), 229-233.

Parmelee, J. T., & Johanson, C. E. (1989). Development of potassium transport capability by choroid plexus of infant rats. *Am J Physiol, 256*(3 Pt 2), R786-791.

Payne, J. A., & Forbush, B., 3rd. (1995). Molecular characterization of the epithelial Na-K-Cl cotransporter isoforms. *Curr Opin Cell Biol, 7*(4), 493-503.

Piala, A. T., Moon, T. M., Akella, R., He, H., Cobb, M. H., & Goldsmith, E. J. (2014). Chloride sensing by WNK1 involves inhibition of autophosphorylation. *Sci Signal, 7*(324), ra41. doi:10.1126/scisignal.2005050

Piechotta, K., Lu, J., & Delpire, E. (2002). Cation chloride cotransporters interact with the stress-related kinases Ste20-related proline-alanine-rich kinase (SPAK) and oxidative stress response 1 (OSR1). *J Biol Chem, 277*(52), 50812-50819. doi:10.1074/jbc.M208108200

Plotkin, M. D., Kaplan, M. R., Peterson, L. N., Gullans, S. R., Hebert, S. C., & Delpire, E. (1997). Expression of the Na(+)-K(+)-2Cl- cotransporter BSC2 in the nervous system. *Am J Physiol, 272*(1 Pt 1), C173-183.

Plum, C. M. (1958). Electrolyte variations in the cerebrospinal fluid in various pathological conditions. *Acta Psychiatr Neurol Scand, 33*(4), 477-489.

Praetorius, J., & Damkier, H. H. (2017). Transport across the choroid plexus epithelium. *Am J Physiol Cell Physiol, 312*(6), C673-C686. doi:10.1152/ajpcell.00041.2017

Preston, J. E., Dyas, M., & Johanson, C. E. (1993). Development of chloride transport by the rat choroid plexus, in vitro. *Brain Res, 624*(1-2), 181-187.

Rao, V. V., Dahlheimer, J. L., Bardgett, M. E., Snyder, A. Z., Finch, R. A., Sartorelli, A. C., & Piwnica-Worms, D. (1999). Choroid plexus epithelial expression of MDR1 P glycoprotein and multidrug resistance-associated protein contribute to the blood-cerebrospinal-fluid drug-permeability barrier. *Proc Natl Acad Sci U S A, 96*(7), 3900-3905.

Redzic, Z. B., & Segal, M. B. (2004). The structure of the choroid plexus and the physiology of the choroid plexus epithelium. *Adv Drug Deliv Rev, 56*(12), 1695-1716. doi:10.1016/j.addr.2004.07.005

Robertson, M. A., & Foskett, K.J. (1995). Fluorescence Measurements of Cytosolic Sodium Concentration. In J. Kraicer, and Dixon, S.J. (Ed.), *Measurement and Manipulation of Intracellular Ions* (Vol. 27, pp. 274-288): Academic Press, Inc.

Rocha-Gonzalez, H. I., Mao, S., & Alvarez-Leefmans, F. J. (2008). Na+,K+,2Cl-cotransport and intracellular chloride regulation in rat primary sensory neurons: thermodynamic and kinetic aspects. *J Neurophysiol, 100*(1), 169-184. doi:01007.2007 [pii]

10.1152/jn.01007.2007

Roder, P., & Hille, C. (2014). ANG-2 for quantitative Na(+) determination in living cells by time-resolved fluorescence microscopy. *Photochem Photobiol Sci, 13*(12), 1699-1710. doi:10.1039/c4pp00061g

Rose, C. R., & Ransom, B. R. (1996). Intracellular sodium homeostasis in rat hippocampal astrocytes. *J Physiol, 491 ( Pt 2)*, 291-305.

Ruess, L. (1988). Cell volume regulation in nonrenal epithelia. *Renal Physiol. Biochem., 11*.

Russell, J. M. (2000). Sodium-potassium-chloride cotransport. *Physiol Rev, 80*(1), 211-276.

Saito, Y., & Wright, E. M. (1983). Bicarbonate transport across the frog choroid plexus and its control by cyclic nucleotides. *J Physiol, 336*, 635-648.

Saito, Y., & Wright, E. M. (1984). Regulation of bicarbonate transport across the brush border membrane of the bull-frog choroid plexus. *J Physiol, 350*, 327-342.

Saito, Y., & Wright, E. M. (1987). Regulation of intracellular chloride in bullfrog choroid plexus. *Brain Res, 417*(2), 267-272.

Shekarabi, M., Zhang, J., Khanna, A. R., Ellison, D. H., Delpire, E., & Kahle, K. T. (2017). WNK Kinase Signaling in Ion Homeostasis and Human Disease. *Cell Metab, 25*(2), 285-299. doi:10.1016/j.cmet.2017.01.007

Silva, P., Stoff, J., Field, M., Fine, L., Forrest, J. N., & Epstein, F. H. (1977). Mechanism of active chloride secretion by shark rectal gland: role of Na-K-ATPase in chloride transport. *Am J Physiol, 233*(4), F298-306.

Smith, Q. R., & Johanson, C. E. (1985). Active transport of chloride by lateral ventricle choroid plexus of the rat. *Am J Physiol, 249*(4 Pt 2), F470-477.

Somjen, G. G. (2002). Ion regulation in the brain: implications for pathophysiology. *Neuroscientist, 8*(3), 254-267.

Spector, R., & Johanson, C. E. (1989). The mammalian choroid plexus. *Sci Am, 261*(5), 68-74.

Spector, R., Keep, R. F., Robert Snodgrass, S., Smith, Q. R., & Johanson, C. E. (2015). A balanced view of choroid plexus structure and function: Focus on adult humans. *Exp Neurol, 267*, 78-86. doi:10.1016/j.expneurol.2015.02.032

Strahle, J., Garton, H. J., Maher, C. O., Muraszko, K. M., Keep, R. F., & Xi, G. (2012). Mechanisms of hydrocephalus after neonatal and adult intraventricular hemorrhage. *Transl Stroke Res, 3*(Suppl 1), 25-38. doi:10.1007/s12975-012-0182-9

Stummer, W., Keep, R. F., & Betz, A. L. (1994). Rubidium entry into brain and cerebrospinal fluid during acute and chronic alterations in plasma potassium. *Am J Physiol, 266*(6 Pt 2), H2239-2246.

TEFLabs, I. (2012). Asante NaTRIUM Green 2 Data. Retrieved from http://www.teflabs.com/ion-indicators/sodium-indicators/asante-natrium-green-2

Terker, A. S., Zhang, C., Erspamer, K. J., Gamba, G., Yang, C. L., & Ellison, D. H. (2016). Unique chloride-sensing properties of WNK4 permit the distal nephron to modulate potassium homeostasis. *Kidney Int, 89*(1), 127-134. doi:10.1038/ki.2015.289

Thastrup, J. O., Rafiqi, F. H., Vitari, A. C., Pozo-Guisado, E., Deak, M., Mehellou, Y., & Alessi, D. R. (2012). SPAK/OSR1 regulate NKCC1 and WNK activity: analysis of WNK isoform interactions and activation by T-loop trans-autophosphorylation. *Biochem J, 441*(1), 325-337. doi:10.1042/BJ20111879

Unterberg, A. W., Stover, J., Kress, B., & Kiening, K. L. (2004). Edema and brain trauma. *Neuroscience, 129*(4), 1021-1029. doi:10.1016/j.neuroscience.2004.06.046

Valverde, M. A., Bond, T. D., Hardy, S. P., Taylor, J. C., Higgins, C. F., Altamirano, J., & Alvarez-Leefmans, F. J. (1996). The multidrug resistance P-glycoprotein modulates cell regulatory volume decrease. *EMBO J, 15*(17), 4460-4468.

Verkman, A. S., Sellers, M. C., Chao, A. C., Leung, T., & Ketcham, R. (1989). Synthesis and characterization of improved chloride-sensitive fluorescent indicators for biological applications. *Anal Biochem, 178*(2), 355-361.

Vogh, B. P., & Langham, M. R., Jr. (1981). The effect of furosemide and bumetanide on cerebrospinal fluid formation. *Brain Res, 221*(1), 171-183.

Walcott, B., Birzgalis, A., Moore, L. C., & Brink, P. R. (2005). Fluid secretion and the Na+-K+-2Cl- cotransporter in mouse exorbital lacrimal gland. *Am J Physiol Cell Physiol, 289*(4), C860-867. doi:10.1152/ajpcell.00526.2004

Wang, G., Huang, H., He, Y., Ruan, L., & Huang, J. (2014). Bumetanide protects focal cerebral ischemia-reperfusion injury in rat. *Int J Clin Exp Pathol, 7*(4), 1487-1494.

Watts, A. G., Sanchez-Watts, G., Emanuel, J. R., & Levenson, R. (1991). Cell-specific expression of mRNAs encoding Na+,K(+)-ATPase alpha- and beta-subunit isoforms within the rat central nervous system. *Proc Natl Acad Sci U S A, 88*(16), 7425-7429.

Welch, K., & Sadler, K. (1965). Electrical Potentials of Choroid Plexus of the Rabbit. *J Neurosurg, 22*, 344-351. doi:10.3171/jns.1965.22.4.0344

Wright, E. M. (1978). Transport processes in the formation of the cerebrospinal fluid. *Rev Physiol Biochem Pharmacol, 83*, 3-34.

Wu, Q., Delpire, E., Hebert, S. C., & Strange, K. (1998). Functional demonstration of Na+-K+-2Cl- cotransporter activity in isolated, polarized choroid plexus cells. *Am J Physiol, 275*(6 Pt 1), C1565-1572.

Zeuthen, T. (1978). Intracellular gradients of ion activities in the epithelial cells of the Necturus gallbladder recorded with ion-selective microelectrodes. *J Membr Biol, 39*(2-3), 185-218.

Zeuthen, T. (1987). The effects of chloride ions on electrodiffusion in the membrane of a leaky epithelium. Studies of intact tissue by microelectrodes. *Pflugers Arch, 408*(3), 267-274.

Zeuthen, T. (1994). Cotransport of K+, Cl- and H2O by membrane proteins from choroid plexus epithelium of Necturus maculosus. *J Physiol, 478 ( Pt 2)*, 203-219.

Zeuthen, T., Christensen, O., Baerentsen, J. H., & la Cour, M. (1987). The mechanism of electrodiffusive K+ transport in leaky epithelia and some of its consequences for anion transport. *Pflugers Arch, 408*(3), 260-266.

Zeuthen, T., & Macaulay, N. (2012). Cotransport of water by Na(+)-K(+)-2Cl(-) cotransporters expressed in Xenopus oocytes: NKCC1 versus NKCC2. *J Physiol, 590*(Pt 5), 1139-1154. doi:jphysiol.2011.226316 [pii]

10.1113/jphysiol.2011.226316

Zeuthen, T., & Wright, E. M. (1981). Epithelial potassium transport: tracer and electrophysiological studies in choroid plexus. *J Membr Biol, 60*(2), 105-128.

Zhang, J., Karimy, J. K., Delpire, E., & Kahle, K. T. (2017). Pharmacological targeting of SPAK kinase in disorders of impaired epithelial transport. *Expert Opin Ther Targets, 21*(8), 795-804. doi:10.1080/14728222.2017.1351949

Zhang, J., Pu, H., Zhang, H., Wei, Z., Jiang, X., Xu, M., . . . Chen, L. (2017). Inhibition of Na+-K+-2Cl- cotransporter attenuates blood-brain-barrier disruption in a mouse model of traumatic brain injury. *Neurochem Int*. doi:10.1016/j.neuint.2017.05.020

Zhao, H., & Muallem, S. (1995). Na+, K+, and Cl- transport in resting pancreatic acinar cells. *J Gen Physiol, 106*(6), 1225-1242.

Zhao, H., Nepomuceno, R., Gao, X., Foley, L. M., Wang, S., Begum, G., . . . Sun, D. (2017). Deletion of the WNK3-SPAK kinase complex in mice improves radiographic and clinical outcomes in malignant cerebral edema after ischemic stroke. *J Cereb Blood Flow Metab, 37*(2), 550-563. doi:10.1177/0271678X16631561

Zhu, W., Begum, G., Pointer, K., Clark, P. A., Yang, S. S., Lin, S. H., . . . Sun, D. (2014). WNK1-OSR1 kinase-mediated phospho-activation of Na+-K+-2Cl- cotransporter facilitates glioma migration. *Mol Cancer, 13*, 31. doi:10.1186/1476-4598-13-31

## *APPENDIX A*

## *Pilot Experiment, Immunohistochemical verification of the expression of NKATP$\alpha$1 and AQP1 in NKCC1 -/- CPECs.*

AQP1 and NKATP are both expressed on the apical membrane of CPECs (Wu et al., 1998). Given that AQP1 is the only known water channel expressed in on the apical membrane of CPECs, and that NKATP is the other $K^+$ uptake mechanism with an unusual location in this secretory epithelial cell, we decided to perform a screening to determine whether the location of either of these membrane proteins was changed in the NKCC1 -/- mouse. A change in the location of either AQP1 or NKATP in the NKCC1 -/- mouse would suggest that NKCC1 somehow participates in membrane protein sorting. The ultimate goal of this screening is to compare all of the known ion transporters in the NKCC1 -/- mouse CP to WT controls; however, we chose to begin with the two apical proteins that may interact with the $K^+$-induced changes in CWV presented above. The expression pattern of both AQP1 and NKATP in CPECs from NKCC1 KO mice appeared to be the same as in WT, n = 1 (Figure A1). There may be a difference the intensity of the antibody staining in the NKCC1 -/- mouse, which supports further investigation to quantify the fluorescence.

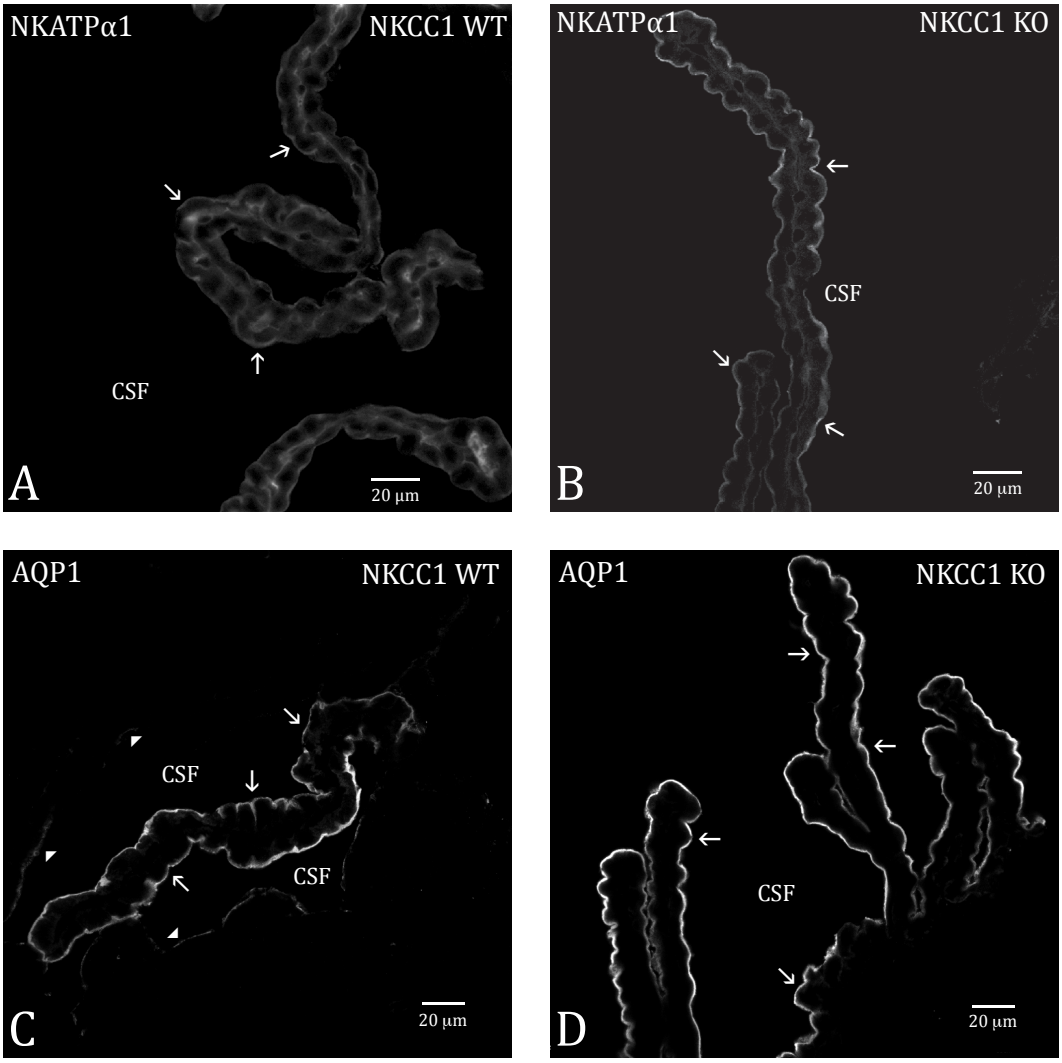


***Figure A1: NKCC1 KO CPECs maintain their apical expression of NKATPα1 and AQP1.*** *Brain tissue obtained from male sibling WT and NKCC1 -/- mice, postnatal age 19 days.* ***A*** *and* ***B*** *revealed the apical expression pattern of NKATPα1 on the CP in WT* ***(A)*** *and NKCC1 KO* ***(B)****. In* ***C*** *and* ***D****, a similar apical expression pattern existed for CP from the WT* ***(C)*** *and NKCC1 -/-* ***(D)****.*

## *APPENDIX B*

## *Animal means from the experimental data.*

The following supplemental data of the individual animal statistics is presented in the same order as it appears in the main text. Data labels show the individual animal means ± standard deviations, with n = number of cells from that animal.

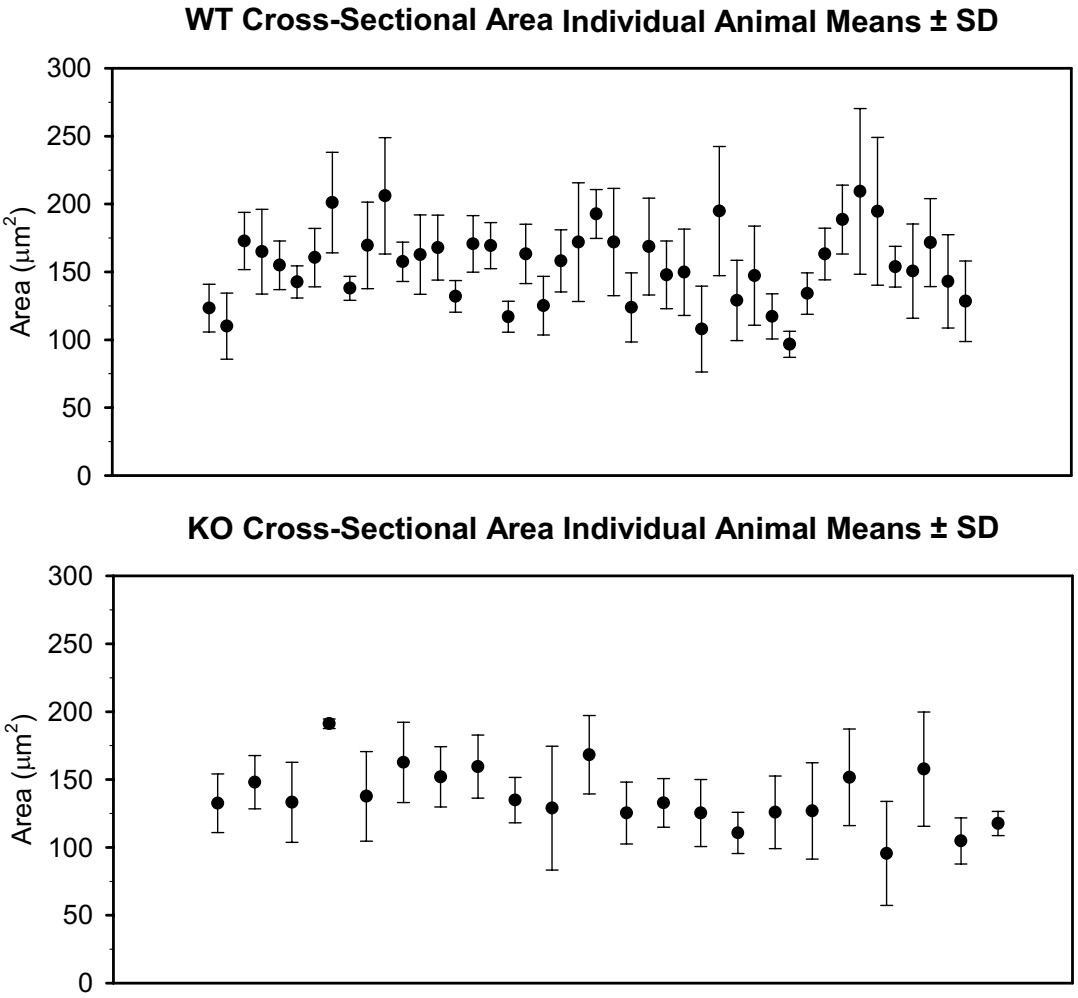


***Figure B1: WT and NKCC1 KO cross-sectional area animal data.*** *Individual statistics presented in tables on the following pages with left to right graph data presented top to bottom in table.*

**Table B1A: WT cross-sectional Areas (CSA)**

| Animal ID | n = cells | Mean CSA (µm²) | standard deviation |
|---|---|---|---|
| 12.2 | 9 | 123.4233 | 17.6 |
| 12.1 | 12 | 110.158 | 24.4 |
| 8.3 | 7 | 172.8159 | 21.1 |
| 6.4 | 6 | 164.9738 | 31.3 |
| 9.4 | 7 | 154.9809 | 17.9 |
| 7.3 | 5 | 142.6804 | 11.9 |
| 36.2 | 7 | 160.6699 | 21.5 |
| 40.6 | 15 | 201.1547 | 37.0 |
| 40.3 | 6 | 138.0045 | 8.8 |
| 40.1 | 9 | 169.6126 | 31.9 |
| 38.1 | 9 | 206.1038 | 42.9 |
| 38.3 | 7 | 157.5668 | 14.5 |
| 36.5 | 11 | 162.8289 | 29.2 |
| 16.4 | 7 | 167.9831 | 23.9 |
| 7.6 | 7 | 132.0074 | 11.7 |
| 2.1 | 8 | 170.7131 | 20.8 |
| 2.2 | 6 | 169.3866 | 17.0 |
| 85.6 | 5 | 117.0302 | 11.4 |
| 76.2 | 9 | 163.3088 | 21.8 |
| 75.6 | 7 | 125.1456 | 21.6 |
| 72.1 | 9 | 158.1353 | 22.9 |
| 69.3 | 7 | 171.9388 | 43.7 |
| 50.1 | 4 | 192.7865 | 18.0 |
| 48.5 | 16 | 172.1032 | 39.5 |
| 48.4 | 16 | 123.9412 | 25.4 |
| 47.4 | 13 | 168.7268 | 35.7 |
| 46.6 | 10 | 147.9214 | 24.9 |
| 44.7 | 9 | 149.7962 | 31.8 |

| | | | |
|---|---|---|---|
| 42.5 | 16 | 107.9828 | 31.6 |
| 37.5 | 24 | 194.9336 | 47.6 |
| 36.6 | 10 | 129.0399 | 29.6 |
| 33.5 | 12 | 147.3018 | 36.6 |
| 33.4 | 17 | 117.2521 | 16.6 |
| 32.5 | 5 | 96.7644 | 9.6 |
| 29.2 | 8 | 134.1625 | 15.3 |
| 26.7 | 15 | 163.2957 | 19.0 |
| 4.6 | 5 | 188.6032 | 25.3 |
| 80.3 | 6 | 209.4189 | 61.0 |
| 78.2 | 13 | 194.7071 | 54.4 |
| 77.1 | 7 | 153.8979 | 15.0 |
| 75.1 | 30 | 150.6935 | 34.7 |
| 74.2 | 28 | 171.6309 | 32.4 |
| 68.6 | 15 | 143.0997 | 34.4 |
| 44.2 | 36 | 128.4247 | 29.6 |

**Table B1B: NKCC1 KO cross-sectional areas (CSA)**

| Animal ID | n = cells | Mean CSA (μm²) | standard deviation |
|---|---|---|---|
| 71.1 | 4 | 132.4749 | 21.6 |
| 70.9 | 7 | 148.005 | 19.6 |
| 70.7 | 3 | 133.1665 | 29.4 |
| 63.4 | 2 | 191.1266 | 3.5 |
| 14.6 | 9 | 137.6215 | 33.0 |
| 62.2 | 11 | 162.6473 | 29.6 |
| 41.2 | 14 | 151.9135 | 22.2 |
| 41.4 | 12 | 159.4426 | 23.2 |
| 34.1 | 9 | 134.7757 | 16.7 |
| 33.8 | 9 | 128.9164 | 45.6 |
| 20.1 | 15 | 168.2091 | 28.9 |
| 19.2 | 21 | 125.3188 | 22.8 |
| 10.1 | 20 | 132.7343 | 17.9 |
| 4.5 | 11 | 125.2148 | 24.7 |
| 83.1 | 8 | 110.6741 | 15.1 |
| 83.4 | 13 | 125.8348 | 26.8 |
| 67.3 | 22 | 126.7616 | 35.5 |
| 47.2 | 21 | 151.5516 | 35.6 |
| 21.1 | 11 | 95.5485 | 38.3 |
| 12.2 | 17 | 157.6301 | 42.0 |
| 12.5 | 10 | 104.8059 | 17.0 |
| 6.4 | 15 | 117.6413 | 8.9 |

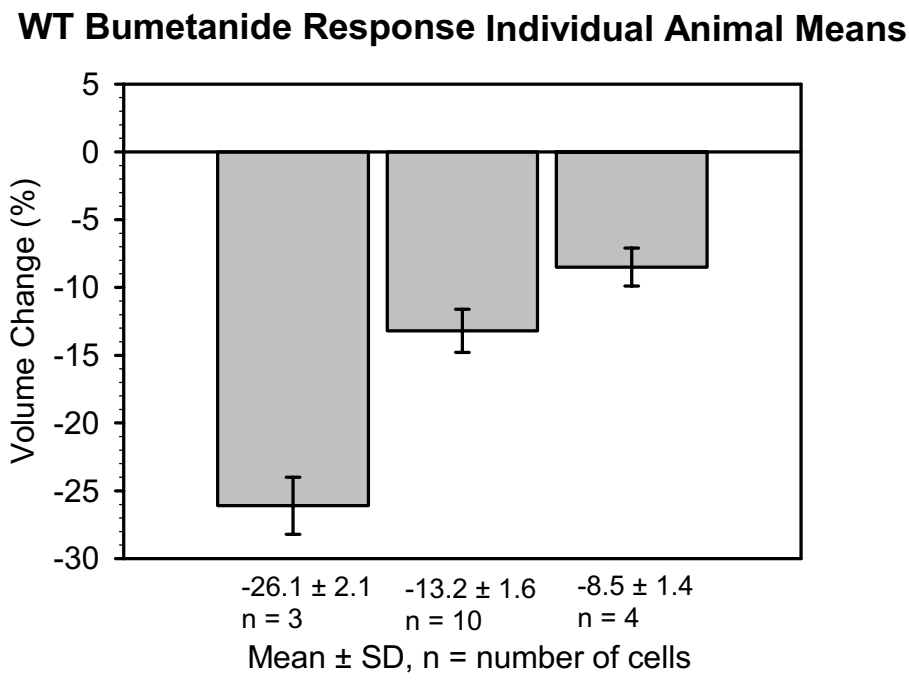


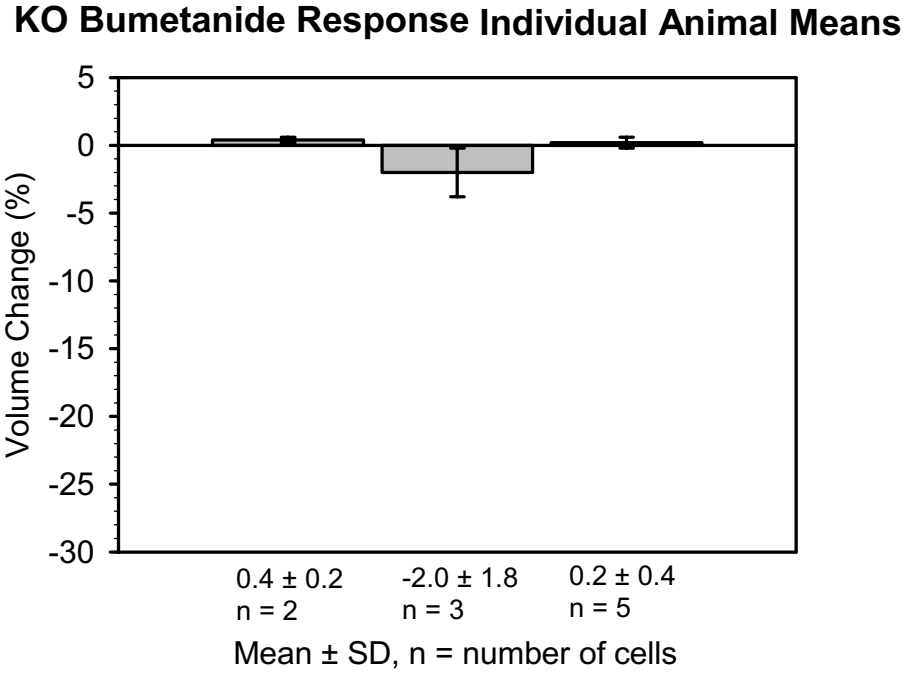


***Figure B2: CPEC volume response to 10 μM bumetanide***

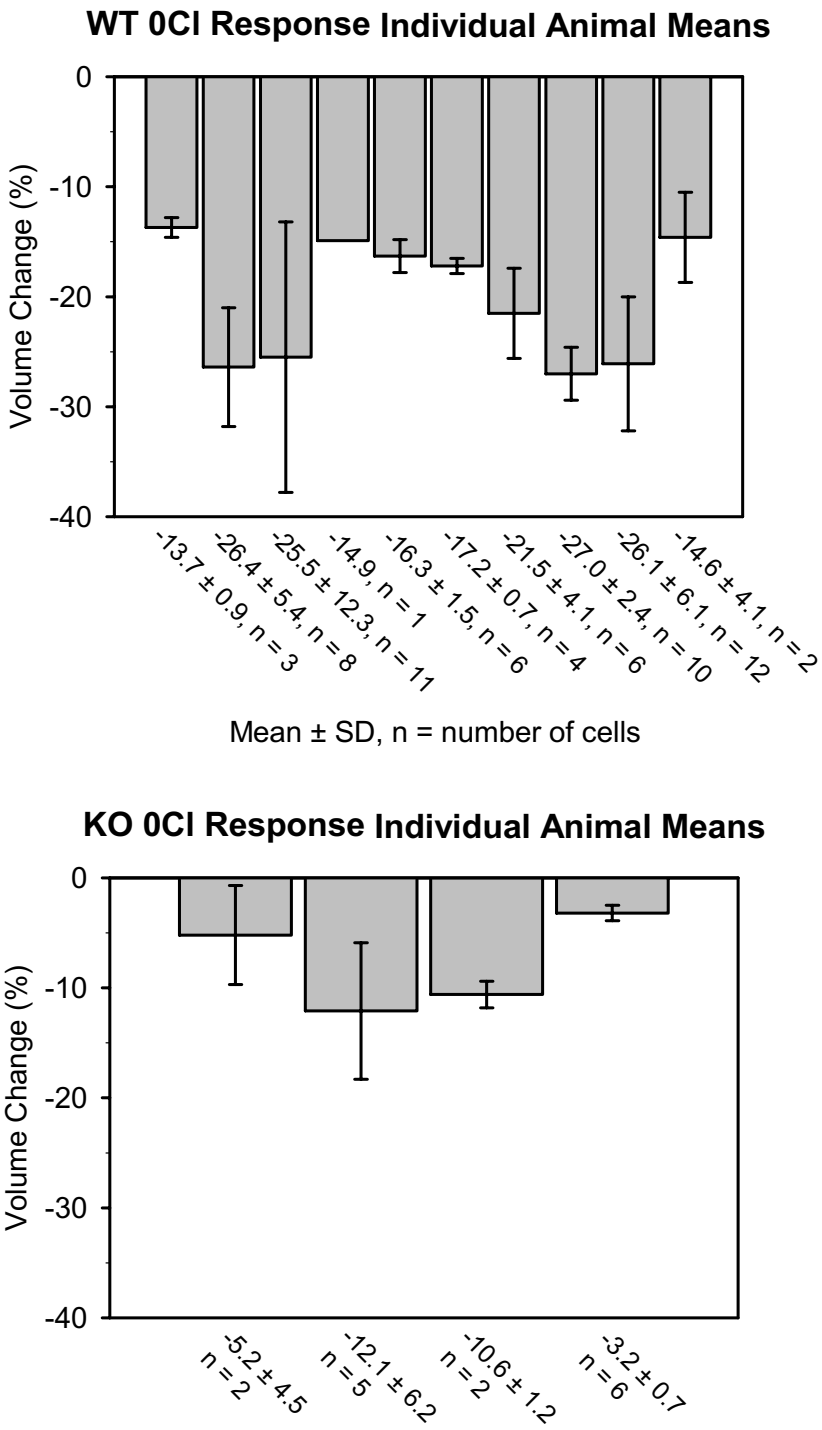


***Figure B3: CPEC volume response to 0Cl***

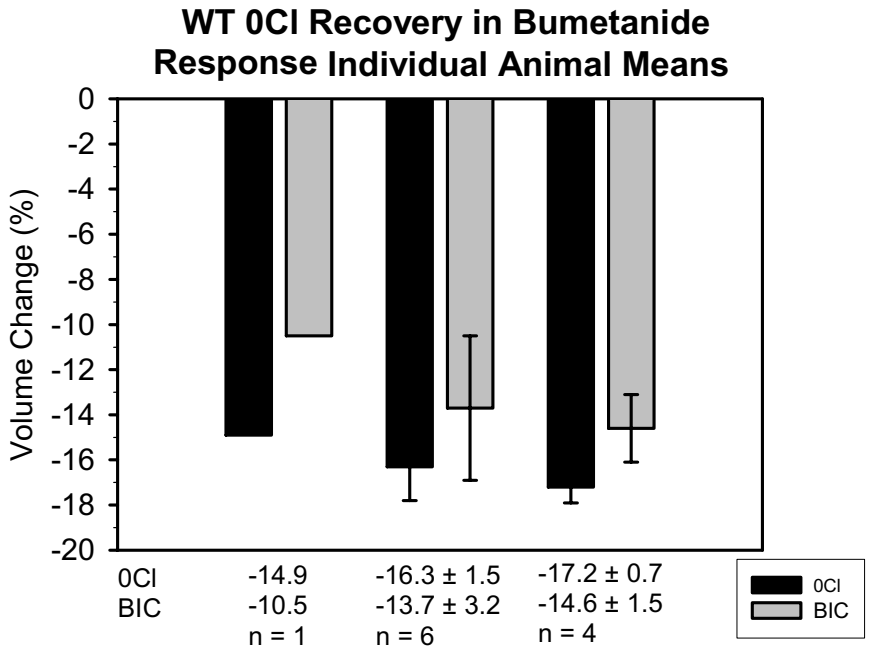


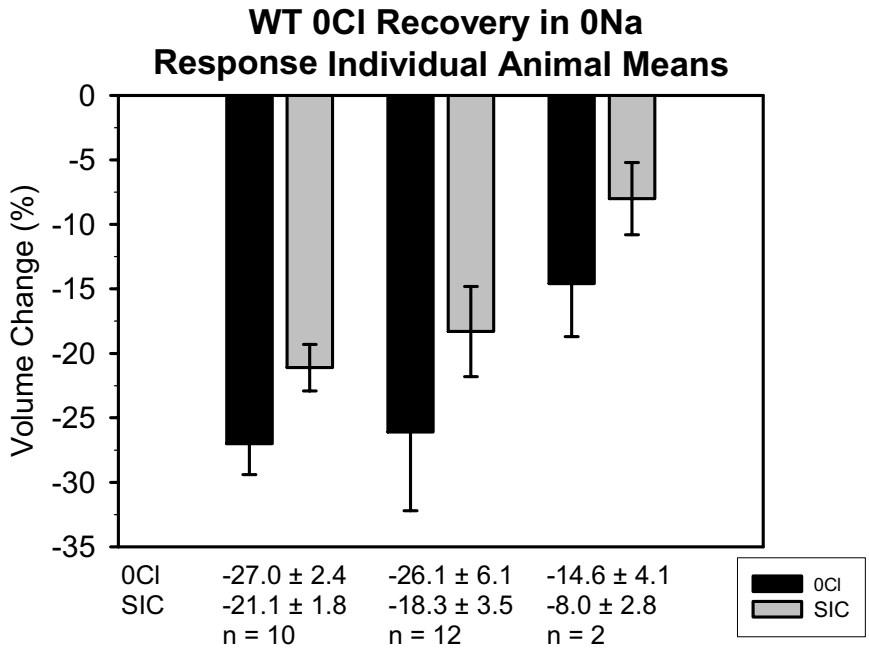


***Figure B4: CPEC volume recovery from 0Cl.***

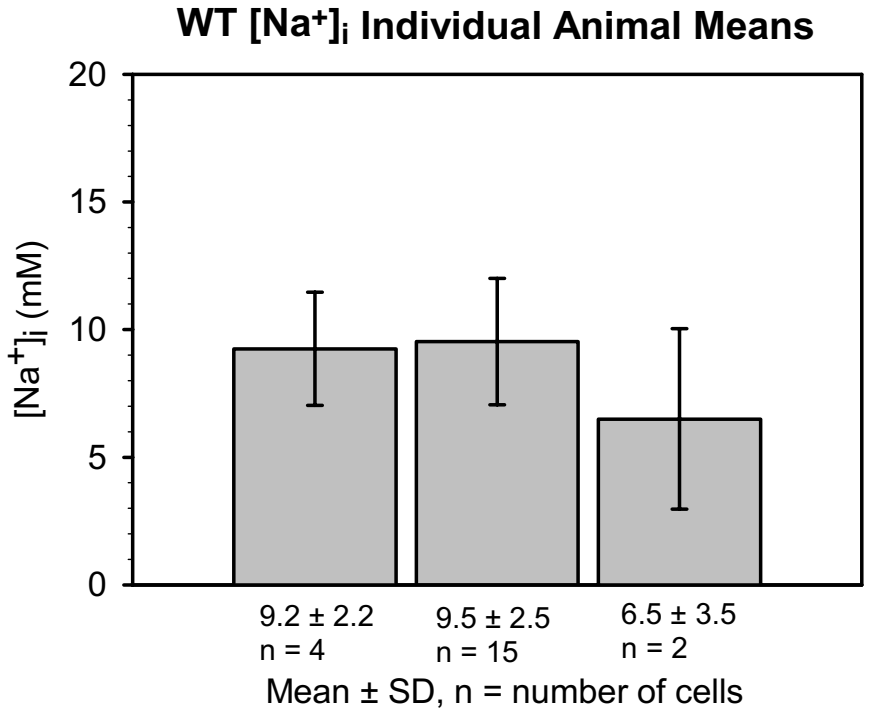


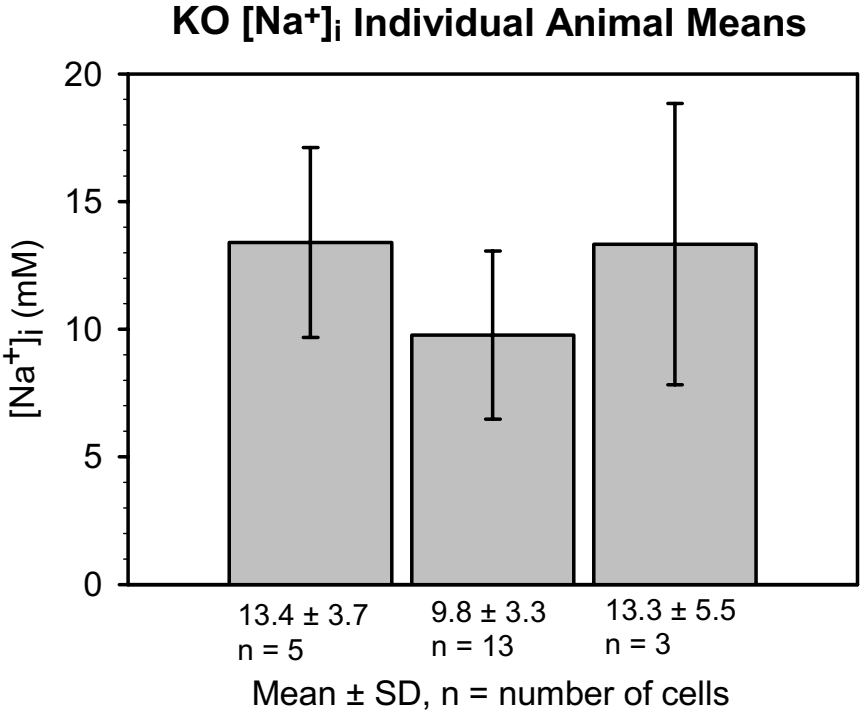


***Figure B5: ANG-2 $[Na^+]_i$ measurements***

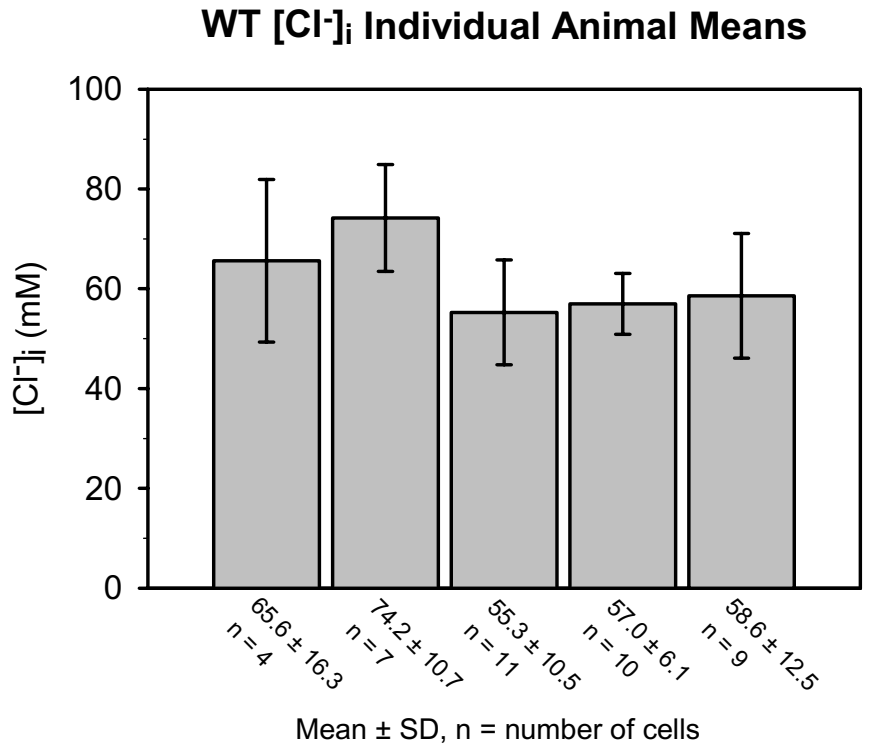


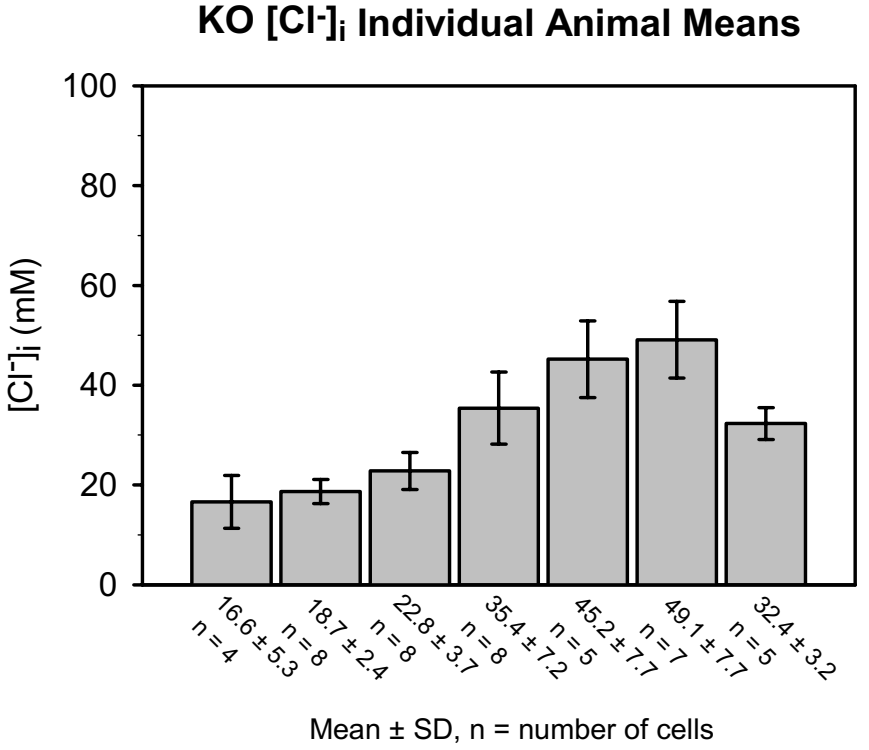


***Figure B6: MQAE $[Cl^-]_i$ measurements***

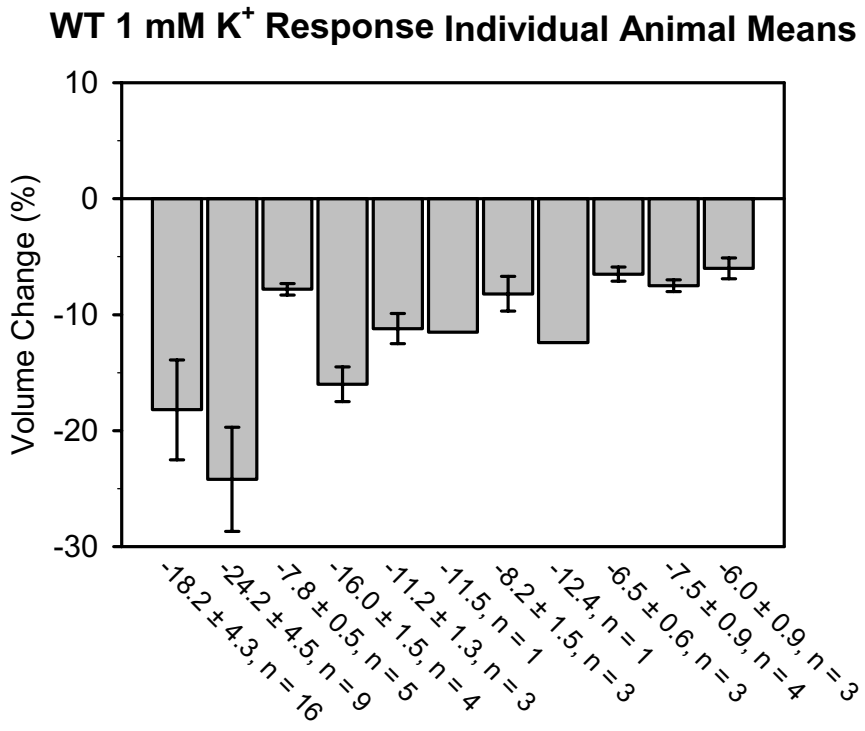


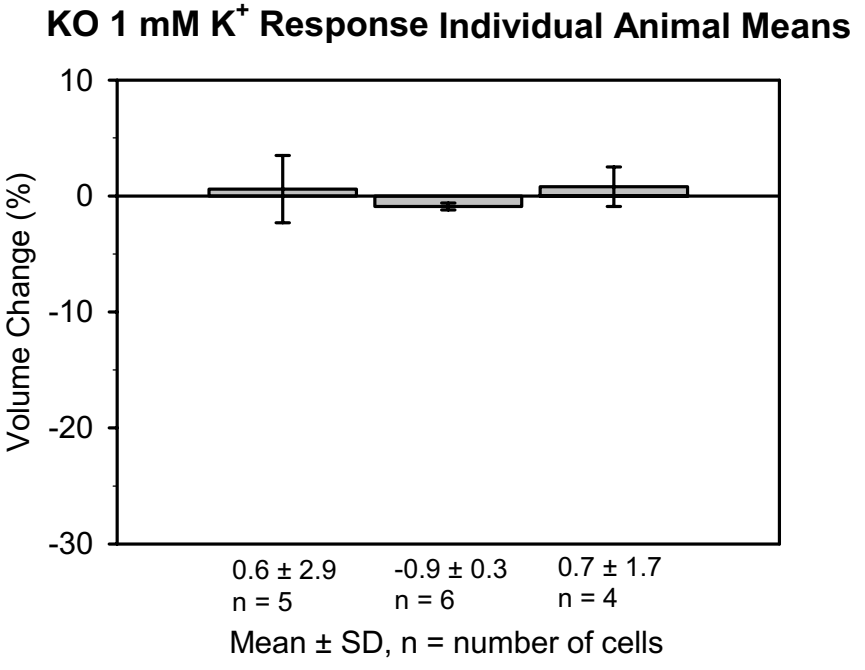


***Figure B7: CPEC volume response to 1 mM $K^+$***

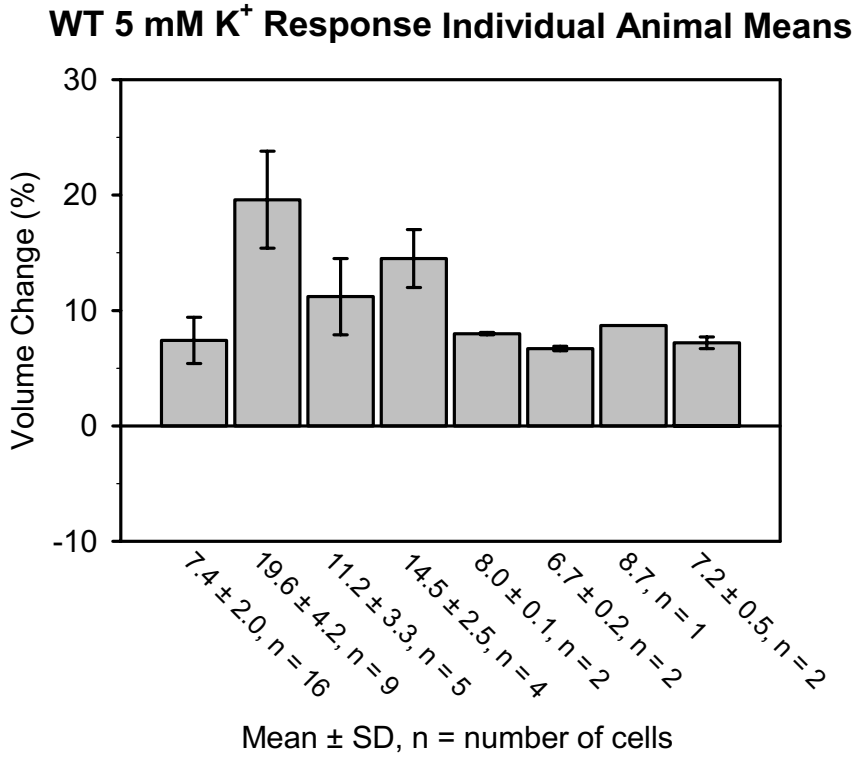


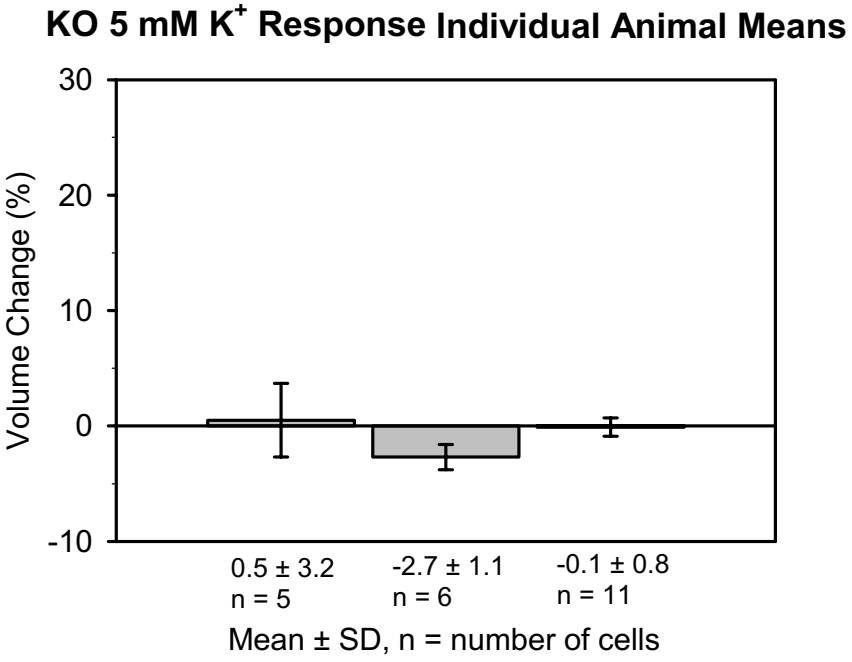


***Figure B8: CPEC volume response to 5 mM $K^+$***

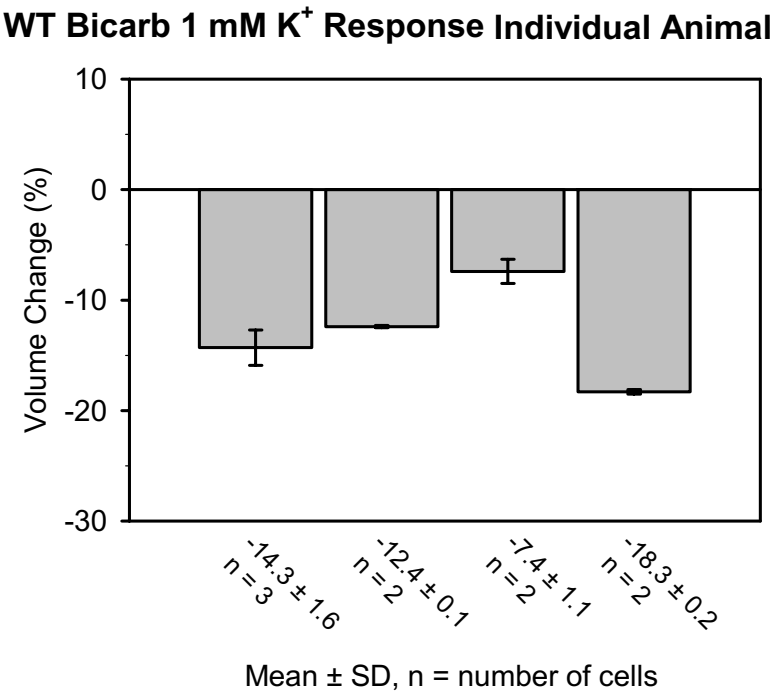


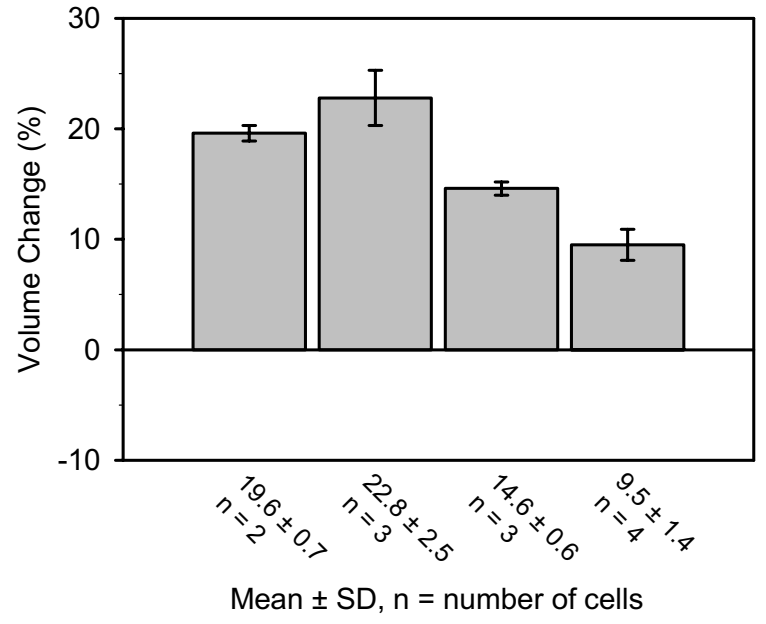


***Figure B9: CPEC volume response to 1 and 5 mM $K^+$ in $HCO_3^-$ buffered solutions.***